

Study on Localization System for Agricultural Vehicle Navigation Using Omnidirectional Vision

(全方位カメラによる農業用車両のナビゲーションのための
ロカライゼーションシステムに関する研究)

Ming Li

李明

ABSTRACT

With the problem dwindling in numbers of farm labor force and satisfying with precision agriculture necessary, agricultural vehicle automation is becoming more important. GPS is the most popular method for agricultural vehicle navigation. However, there are some limitations. First, its accuracy depends on the position of the satellites. In rural environments, especially in valley, hills or trees can obscure the microwave beams from satellites, resulting in a considerable drop in accuracy. To overcome this problem, the GPS sensor must be fused with other sensors, such as dead-reckoning sensors and machine vision sensors. Second, kinematic GPS for agricultural application is very expensive. Machine vision is also a popular method and other methods like GDS are not matured for application. Machine vision is a kind of cheaper and passive sensor, which has some excellent computer algorithms and matured success researches to support. GPS guidance system provides an absolute guidance system based on GPS base station on the ground, which is not affected by environments varying. The best solution on technology is a guidance system fusing with the technologies of GPS and machine vision.

Recently, omnidirectional vision sensors are very attractive for autonomous navigation system. An omnidirectional vision sensor is cheap and simply composed of a digital camera aiming at a catadioptric mirror. The images (obtained without rotating the robot) are 360° view of the environment and therefore are not sensitive to wheel slippage and small vibrations. Although it is not straightforward to obtain distance estimations from an omnidirectional image due to shape of the mirror, the apparent angles of objects from the robot are relatively accurate and easy to derive from the image.

In order to compensate for GPS that can use in the places where hills or trees obscure the microwave beams from satellites, resulting in a considerable drop in accuracy and develop a localization system substitute for GPS is used in the forage production and apply for precision agriculture. We developed a new localization system based on low-cost omnidirectional vision and artificial landmarks which estimates an absolute position relative to the landmark-based

coordinate system on the ground. In this work, we used an integrated-type omnidirectional vision consisting of a conventional USB camera and a hyperbolic mirror.

The field localization system for agricultural vehicle indoor and outdoor environments consists of four artificial landmarks, an omnidirectional vision sensor, PC and operating vehicle. The system sets four red artificial landmarks as a rectangle in the corners of an operating spot and estimates an absolute position relative to the landmark-based coordinate system on the ground. The principle of localization is that the omnidirectional vision sensor takes the image of the landmarks and estimates the directional angles of landmarks in the image. Camera location is estimated based on the directional angles. The system is not only a potential substitute for the GPS guidance system to localize agricultural vehicles, but it can also operate common computer vision functions to support localization and obstacle avoidance. Based on the analysis of system features, we know that agricultural vehicles equipped with the localization system will likely carry out navigation using their “eyes” in the same way that mammals move around in the world.

The recognition of landmarks and extraction of features is pivotal to realizing localization. In farm fields, the same crop usually shows a homologous color pattern, which makes it very difficult to utilize natural crop landmarks as features for processing images. Omnidirectional vision having a 360° view can capture landmark images in different directions. In order to ensure that images are captured in all directions and provide the same results, the landmarks were designed as a right circular red cone. Furthermore, to distinguish the landmarks from environmental interferences, we proposed a color model with red and blue patches.

One algorithm is about landmark tracking extraction in which red landmark pixels beyond the threshold were extracted as a small area and the center of gravity was calculated for the extracted small area representing the candidate of one landmark. Generally, providing the blue patch as compensation to further distinguish the landmark from other objects in a complex environment, blue patch pixels beyond the threshold were extracted as a small area and the center of gravity was calculated and judged the candidate of landmark by the distance between the two centers of gravity. Then the positions of four representative landmarks were obtained.

One image processing is about noise smoothness, which the classical low-pass filter (LPF) was employed to remove high spatial frequency noise from digital images. We multiplied convolution kernel elements by the least common multiple to compute the weighted sum and then divide the summation with the least common multiple to obtain the real results to improve computational speed.

The second algorithm is about estimation of the position of vehicle installed with camera. Based on the obtained positions of four landmarks via the landmark tracking extraction algorithm, and then estimated the four directional angles of the landmarks centered by camera principal point using only one omnidirectional image. Vehicle location was estimated using the center of gravity of the four intersections formed by four arcs according to geometric transformation based on the four directional angles of the landmarks. If only find three landmarks, we also utilized the directional angles to estimate the vehicle location.

In the test, if we used PC (Intel Core 2, 2.33GHz) to process a piece of image resolution 1024x768, it took only about 0.1~0.2 s. The tracking extraction, position estimation algorithms and image processing (LPF) are robustness.

In the localization algorithm, the principal point in the image is pivotal position and other calibration parameters are useful for improving the accuracy of locating. The calibration method utilized a 2D calibration pattern that can be freely moved. Without a priori knowledge of the motion, the boundary ellipse of the catadioptric image and field of view (FOV) were used to obtain principal point and focal length. Then, the explicit homography between the calibration pattern and its virtual image was used to initialize the extrinsic parameters. Last, the intrinsic and extrinsic parameters were refined by nonlinear optimization. Experimental results are proved to the calibration method which is feasible and effective. Localization application experimental results show that calibration can provide with the principal point value and improve the accuracy of localization about 1.6 cm in a 0.9 m x 1.8 m area. The role of calibration is very obvious.

For the fast and accurate self-localization applying for agriculture, artificial landmarks can be used very efficiently in the natural environment. Based on the proposed artificial color landmark model, balancing distance between landmark and camera, landmark height and

camera height to enlarge the application area was considered. We theoretically analyzed the necessary to balance camera height and landmark height to enlarge application area. Experimental results show that adjusting camera height and landmark height can enlarge application area for agricultural vehicle localization and we can decide the landmark size by the relations about landmark image size with distance between landmark and camera, landmark height and camera height, respectively.

In order to prove the localization system, we have done indoor experiments and outdoor experiments to verify the feasibility and effectiveness for indoor and outdoor field. The agricultural vehicle often operates on uneven ground and vibrates, camera tilt experiments also have done to test the errors caused by tilt angle. Indoor experiments were conducted under daylight lamps in a 5.8 m×3.53 m rectangular area of the laboratory, and outdoor experiments were conducted under natural sunlight in a 50 m×50 m square area to verify the system. Indoor experimental results showed that the maximum and RMS errors were less than 8 cm in an illuminated and small environment. Outdoor experimental results showed that the maximum and RMS distance errors were about 46.96 and 34.24 cm, respectively; camera tilt experiments showed that the tilt angle had some effect on errors, but not to an obvious level, and it was not necessary to compensate for the errors caused by camera tilt. Combined with camera tilt, the position distance RMS error is about 40 cm, although overall accuracy is a little lower, the localization system can compensate for GPS utilizing in the valley, apply for the forage operation agricultural vehicle navigation and improve the precision agriculture, e.g. mapping localization and mapping operation. In conclusion, the system is feasible and a potential compensation or substitute for GPS in agricultural vehicle navigation required for our objectives.

We introduced a new localization method on road for agricultural field utilizing omnidirectional camera with two landmarks. Image process extracted landmark candidate in the image and estimated the image distance between landmark and camera. The localization algorithm estimated the absolute location of vehicle based on the distance computational model between landmark image distance and spatial distance, and the directional angle of landmarks. Experimental results show that the RMS distance error is about 15 cm on a 20 m

distance road test. The proposed localization method is feasible and effective for agricultural vehicles field road navigation.

In a whole, we divide agricultural vehicles localization into two solutions to realize navigation: Field localization and Field road localization. This study mainly developed a localization system for agricultural vehicle in the indoor and outdoor field. We also developed a localization system for agricultural vehicle in the field road. Both of them use an omnidirectional vision sensor and artificial landmarks with simple construction and easy operation. In this study, we have done the experiments on the even ground and the system is feasible. We should apply the system working on the slope and consider it to practical application in next work.

FIGURE LIST

Fig. 1-1 Framework of agricultural vehicle autonomous guidance system	5
Fig.1-2 Row detection from the segmented binary image	7
Fig.1-3 Schematic diagram of dual-spectral camera system	9
Fig.1-4 Automated rice transplanter	12
Fig.1-5 Rectangular box substitute for a line	17
Fig.1-6 Row location: (a) uniform lighting conditions; (b) with deep shadows	18
Fig.1-7 The middle line was guiding row line	19
Fig.1-8 Comparison of navigation accuracy in vehicle offset from the desired path using sensor fusion, vision only, and GPS-FOG only based navigation controls.	22
Fig. 3-1 Position constrained by landmarks and distances.....	40
Fig. 3-2 Position constrained by landmarks and angles	40
Fig. 3-3 System architecture	42
Fig. 3-4 Signal processing diagram	42
Fig. 3-5 Panoramic view.....	43
Fig. 3-6 Omnidirectional vision system structure	44
Fig. 3-7 Omnidirectional vision system cross section and its point imaging	44
Fig. 3-8 Top view of imaging	45
Fig. 3-9 Illustration of vision area	46
Fig. 3-10 Landmark models	47
Fig. 4-1 Red landmark model tracking flow chart.....	53
Fig. 4-2 Red and blue combined landmark model tracking flow chart	54
Fig. 4-3 Position determination from four landmarks	57
Fig. 4-4 Position determination from three landmarks	58
Fig. 4-5(a) Original image with landmark and interference	59
Fig. 4-5(b) Landmarks extraction	59
Fig. 4-6(a1) Original image (only one landmark)	60

Fig. 4-6(b1) Smoothed image	60
Fig. 4-6(a2) Histogram of R, G and B before smoothness	61
Fig. 4-6(b2) Histogram of R, G and B after smoothness	61
Fig. 4-6(a3) Results of landmark extraction before smoothness	62
Fig. 4-6(b3) Results of landmark extraction after smoothness	62
Fig. 4-7 Program interface for four landmarks extraction	63
Fig. 5-1 Principal point of camera different from image center	67
Fig. 5-2 Directional angles changing with principal point.....	67
Fig. 5-3 Unified image formation	69
Fig. 5-4 Unified image formation with FOV	71
Fig. 5-5 One example of image.....	75
Fig. 5-6 Loading images.....	75
Fig. 5-8 Grids four corners extraction and coordinate	76
Fig. 5-9 Sub-pixel extraction of the corners	77
Fig. 5-10 Errors distribution.....	77
Fig. 5-11 Experimental setting	79
Fig. 6-1 Omnidirectional vision sensor with landmark imaging.....	84
Fig. 6-2 Relation between height of landmark image and X, Y value	85
Fig. 6-3 Relation between height of landmark (h_1) and height of landmark image (h_2)	86
Fig. 6-4 Relation between height of camera (H) and height of landmark image (h_2).....	87
Fig. 6-5 Relation of size (height and width) of landmark image and distance between landmark and camera	88
Fig. 6-6 Relation of size (height and width) of landmark image and height of landmark	90
Fig. 6-7 Illustration of landmark height.....	90
Fig. 6-8 Relation of size (height and width) of landmark image and height of camera.....	91
Fig. 7-1 Experimental device.....	94
Fig. 7-2 Distance measurement tools	94
Fig. 7-3 Landmark (1).....	95
Fig. 7-3 Landmark (2).....	95

Fig. 7-4 One indoor scene.....	96
Fig. 7-5 One outdoor scene	96
Fig. 7-6 Experimental results depicted on a map.....	97
Fig. 7-7 Experimental results for original and estimated positions	99
Fig. 7-8 Equipment for adjusting camera angle	100
Fig. 7-9 Example of x and y values and errors varying with tilt angle	103
Fig. 8-1 (a) Omnidirectional vision with ground point imaging	108
Fig. 8-1 (b) Top view of ground point imaging	109
Fig. 8-2 Simulation on real distance (x_i) and image distance (x_0).....	110
Fig. 8-3 Simulation on image distance (x_i) and height of system (H).....	111
Fig. 8-4 Position candidate calculation method	112
Fig. 8-5 Experimental illustration.....	113
Fig. 8-6 Position tracking result.....	113
Fig. A-1 Geometrical illustration	123

TABLE LIST

Table 1-1 Examples of guidance system developed in the world.....	4
Table 2-1 Objectives and application property.....	33
Table 5-1 Absolute errors ($\Delta\theta$) of directional angle	80
Table 5-2 Errors of x, y and distance (D) by original images.....	80
Table 5-3 Errors of x, y and distance (D) by rectification images.....	80
Table 7-1 Errors in x, y and distance (D) in indoor experiment	98
Table 7-2 Errors in x, y and distance (D) in outdoor experiment	99
Table 7-3 Errors in x, y and distance (D) relative to zero degree position.....	104
Table 7-4 Errors in distance (D) relative to zero degree position with varying tilt angle...	104
Table 7-5 Errors in x, y and distance (D) with camera tilt	104
Table 8-1 Errors in x, y and distance (D) on 20 m distance road experiment	114

ABBREVIATIONS

2D	: two dimension
3D	: three dimension
BCG	: blue pixels center of gravity
CCD	: charge coupled device
FL	: fuzzy logic
FOG	: fiber optical gyroscope
FOV	: field of view
FPID	: feed-forward PID
GDS	: geomagnetic direction sensor
GPS	: global positioning system
IMU	: inertial measurement unit
INS	: Inertial Navigation System
LPF	: low-pass filter
MAE	: mean absolute error
NN	: neural network
PC	: personal computer
PID	: Proportional-Integral-Differential
RCG	: red pixels center of gravity
RMS	: Root Mean Square
RTKGPS	: Real-time Kinematic GPS
WLAN	: wireless communication system

NOTATION

LATIN SYMBOLS

a	: structural parameter for the hyperbolic mirror surface, real axis length
b	: structural parameter for the hyperbolic mirror surface, imaginary axis length
be	: extracted blue pixel intensity
blevelmax	: extracted maximum blue intensity in the image
c	: structural parameter for the hyperbolic mirror surface which decides by a and b, the focus of hyperbola
cg	: center of gravity
d	: width of the formed landmark rectangular
f	: focal length of camera
g	: length of the formed landmark rectangular
H	: height of omnidirectional vision system
h1	: height of landmark
h2	: height of landmark in the image
I_1, I_2, I_3, I_4	: intersections of circular arcs defining camera (vehicle or robot) position
m_Height	: height of bitmap (pixel)
m_nmark	: number of landmark candidate
m_npoint1	: number of pixels satisfied with more than $Rlevelmax-C_1$
m_npoint2	: number of pixels satisfied with more than $Blevelmax-C_2$
ncorner1	: number groups of red pixels
ncorner2	: number groups of blue pixels
$p(x, y)$: an image point of P in the image plane
r_1, r_2	: spatial distance between landmark and camera position

r_e	: extracted red pixel intensity
$r_{levelmax}$: extracted maximum red intensity in the image
s	: image plane
t	: translation 3-vector
x_0	: image distance landmark imaging
x_i	: spatial line distance between camera and landmark
B	: blue pixel intensity
B_i	: selected blue pixels
C_1, C_2	: circular arcs defining camera position
D	: distance between original position and estimated position
G	: green pixel intensity
K	: camera intrinsic matrix
$K_i (i=1-5)$: calibration parameters
L	: distance between camera and landmark
L_{12}	: distance between landmark and landmark
L_1, L_2, L_3, L_4	: landmarks' positions
N_1, N_2, N_3, N_4, N_5	: threshold coefficient defined by image processing test
O	: original point
O_c	: principal point of the camera lens
$O_{c'}$: principal point of the virtual camera lens
O_M	: focus of the hyperbolic mirror
$P(S, Z)$: a random point in space with SZ coordinate system
$P(X, Y, Z)$: a random point in space with XYZ coordinate system
$P(x, y)$: estimated position determined by the image processing
R	: red pixel intensity
R_i	: selected red pixels
S	: plane of X and Y
S_1, S_2, S_3, S_4	: circular arcs in the ground coordinate system
$W_i (i=1, 2, 3, 4)$: divided crops area window

X_{be}	: the x-axis value of landmark position candidate decided by selected blue pixels
X_{re}	: the x-axis value of landmark position candidate decided by selected red pixels
Y_{be}	: the y-axis value of landmark position candidate decided by selected blue pixels
Y_{re}	: the y-axis value of landmark position candidate decided by selected red pixels
(x_a, y_a)	: location of the landmark L_1
(x_b, y_b)	: location of the landmark L_2
(x_0, y_0)	: location of the centroid point within a window W_i
(x_0, z_0)	: point of landmark
(x_i, z_i)	: point on the image plane corresponding point (x_0, z_0)
(x_m, z_m)	: point (x_0, z_0) reflected on the hyperbolic mirror
(u_0, v_0)	: principal point

GREEK SYMBOLS

α	: geometrical inclination angle of a point in space
α_1	: a subangle of directional angle θ_1
α_2	: a subangle of directional angle θ_2
β	: an arbitrary scalar
β_1	: a subangle of directional angle θ_1
β_2	: a subangle of directional angle θ_2
γ	: geometrical elevation angle of a image point
δ	: angle of perspective center by a virtual camera
$\delta^{(r)}$: radial distortion
$\delta^{(t)}$: tangential distortion
ζ	: distortion parameters' representation
θ	: direction angle of a point in space

θ'	: orientation angle on row crops
$\theta_1, \theta_2, \theta_3, \theta_4$: angle of the direction between neighboring landmarks
λ	: aspect ratio
μ	: a nonzero scalar
ξ	: mirror parameter
ρ	: radius
Φ	: angle of FOV
ω	: calculating relation with ξ, Φ
$\hat{\mathbf{R}}$: rotation matrix
$\Delta\theta_1, \Delta\theta_2, \Delta\theta_3, \Delta\theta_4$: angle errors

TABLE OF CONTENTS

Abstract	I
Figure list.....	VI
Table list.....	IX
Abbreviations.....	X
Notation	XI
Table of contents.....	XV
1 Introduction.....	1
1.1 Preface.....	1
1.2 Agricultural vehicle autonomous guidance research	2
1.2.1 Features of agricultural vehicles implement	5
1.2.2 Navigation sensors	6
1.2.2.1 Machine vision	6
1.2.2.3 Global positioning system	10
1.2.2.3 Dead reckoning sensors.....	12
1.2.2.4 Laser-based sensors.....	13
1.2.2.5 Inertial sensors.....	14
1.2.2.6 Geomagnetic direction sensor	15
1.2.3 Computational methods.....	16
1.2.3.1 Hough transform	16
1.2.3.2 Kalman filter	17
1.2.3.3 Other methods	18
1.2.4 Navigation planning	19
1.2.4.1 Tracking methods	19
1.2.4.2 Vehicle motion models	20
1.2.5 Steering controller	22
1.3 Discussion.....	24
1.4 Conclusions	26
2 Problem description, objectives and outline.....	28
2.1 Problem description	28
2.1.1 Dwindling in numbers of farming labor force and precision agriculture necessary	28
2.1.2 Limitations of GPS for agricultural vehicle navigation	29
2.1.3 Shortcomings of guidance system prototype in the laboratory	29
2.2 Status quo analysis.....	30

2.3 Objectives	33
2.4 Outline.....	35
3 Field localization system architecture and feature	37
3.1 Introduction	37
3.2 Landmarks based methods principle	38
3.3 Architecture of system	41
3.3.1 System architecture	41
3.3.2 Omnidirectional vision system	43
3.3.3 Landmark model.....	47
3.4 Features about system	48
3.4.1 Localization role.....	48
3.4.2 Computer vision role.....	48
3.5 Conclusions	49
4 Algorithms and program.....	50
4.1 Introduction	50
4.2 Proposed algorithm.....	51
4.2.1 Landmark tracking algorithm	51
4.2.2 Smoothness.....	55
4.2.3 Estimating position	55
4.2.3.1 Four landmarks extraction.....	55
4.2.3.2 Three landmarks extraction	58
4.3 Results of program running	58
4.3.1 Landmark extraction	58
4.3.2 Smoothness result	59
4.3.3 Position estimation result.....	62
4.4 Conculusions	63
5 Omnidirectional vision camera calibration	64
5.1 Introduction	64
5.2 Calibration requirements.....	66
5.2.1 Principal point	66
5.2.2 Omnidirectional vision system distortion	67
5.3 Catadioptric camera projection models	68
5.3.1 Pinhole camera model.....	68
5.3.2 Central catadioptric camera model.....	68
5.3.3 Distortion.....	69
5.4 Calibration algorithm	70
5.4.1 Mirror boundary extraction for principal point estimation	70
5.4.2 Initialization of focal length	71

5.4.3 Homography between the calibration pattern and its virtual image	72
5.4.4 Nonlinear optimization	73
5.4.5 Calibration Steps	73
5.5 Calibration experiments	74
5.5.1 Materials and methods	74
5.5.2 Experimental process	74
5.5.3 Results	77
5.5.3.1 Analysis of errors	77
5.5.3.2 Calibration results	78
5.6 Application experiments	78
5.6.1 Materials and methods	78
5.6.2 Results	79
5.7 Conclusions	80
6 Landmark imaging influence analysis	82
6.1 Introduction	82
6.2 Two related problems	82
6.2.1 Landmark detection	82
6.2.2 Application area	83
6.3 Enlarging application area analysis	83
6.3.1 Landmark imaging	84
6.4 Experiments	87
6.4.1 Materials and methods	87
6.4.2 Results and analysis	88
6.4.2.1 Relation of size of landmark image and distance between landmark and camera	88
6.4.2.2 Relation of size of landmark image and landmark setting height	89
6.4.2.3 Relation of size of landmark image and height of camera	91
6.5 Conclusions	92
7 Evaluation of the system	93
7.1 Experimental devices and scenes	93
7.1.1 Devices	93
7.1.1.1 Camera system	93
7.1.1.2 Measurement	94
7.1.1.3 Landmark	95
7.1.2 Scenes	96
7.1.2.1 Indoor scene	96
7.1.2.2 Outdoor scene	96
7.2 Indoor experiment	96

7.2.1 Methods	96
7.2.2 Results and discussion	97
7.3 Outdoor experiment	98
7.3.1 Methods	98
7.3.2 Results and discussion	98
7.4 Camera tilt experiment	99
7.4.1 Methods	99
7.4.2 Results and discussion	101
7.4.3 Position errors with camera tilt	104
7.5 Conclusions and future work	105
8 Field road localization	107
8.1 Introduction	107
8.2 Landmarks model and tracking algorithm	107
8.3 Distance computation model	108
8.4 Camera position estimation method	111
8.5 Experiments	113
8.5.1 Results and discussion	113
8.6 Conclusions	114
9 General conclusions and future work	115
9.1 General conclusions	115
9.1.1 The main original contributions of this work	118
9.1.2 A few critical aspects requiring improvement	119
9.2 Future work	120
Appendix A–Position estimation via geometry	123
Appendix B–focal length calculation via geometry	125
Appendix C–Screenshots of user interfaces of program	126
Appendix D–Screenshot of user interfaces of calibration program	127
Appendix E–Main program code	128
List of publications	141
References	143
Acknowledgements	155

1 INTRODUCTION

1.1 PREFACE

With the background of the development trend of international agricultural engineering in 21st century, modern technologies of electronics, information and automation are introduced into traditional agricultural vehicles to realize visual navigation, which will become the base of agricultural machine possessing abilities to exert precision agriculture, so that labor can be reduced, pollution caused by agricultural chemicals can be avoided and agricultural cost can be decreased. Field robots will be one way to improve the precision agriculture, which can be satisfied with the demand of future agriculture with high yield, food safety, high working efficiency, environment protection and precision horticulture. The navigation technologies of field robot are one of the basic technologies that must be realized.

There are many researches for agricultural vehicle navigation. Some navigation sensors provide vehicle position and vehicle heading, but also some sensors provide the current state of the vehicle (speed, wheel position, etc.). Some sensors provide information for absolute positioning and others only provide relative positioning (e.g. mechanical feelers and machine vision) between the vehicle and the guidance directrix. The key position sensors have been GPS and machine vision. The key heading sensors have included machine vision, GPS, with some work taking place with geomagnetic direction sensors (GDS) and inertial sensors.

Recently, omnidirectional vision has been used for navigation. This idea has much in common with biology where the majority of insects and arthropods benefit from a wide field of view and the omnidirectional vision is able to capture almost a hemi-spherical field of view. Many papers have been published on the applications of omnidirectional vision for navigation and made a better result to realize the guidance for indoor robots and non-stationary environments robots. However the applications for agricultural environments robots and agricultural vehicles are very few involved. At the same time, GPS is expensive for agricultural application and its accuracy is liable to be influenced by microwave shades such

as trees, houses. Machine vision and other methods like mechanical feelers are still not matured in application for agricultural vehicle. Therefore, the research using omnidirectional vision is worthy of going forward and hoping.

This chapter mainly focuses on the development of agricultural vehicle autonomous guidance research in recent 20 years. A brief review of research in agricultural vehicle guidance technologies is presented. We propose the conceptual framework of an agricultural vehicle autonomous guidance system, and then analyze its device characteristics. Mainly introduces navigation sensors, computational methods, navigation planners and steering controllers. Sensors include global positioning systems (GPS), machine vision, dead-reckoning sensors, laser-based sensors, inertial sensors and geomagnetic direction sensors. Computational methods for sensor information are used to extract features and fuse data. Planners generate movement information to supply control algorithms. Actuators transform guidance information into changes in position and direction. A number of prototype guidance systems have been developed but have not yet proceeded to commercialization. GPS and machine vision fused together or one fused with another assistant technology is becoming the trend development for agricultural vehicle guidance systems. Application of new popular robotic technologies will augment the realization of agricultural vehicle automation in the future.

1.2 AGRICULTURAL VEHICLE AUTONOMOUS GUIDANCE RESEARCH

Over history, agriculture has evolved from a manual occupation to a highly industrialized business, utilizing a virtually infinite variety of tools and machines (Tamaki, 2006). We are now looking towards the realization of autonomous agricultural vehicles. The first stage of development, automatic vehicle guidance, has been studied for many years, with a number of innovations explored as early as the 1920s (Willrodt, 1924; Sissons, 1939). The concept of fully autonomous agricultural vehicles is far from new; examples of early 'driverless tractor' prototypes using leader cable guidance systems date back to the 1950s and 60s (Morgan, 1958).

In the 1980s, the potential for combining computers with image sensors provided opportunities for machine vision based guidance systems. During the mid-1980s, researchers at Michigan State University and Texas A&M University were exploring machine vision guidance. Also during that decade, a program for robotic harvesting of oranges was successfully performed at the University of Florida (Harrell et al., 1990). In 1997, agricultural automation had become a major issue along with the advocacy of precision agriculture. The potential benefits of automated agricultural vehicles include increased productivity, increased application accuracy, and enhanced operation safety. Additionally, the rapid advancement in electronics, computers, and computing technologies has inspired renewed interest in the development of vehicle guidance systems. Various guidance technologies, including mechanical guidance, optical guidance, radio navigation, and ultrasonic guidance, have been investigated (Reid et al., 2000; Tillett, 1991).

Table 1-1 summarizes examples of research systems that have been developed around the world. Autonomous navigation systems for agricultural vehicles is now regarded as an important advance in precision agriculture and a promising alternative to the dwindling farming labor force, in addition to satisfying the quest for higher production efficiency and safer operation (Reid et al., 2000; Murakami et al., 2006).

Research on autonomous agricultural vehicles has become very popular, and the robotics industry has developed a wide range of remarkable robots. In the near future, we will be using affordable, dependable autonomous vehicles for agricultural application.

Section 1.2.1 includes an analysis of the device characteristics of agricultural vehicle guidance systems; then, a brief overall review of the past 20 years of global research in agricultural vehicle guidance technologies is presented in terms of a framework for agricultural vehicle autonomous guidance systems, as shown in Fig. 1-1. The key elements are navigation sensors, computational methods, navigation planners and steering controllers. The final section addresses some of the barriers to development and discusses the potential for new development.

Table 1-1 Examples of guidance system developed in the world

Institute (Country)	Sensor	Machine or test device	Performance results	Literature
University of Illinois, USA	Machine vision, GPS, GDS	Case 8920 MFD and 2WD Tractors	Vision guidance at 16 km/h on row crops	Zhang et al. (1999, 2002); Benson et al. (1998, 2003)
Stanford University, USA	GPS	John Deere 7800 Tractor	1° accuracy in heading, line tracking accuracy with 2.5-cm deviation	O'Connor et al. (1996)
University of Florida, USA	GPS, laser radar	Tractor	Average error of 2.8 cm using machine vision guidance and average error of 2.5 cm using radar guidance	Subramanian et al. (2006)
University of Halmstad, Sweden	Machine vision, Mechanical sensor, GPS	Tractor with row cultivator	Standard deviation of position of 2.7 and 2.3 cm	Åstrand and Baerveldt, (2005); Åstrand (2005)
Bygholm Research Center, Denmark	Machine vision	Tractor	Accuracy of less than 12 mm	Søgaard and Olsen, (2003)
University of Tokyo, Japan	FOG, Ultrasonic Doppler sensor	Tractor (Mitsubishi Co.)	Lateral displacement from the reference line was less than 10 cm at speeds of 0.7 to 1.8 m/s on a straight line	Imou et al. (1998)
National Agriculture Research Center, Japan	RTK GPS, FOG	PH-6, Iseki Co., Ehime transplanter	Less than 12 cm, yaw angle offset of about 5.5 cm at 2.52 km/h	Nagasaka et al. (2004)
BRAIN, Japan	Machine vision and laser range sensor	Tractor	Error about 5 cm at the speed of 0.4 m/s	Yukumoto (1997)
Hokkaido University, Japan	GDS, laser scanner	Tractor	Average error less than 1 cm	Noguchi et al. (1997,2002); Tsubota et al. (2004)
National Centre for Engineering in Agriculture, Australia	Machine vision	Tractor	Accuracy of 2 cm	Billingsley et al. (1997)

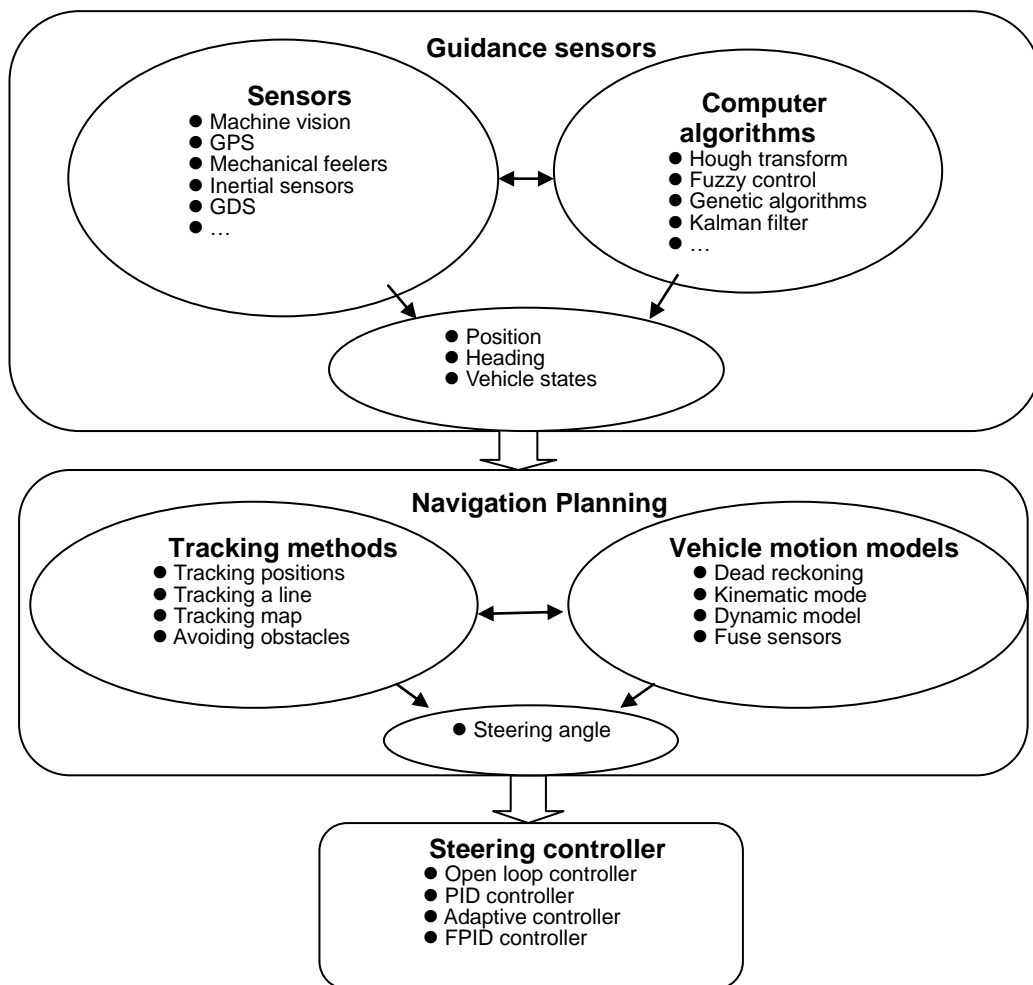


Fig. 1-1 Framework of agricultural vehicle autonomous guidance system

1.2.1 FEATURES OF AGRICULTURAL VEHICLES IMPLEMENT

The agricultural environment offers a very different set of circumstances to that encountered by a laboratory mobile robot. In one respect, operation is simplified by the absence of clutter typically present in the indoor environment; however, a number of additional complications are raised. For example, the operating areas are large; ground surfaces may be uneven; depending on the operation, wheel slippage may be far from negligible. Cultivation may interfere with underground cables, colors may change with plant growth, and soil quality may vary. Environmental conditions (rain, fog, dust, etc.) may affect sensor function; moreover, a low-cost system is required.

These disadvantages make it more difficult to realize agricultural automation. Companies are unwilling to invest in commercialization because it is not seen as a worthwhile money-making venture, and farmers are not financially able to participate. Other major reasons include the need to improve the technology and decrease the cost (Hague, 2000).

Compared with these complicating factors, agricultural farm fields have several advantages to developing autonomous guidance systems. For example, the working areas generally do not change; landmarks can be easily set up around the corners of a field and be taken as a stationary environment. The crops are always at the same places and can be easily distinguished. Therefore, even though there are more disadvantages than advantages for realizing agricultural vehicle autonomous guidance, there are enough research achievements to promote its development.

1.2.2 NAVIGATION SENSORS

1.2.2.1 *Machine vision*

Machine vision sensors measure the relative position and heading using the image sensor mounted on the vehicle. There are several aspects of machine vision based sensing. Different types of sensor modalities can be selected to measure the guidance information. Positioning of the sensor on the vehicle requires an understanding of the geometric relationship between the image sensor, the vehicle and the field-of-view that the sensor uses for guidance information. Fig. 1-2 shows one example. Researchers have explored the use of vision sensors for detecting a guidance directrix on row crops, soil tillage, and the edges along harvested crops. Various methodologies of image processing have been investigated for extracting the guidance information. The processed images provide output signals that can be used to provide steering signals for the vehicle.

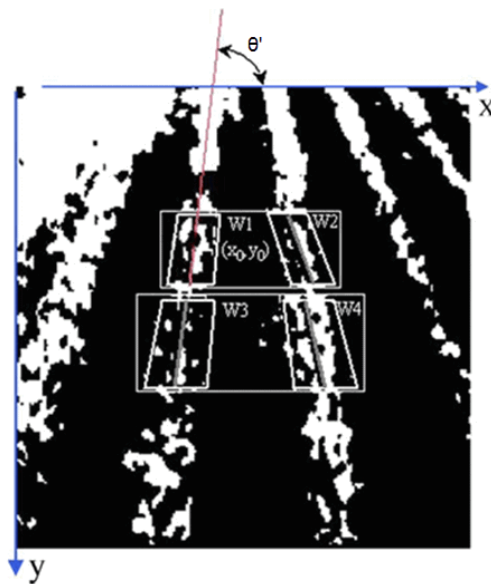


Fig.1-2 Row detection from the segmented binary image (Han et al., 2004)

One of the most commonly used machine vision methods is for detecting a guidance directrix on row crops, soil tillage, and the edges along harvested crops. Benson et al. (2003) developed a guidance combine harvester based on the lateral position of the crop cut edge. Marchant and Brivot (1995) used the Hough transform for row tracking in real time (10 Hz) and noted that their technique was tolerant to outliers (i.e., weeds) only when their number was reasonably small compared to the number of true data points. Marchant et al. (1997) reported an overall root mean square (RMS) error of 20 mm in the lateral position at a travel speed of 0.7 m/s using this technique to guide an agricultural vehicle in a transplanted cauliflower field.

The threshold method has been applied in many vision applications to separate objects of interest from imagery. For reliably extracting crop row features from field images, the major challenge of the threshold method is the difficulty in determining an adequate effective threshold value under varying ambient light conditions or changing crop growth stages. The effectiveness of distinguishing crops from weeds is another challenge in determining a pathway using the obtained field images. Research has been reported on attempts to improve the reliability of crop feature extraction and pathway determination for vision-based guidance systems. Hague and Tillett (2001) exploited a method using a bandpass filter to attenuate the

grey level of weeds and shadows in field images. Pinto et al. (2000) attempted to apply the principal component analysis method to extract crop row features from field images. Søggaard and Olsen (2003) also developed a machine vision guidance method that did not require a plant segmentation step, replacing it with a less intensive computation of the center of gravity for row segments in the image and weighted linear regression to determine the position and orientation of the rows.

Han et al. (2004) developed a row segmentation algorithm based on k-means clustering to segment crop rows. This information was then used to steer a tractor. The guided tractor was able to perform field cultivation in both straight and curved rows. Okamoto et al. (2002) developed an automatic guidance system for a weeding cultivator. A color CCD camera acquired the crop row images, which were then processed by computer and used to determine the offset between the machine and the target crop row.

Other techniques and systems have been investigated for machine vision guidance, and many of them have improved the robustness and dependability of machine vision. Billingsley and Schoenfisch (1997) reported a vision guidance system that is relatively insensitive to additional visual 'noise' from weeds. They used linear regression in each of three crop row segments and a cost function analogous to the moment of the best-fit line to detect lines fitted to outliers (i.e., noise and weeds) as a means of identifying row guidance information. They showed that their system is capable of maintaining an accuracy of 2 cm.

Tillett and Hague (1999) developed a machine vision guidance system for cereal crops, using the midpoints of 15 rows extracted from a single view of three adjacent crop rows (five midpoints per row). They tested the system in a single barley field with light to moderate weed pressure under uniform natural lighting and obtained a standard error in hoe position of 13 mm at travel speeds up to 6 km/h. Hague and Tillett (2001) used the analysis of the periodic near-infrared intensity function in a lateral path across five wheat rows in a plane view of the field rather than a traditional row segmentation method to obtain row guidance information. They obtained a RMS position error of 15.6 mm at a travel speed of 5.8 km/h.

For more complete crop or field information, some researchers used a stereovision system to provide a three-dimensional (3D) field image by combining two monocular field images

taken simultaneously from a binocular camera. Such 3D images are reconstructed based on the different-disparity monocular images to decrease the ambient light influence. Kise et al. (2005) developed a stereovision-based agricultural machinery crop-row tracking navigation system. The RMS error of lateral deviation was 3–5 cm following both straight and curved rows at speeds up to 3.0 m/s. The method required some weed-free areas to provide sufficient information for detecting the navigation points.

Åstrand and Baerveldt (2005) developed a machine vision guidance system that achieved good performance in detecting plants in near-infrared images acquired under non-uniform natural illumination by performing grayscale opening on the raw near-infrared image and subtracting it from the original prior to segmentation. Their method, based upon the Hough transform, used multiple rectangular regions (one for each row viewed) with the rectangle width adjusted for crop size. The information from multiple rows was fused together to obtain a common estimate of the row position. The accuracy of position estimation was less than 1.2 cm with a standard error depending on plant size. Field tests showed that the system had sufficient accuracy and speed to control the cultivator and mobile robot in a closed-loop fashion with a standard deviation of position of 2.7 and 2.3 cm, respectively, with incomplete row structures due to missing plants combined with high weed density (up to 200 weeds/m²).

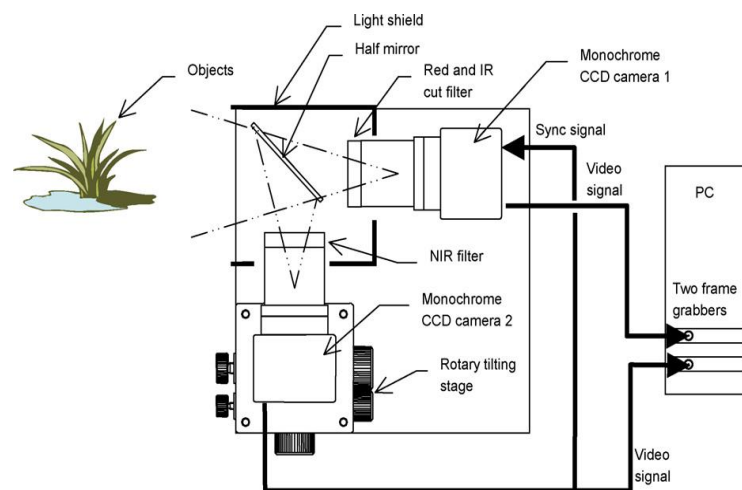


Fig.1-3 Schematic diagram of dual-spectral camera system (Kaizu and Imou, 2008)

Kaizu and Imou (2008) developed a dual-spectral camera system, shown as Fig. 1-3, for paddy rice seedling row detection. The system used a pair of low-cost monochrome cameras with different spectral filters. It matched a near-infrared image and a red image and it worked in the strong reflections on the water surface under cloudy conditions from morning to dusk.

1.2.2.3 Global positioning system

Since the early 1990s, Global Positioning System (GPS) receivers have been widely used as global guidance sensors (Larsen et al., 1994; Gan-Mor et al., 1997; Bell, 2000; Yukumoto et al., 2000). GPS-based guidance technology can be used for many field operations such as sowing, tilling, planting, cultivating, weeding and harvesting (Abidine et al., 2002; Gan-Mor et al., 2002). GPS-based navigation systems are the only navigation technologies that have become commercially available for farm vehicles. Many tractor manufacturing companies now offer the RTK GPS based auto steering system as an option on their tractors. The position information from the RTK GPS can be used for both guidance and other applications such as seed mapping, traffic control, and tillage control. GPS guidance systems provide an absolute guidance system in contrast to the relative guidance provided by machine vision, which requires that the crop be planted using a GPS-guided planting system or the crop rows mapped using some type of geo-referenced mapping technique. GPS guidance systems also require that a GPS base station is located within approximately 10 km of the RTK GPS guided tractor or agricultural robot. However, since GPS systems do not depend upon the visual appearance of the crop, they are not adversely affected by weed density, shadows, missing plants or other conditions that degrade the performance of machine vision guidance systems. Another advantage of GPS guidance systems is that they can be easily programmed to follow curved rows (Slaughter et al., 2008).

There appear to be three limitations to using GPS for vehicle guidance. The first is that GPS guidance systems cannot be used in microwave-shielded areas. Also, GPS cannot promise consistent positioning accuracy in the range of centimeters for a variety of field conditions (e.g., presence of buildings, trees or steeply rolling terrain, and interruption in satellite or differential correction signals). The second limitation is the inherent time delay (data latency) required for signal processing to determine locations that might present control

system challenges at higher field speeds. The third is the high cost for agricultural application (although there is a consistent trend of cost reduction with widespread use). However, with the anticipated technology developments, these limitations will undoubtedly be overcome, thereby making GPS a choice candidate for incorporation into vehicle guidance systems.

Stoll and Kutzbach (2000) studied the use of the RTK GPS as the only positioning sensor for the automatic steering system of self-propelled forage harvesters. They found that the standard deviation of steering was less than 100 mm under all conditions. Standard deviation of lateral offset (error) along straight-line paths ranged from 25 to 69 mm depending upon the travel speed.

Kise et al. (2001, 2002) studied the use of an RTK GPS guidance system for control of a tractor as an autonomous vehicle traveling along a curved path. Test results for following a sinusoidal path with a 2.5-m amplitude and 30-m wavelength at 6.5 km/h showed a 6-cm RMS error with a 13-cm maximum error. To compensate for GPS positioning error associated with machinery attitude, researchers at Hokkaido University integrated an inertial measurement unit (IMU) with an RTK GPS to provide more accurate navigation information. This integrated navigation system could guide agricultural machinery performing all field operations, including planting, cultivating and spraying, at a travel speed of up to 3 m/s, with a tracking error of less than 5 cm on both straight and curved paths.

Ehsani et al. (2003) evaluated the dynamic accuracy of several low-cost GPS receivers with the position information from an RTK GPS as reference. They found that these receivers had an average absolute cross-track error of around 1 m when traveling in a straight line. GPS cannot be effectively used for positioning in citrus applications since the vehicle frequently moves under the tree canopy, which blocks the satellite signals to the GPS receiver. Moreover, a system using GPS for guidance requires that a predetermined path be given for the vehicle to follow. Consequently, significant time must be spent in mapping its path.

Nagasaka et al. (2004) used an RTK GPS for positioning, and fiber optic gyroscope (FOG) sensors to maintain vehicle inclination, for an automated six-row rice transplanter (Fig. 4). Root-mean-square deviation from the desired straight path after correcting for the yaw angle

offset was approximately 55 mm at a speed of 0.7 m/s. The maximum deviation from the desired path was less than 12 cm.

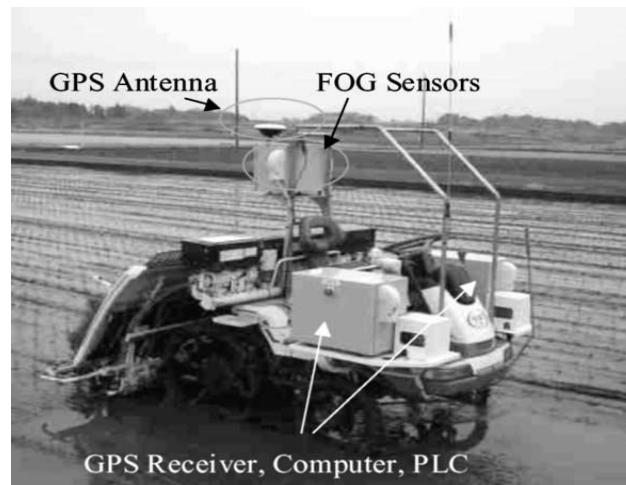


Fig.1-4 Automated rice transplanter (Nagasaka et al., 2004)

1.2.2.3 Dead reckoning sensors

Dead-reckoning sensors are inexpensive, reliable sensors for short-distance mobile robots, using a simple mathematical procedure for determining the present location of a vehicle by advancing a previous position through a known course and velocity information over a given length of time. The simplest form of dead reckoning is referred to as odometry. However, odometry is the integration of incremental motion information over time, which inevitably leads to the unbounded accumulation of errors. Specifically, orientation errors will cause large lateral position errors, which increase proportionally with the distance traveled by the robot. Despite these limitations, researchers use odometry as an important part of robot navigation systems (Borenstein, 1996; Chénavier and Crowley, 1992).

Doppler sensors use the principle based on the Doppler shift in frequency observed when radiated energy reflects off a surface that is moving relative to the emitter. This type of sensor can decrease some of the errors arising from wheel slippage, tread wear, and/or improper tire inflation. Imou et al. (1998) developed an autonomous tractor using an ultrasonic Doppler speed sensor and gyroscope. The results showed that the maximum lateral displacement from the reference line was less than 10 cm at a speed of 4 steps from 0.7 to 1.8 m/s on 50-m straight driving tests.

Imou et al. (2001a, 2001b) developed a new ultrasonic Doppler sensor to achieve high accuracy when measuring the speeds of both forward and reverse motions including low-speed motions.

1.2.2.4 Laser-based sensors

Laser-based sensors have a relatively longer range and higher resolution. The guidance systems need three or more reflectors (landmarks) around the work field. The time at which the laser beam is detected is communicated to the guidance system, which uses triangulation to define the location of the vehicle. The system is not prone to depending on environmental conditions, e.g., strong light change for machine vision and microwave shadowing for GPS, which will make the system inoperable. However, laser-based sensor systems have two drawbacks. They do not work well if the position is changed for any of the artificial landmarks. If natural landmarks are used in the navigation process, map updating is necessary in order to register the landmarks in the map building operation. The second problem is noisy laser measurements when the vehicle is traveling on uneven ground.

Holmqvist (1993) used a laser-optic navigation system for a vehicle moving at a speed of 2 m/s. With an average distance to the reflectors of 50 m, the absolute position error will typically be about 5 cm in each of the X, Y and Z directions. Ahamed et al. (2004) used laser radar for developing a positioning method using reflectors for infield road navigation. They tested differently shaped reflectors to determine the accuracy in positioning. Tatsuno et al. (2005) used a single-laser distance sensor for vehicle navigation experiments, in which the vehicle repeated stop-and-go driving, stopping every 1 m for a distance of 20 m. The calculated RMS localization error in stopping was about 6 mm in the traveling direction and about 12 mm in the transverse direction.

Because the tree canopy frequently blocks the satellite microwaves to the GPS receiver, laser-based sensors are widely applied in orchards. Tsubota et al. (2004) used ladar for navigating a small vehicle through an orchard. They found a guidance system using ladar was found to be more stable than using a GPS in a citrus orchard setting. Barawid et al. (2006) developed an automatic guidance system for navigating between tree rows. Their research used a 56-kW agricultural tractor, 2D laser scanner, RTK GPS and FOG. The results showed

an accuracy of 11 cm lateral error and 1.5° heading error. Subramanian et al. (2006) developed an autonomous guidance system for citrus grove navigation based on machine vision and laser radar. An average error of 2.8 cm using machine vision guidance and 2.5 cm using lidar guidance was observed during vehicle testing on a curved path at a speed of 3.1 m/s.

Tofael (2006) developed a complex autonomous tractor system with a laser rangefinder, RTK GPS and gyroscope. The results of field experiments using the laser rangefinder showed a lateral error of less than 2 cm and a heading error of less than 1°. The accuracy was very high.

1.2.2.5 Inertial sensors

Inertial sensors take measurements of the internal state of the vehicle. A major advantage of inertial sensors is that they are packaged and sealed from the environment, which makes them potentially robust under harsh environmental conditions. The most common types of inertial sensors are accelerometers and gyroscopes. Accelerometers measure acceleration relative to an inertial reference frame. This includes gravitational and rotational acceleration as well as linear acceleration. Gyroscopes measure the rate of rotation independent of the coordinate frame. They can also provide 3D position information and have the potential to detect wheel slippage. Unfortunately, these types of sensors are prone to positional drift (Barshan and Durrant-Whyte, 1993).

Inertial sensors have been used in a number of vehicle applications (SchÖnberg et al., 1996; Yu, et al., 1997; Nagasaka et al., 2004). The most common application of inertial sensors is in the use of a heading gyro (e.g. Imou et al., 1998; Ishida et al., 1998; Barawid, et al., 2007).

Inertial sensors are mostly used in combination with GPS or machine vision. Zhang and Reid (1999) presented an on-field navigation system with a vision sensor, FOG and RTK GPS. The results indicated that the multiple sensor based agricultural navigation system was capable of guiding a tractor between crop rows and showed that the inertial sensor was a good assistant function.

Noguchi et al. (2002) developed an agricultural navigation system consisting of an RTK GPS and an inertial measurement unit. Experiments conducted in a soybean field for tilling, planting, cultivating and spraying demonstrated that the accuracy of the vehicle surpassed that of skilled farmer operation. The lateral error of the guided vehicle was less than 5 cm.

1.2.2.6 Geomagnetic direction sensor

A geomagnetic direction sensor (GDS) is a magnetometer that senses the earth's magnetic field. It can be used as a heading sensor similar to an electronic compass (Reid, et al., 2000). The GDS is generally used to supplement other sensors.

Noguchi et al. (1997) used a GDS to provide heading information to a tillage robot. Benson et al. (1998) used GPS with GDS for vehicle guidance along straight directional lines. One limitation of GDS sensors is the influence of external electromagnetic interference from the outside environment, such as from a nearby set of high-tension electrical wires or the vehicle heater/air conditioner fan. However, by controlling these error sources, they were able to combine GDS with a medium-accuracy GPS system (20 cm) and track a straight line with an average error of less than 1 cm. The maximum overshoot for a 3-m step response was 12%, compared to 50% for GPS alone.

The feasibility of correlating GDS with sensor applications for agricultural guidance systems has been researched. Harper and Mckerrow (2001) used a frequency-modulated ultrasonic sensor to detect plants, setting up a plant database with a return signal containing information about the geometric structure of the plants to improve navigation. Yekutieli and Pegna (2002) used a sensing arm to detect plants in the path for guidance in a vineyard. However, using an arm would require that citrus groves be even with continuous canopy. There are also concerns about damaging the tree branches. Ultrasonic sensors are used for guidance in greenhouses, but they require that the target be perpendicular to the sensor for the ultrasonic waves to be reflected back properly (Subramanian et al., 2004). Dead reckoning is also widely used in combination with other sensors for autonomous vehicles (e.g. Subramanian et al., 2006; Morimoto, 2005).

1.2.3 COMPUTATIONAL METHODS

A computational method is mainly to detect image features by image processing or deal with sensor data fusion successfully for providing with basic information for agricultural vehicle autonomous guidance system. Therefore, the method choice and improvement is very important.

1.2.3.1 Hough transform

The Hough transform technique can be used to isolate the features of a particular shape within an image. The transform was originally concerned with the identification of lines in the image, but later it was extended to identifying the position of arbitrary shapes, most commonly circles or ellipses. The Hough transform as it is universally used today was developed in 1972 by Richard Duda and Peter Hart, who called it a "generalized Hough transform" after the related 1962 patent of Paul V.C. Hough. The main advantage of using a Hough transform is that it is quite robust even if a group of points varies to some extent, and seeking a straight line is still possible. The disadvantage is that in order to plot curves (i.e., sinusoids) for every observation point in Cartesian image space to $r-\theta$ in the polar Hough parameter space, the load of computational complexity is large. As most crops are cultivated in rows, there are a number of publications on deriving guidance signals from plant structures using the Hough transform (Marchant, 1997; Marchant, et al., 1995; Yu and Jain, 1997; Lee, et al., 2001; Åstrand, 2005; Leenmasn and Destain, 2006; Barawid, et al., 2007).

A stereovision based crop row detection method for tractor automated guidance (Kise et al., 2005) used a stereovision-based agricultural machinery guidance system. The algorithm consists of functions of stereo-image processing, elevation map creation and navigation point determination for crop row detection. The research also dealt with crop row detection for autonomous tractor guidance.

Åstrand et al. (2005) modeled a plant row using a rectangular box instead of a line. The width of the box is equal to the average width of the plants and the length of the box is "unlimited" as it fills the whole image. The rectangular box can be described by a set of parallel adjacent lines, which appear in the image as a set of lines that intersect at a virtual point outside the image, as shown Fig.1-5



Fig.1-5 Rectangular box substitute for a line (Åstrand, B.et al., 2005)

1.2.3.2 Kalman filter

The Kalman filter (Kalman, 1960) provides a sound theoretical framework for multi-sensor data fusion. The approach depends upon tracking the position of the vehicle or the state of the system at all times. Kalman filter models are often applied in GPS receivers to provide position estimates from raw GPS signals. In a highly dynamic system that has the potential for significant acceleration, it is necessary to integrate GPS with an Inertial Navigation System (INS) using Kalman filters. Literature on the integration of INS and/or other sensors with GPS is abundant (e.g., Bergeijk et al., 1998; Kubo et al., 1999; Madhukar et al., 1999; Abidine et al., 2002; Gan-Mor et al., 2002; Nagasaka et al., 2004; Nørremark et al., 2008). These integrated systems can improve the positioning accuracy, and more importantly, can provide reliable short-term positioning information if the GPS signal is lost.

Han et al. (2002) applied Kalman filtering to raw DGPS measurement data and effectively removed the DGPS noise and reduced the root-mean-squared (RMS) positioning error. The maximum cross-tracking error was reduced from 9.83 to 2.76 m and the root-mean-squared error was reduced from 0.58 to 0.56 m.

Hague and Tillett (2001) provided a method in which image processing was combined with a bandpass filter and extended Kalman filter. The method does not rely upon segmentation of the plant background to reduce the brightness or color influence. Results are shown in Fig.1-6.

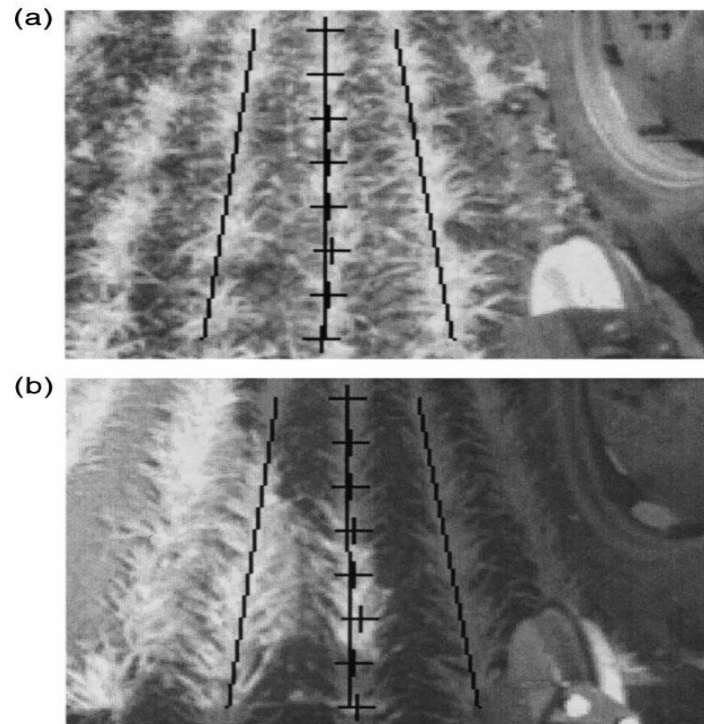


Fig.1-6 Row location: (a) uniform lighting conditions; (b) with deep shadows (Hague and Tillett, 2001)

A new sigma point Kalman filter was proposed and used to improve Kalman filter (Rudolph et al., 2005). Zhang et al. (2008) compared both of them through simulation and found the sigma point Kalman filter was more numerically robust and computationally efficient.

1.2.3.3 Other methods

Søgaard and Olsen (2003) proposed a method based on machine vision for detection and localization of crop rows distinguished by using the generalized Hough transformation method (as shown in Fig.1-7). The method divided the grayscale image into horizontal strips and computed the center of gravity, by vector, as a substitute for the segmentation step to reduce the computational burden on the image processing.

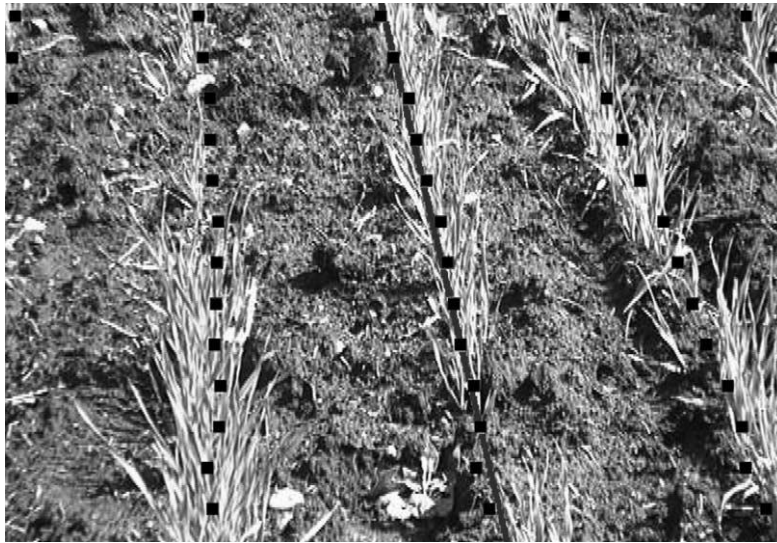


Fig.1-7 The middle line was guiding row line (Søgaard and Olsen, 2003)

Han et al. (2004) used three methods to obtain a guidance directrix, which applied a k -means clustering algorithm for row segmentation, a moment algorithm for row detection, and a cost function for guidance line selection. The soybean field results showed an average RMS offset error of 1.0 cm from 30 images. The corn field results showed an average RMS offset error of 2.4 cm from 15 images.

1.2.4 NAVIGATION PLANNING

Navigation planner plays an important role for agricultural vehicle autonomous control, which transforms the position deviation (heading, position or state) of the vehicle or device into the steering angle. Besides including tracking methods, the navigation planning must consider the sensor information and vehicle motion to guidance in the desirable course.

1.2.4.1 Tracking methods

Navigation planning uses four methods: position tracking, line tracking, map tracking and obstacle avoidance. Most guidance system operations follow some nominal trajectory or directrix line. The method usually uses local information including crop rows, swath edges, and tilled/untilled boundaries. However, if the tracking signal weakens or vanishes, the operation fails. Map tracking is often used in GPS systems, but it is a labor- and time-intensive method.

1.2.4.2 Vehicle motion models

(1) Dead reckoning

Dead reckoning is reliable for short-distance traveling (two positions) on a smooth concrete road. Since motion information is integrated in order to obtain the position of the vehicle, there is a risk of error accumulation leading to positional drift if the sensor produces even a slight bias. On agricultural vehicles, dead-reckoning sensors can be as simple as wheel encoders, which measure the rotation of the vehicle or equipment wheels. Freeland et al. (1992) experimented with a low-cost electronic compass used together with wheel encoders to provide dead-reckoning position information. Dead reckoning is widely used in combination with other sensors for autonomous vehicles. Nagasaka et al. (2004) and Kodagoda et al. (2002) used rotary encoders. Garacía-Pérez et al. (2008) used odometers and a proximity capacitive sensor.

(2) Kinematic model

Kinematic models are very simple and have been used by researchers to describe the lateral error relative to a nominal trajectory without taking into account vehicle dynamics (O'Connor et al., 1996; 2002; Benson et al., 1998; Noguchi et al., 2002; Zhang, et al., 2002). Some of the research showed very good accuracy of less than 5 cm not only on a straight line but also on a curved path as soon as the vehicle satisfied the pure rolling constraints. Unfortunately, pure rolling constraints are almost impossible to satisfy during agricultural tasks due to sliding, deformed tires or change in wheel-ground contact conditions, which degrade the performance and stability of automatic guidance. Some literature is related to improved kinematic models that can adapt to the sliding influence and promise guidance accuracy (e.g. Lenain, et al., 2005, 2006). The sliding effects have been taken into account for trajectory tracking control of agricultural vehicles and three variables characterizing the sliding effects were introduced into the kinematic model based on geometric and velocity constraints. An ideal refined kinematic model was obtained in which sliding effects appeared as additive unknown parameters using linearized approximation (Fang, et al., 2006).

(3) Dynamic model

Dynamic models are fairly complex for agricultural vehicle navigation, since describing all vehicle features (e.g., inertia, sliding, springing) leads to very large, intricate models. In particular, most of the parameter values (mass, wheel-ground contact conditions, tire and wheel deformation) are difficult to obtain even based on experimental identification. However, agricultural vehicle tasks involve mostly dynamic processing and researchers are interested in investigating this (Bevly, et al., 2002; Feng, et al., 2005; Bouton, et al., 2007).

(4) Sensor fusion

The principle of sensor fusion is to combine information from various sensing sources (e.g., GPS and machine vision, GPS and GDS) since an individual sensing technology cannot satisfy vehicle automation navigation operation for all models and all methods of use in different environments. The appropriate sensor will function at the appropriate field status during operation. Nevertheless, even under a given field operation, the availability of data from multiple sensors provides the opportunity for better data integration to provide superior results compared to those using an individual sensor. Sensor fusion technology is becoming increasingly popular for agricultural navigation (Benson et al., 1998; Noguchi et al., 2004; Han et al., 2004).

Zhang et al. (1999) developed an on-field navigation system using a vision sensor, FOG and RTK GPS. Fig.1-8 showed the comparison results. Garacía-Pérez et al. (2008) developed a hybrid agent for behavior architecture adapted to agricultural navigation. The farming vehicle was equipped with several positioning sensors (DGPS, digital compass and dead-reckoning system) and safety sensors (laser rangefinder, bumper, inclinometers, emergency stops) as well as an on-board processor, wireless communication system (WLAN) and electro hydraulic actuators. Sensor-fusion algorithms were proposed to overcome the absence of GPS signals so as to obtain continuous and precise positioning.

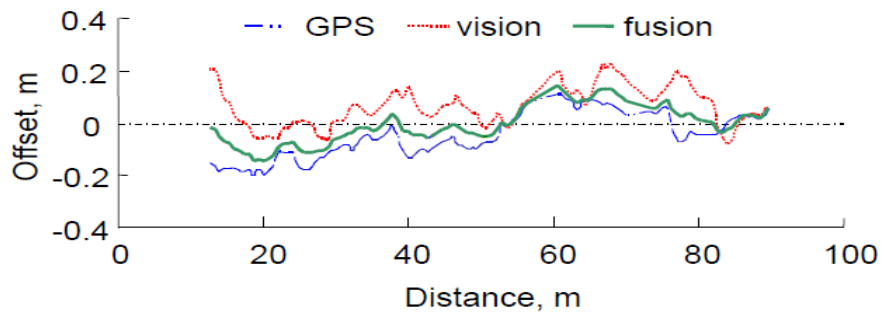


Fig.1-8 Comparison of navigation accuracy in vehicle offset from the desired path using sensor fusion, vision only, and GPS-FOG only based navigation controls (Zhang et al., 1999).

(5) Neural steer model

Noguchi and Terao (1997) designed a neural network (NN) vehicle controller in which the motion of the mobile agricultural robot was specified as a nonlinear system with high learning ability. This NN model was applied to navigation on an asphalt surface, with an accuracy of 0.08 m in the offset. Noguchi et al. (1997) used an NN model to correct the geomagnetic direction sensor for the inclination of the vehicle. A field test was conducted on a square path (40-m sides) in a meadow. The maximum directional angle error was 14° using the conventional method, but only 1° using the NN. Zhu et al. (2005) designed an NN vehicle model for estimating vehicle behavior on sloping terra. Bernoulli's lemniscate was employed to acquire training pairs. Genetic algorithms and back propagation algorithms were used to train the NN vehicle model. The tractor was successfully guided along a predetermined path with mean and standard lateral deviation of 5 mm and 6.7 cm, respectively. Ryerson and Zhang (2007) chose genetic algorithms to plan optimal path that guided vehicle to avoid known obstacles.

1.2.5 STEERING CONTROLLER

A good control system is necessary irrespective of the guidance sensor. The controller translates sensor position deviation signals into a voltage signal that is used to open a valve forcing the hydraulic ram in the steering circuit to change the steering angle of the front or rear axle, or, in the case of side shifting the equipment, an additional ram to adjust the position of the equipment relative to the tractor or the row of plants.

Agricultural vehicles often work on different types of terrain, even and uneven, or changing and unpredictable terrain ranging from asphalt to spongy topsoil in the field. In the case of automatic or autonomous navigation, steering controllers should be able to provide appropriate steering action in response to the variation in equipment operation state, traveling speed, tire cornering stiffness, ground conditions, and many other parameters influencing steering dynamics. Consequently, steering controller design for agricultural vehicles is a difficult challenge.

Most modern agricultural vehicles employ some form of hydraulic steering system, and recent developments in automatic steering controllers include advanced modifications to the existing hydraulic system considering vehicle dynamics, such as terrain conditions and vehicle status (speed and/or acceleration). Various steering controllers, including PID, feed-forward PID (FPID), and fuzzy logic (FL) controllers, have been developed and implemented in guidance systems (Qiu et al., 1999; Wu et al., 1999; Zhang, 1999). O'Connor et al. (1996) used a steering controller based on a set of linear motion equations. Inoue et al. (1997) developed an adaptive steering controller that corrects steering system delay. Cho and Lee (2000) used a fuzzy controller for an autonomous operation of an orchard speed sprayer. Kise et al. (2002) developed an optimal steering controller and obtained good curved-path guidance results. Zhang et al. (2002) put forward a kinematic model in which the steering linkage geometry provided the gain between the hydraulic actuator and the front wheels. The system model was used to close the steering control loop based on the feedback signal from the hydraulic steering actuator rather than from the front wheels. Lenain et al. (2006) considered agricultural vehicle sliding and pseudo-sliding on slippery ground and used predictive model control to preserve accuracy.

An actuator, combined with the vehicle status, was used to convert the control signal from a feedback controller to the appropriate mechanical adjustment in steering angle to provide the position of the vehicle.

1.3 DISCUSSION

Since the time when the first 'driverless tractor' prototype was created 50 years ago (Morgan, 1958), research into automatic guidance has steadily progressed, particularly in the case of guidance system technologies, which have improved remarkably in the last two decades. However, with the exception of GPS receivers, vision sensors, laser rangefinders, gyroscopes and GDS, the commercialization of prototype agricultural guidance systems is very low. Various reasons are behind the absence of funds for developing these prototypes into commercial products. Some cases have fallen into disuse as society has developed. For example, new technology or production causes the prototype market to devalue, and performance standards for environmental protection and implementing tractors are changing. Nevertheless, some general conclusions can be drawn regarding the failure of many prototype 'service robots' to reach commercial viability.

The environmental and performance requirements for agricultural vehicle guidance operation are extremely strict (section 1.2). In addition to this barrier (a more difficult consideration than other guidance applications), there are other barriers that have not yet been resolved from many years ago. Hague et al. (2000) concluded that dead-reckoning sensors lead to the accumulation of errors resulting in positional drift; laser or radar and image based artificial landmark positioning systems are a direct function of positioning, and not prone to accumulating drift errors, but the beacons take time to set up and may result in ambiguous and unreliable results due to false detection and failure to detect obscured beacons. The popular machine vision and GPS also have their respective advantages and disadvantages. Machine vision is an inexpensive and passive sensor, which has some excellent computer algorithms to support and advance successful research (Subramanian, et al., 2006; Han, et al., 2004). However, it also has difficulty dealing with changing light conditions, shadows, direct sunlight and other difficulties with extracting guidelines from the images captured in the working environment. Although most problems can be solved with electronic shutters, automatic diaphragms, color differences and the right position and adjustment of the camera, a row of plants or a furrow is needed to guide the vehicle using image processing, and tasks such as spraying or fertilizing uncultivated fields need another

strategy. GPS is different than machine vision, as it is not affected by environmental variations, and real-time kinematic (RTK) GPS can provide better accuracy. Nevertheless, GPS sensor accuracy depends on the position of the satellites. In urban environments, especially in narrow streets (urban canyons), buildings can shield the microwaves from satellites. Moreover, a system using GPS for guidance requires that a predetermined path be given for the vehicle to follow. Secondly, a kinematic GPS is very expensive. GPS guidance systems pose a problem in terms of positioning the antenna on the roof of the agricultural vehicle with the equipment working at the ground level. This means that on sloping ground and with changing soil conditions, deviations can occur between the virtual guideline and the path described by the equipment. Solving this problem requires attitude measurement.

With the advent of computer vision and GPS and their declining prices, it seems inevitable that these two technologies will be 'fused' together or one of them will be 'fused' with another technology, such as gyroscope (Morimoto, 2005; Nagasaka, et al., 2004), GDC (Benson et al., 1998), or laser radar (Subramanian, et al., 2006) to realize autonomous vehicles in agriculture, allowing real-time image processing with a digital controller on a simple PC, precision positioning with an RTK DGPS system or heading computation with a traditional gyroscope.

However, if the guidance system for agriculture is commercialized, the following product research will be needed as single technologies mature. An integrated consideration may be better.

(1) Evaluation of economic feasibility. Electronics, computers, sensors and attachments are declining in price, mostly because high commercial demand enabled their manufacture at great economies of scale; however, the cost of designing and producing the special-purpose parts for agricultural guidance systems will increase markedly. An evaluation of economic feasibility is necessary to determine the market value and understand the difference compared with old conventional systems.

(2) Improvement of robustness in versatility and dependability of mechanical technology. The agricultural machine operates in a harsher environment (often in paddy fields), but its seasonality is stronger than other machines for harvesting, sowing and spraying and the

operating seasons are usually pivotally related to benefit the farmers. Hence, such machines should be sufficiently robust to work effectively under varying conditions. Today's technologies have not always proven capable of delivering this performance.

(3) Addition of safety to avoid the risk of damage resulting from the use of such machines.

(4) Provision of service system. A sophisticated machine that is broken cannot do a better job than a primitive machine. As machines become more complicated, the skills required for their operation and maintenance increase in proportion. For agricultural application, the service system will be more important than in a factory environment, because there are very few, if any, technicians who will have the expertise or equipment for repairs and maintenance.

With the emergence of new technologies in the industry, research into their application to agricultural vehicle guidance systems will contribute to the realization of autonomous agricultural vehicles or robots in the future. For example, omnidirectional vision sensors (Ayako et al., 2006) have become increasingly attractive for autonomous navigation systems. The camera and mirror are mounted at the top of the mobile robot's platform. Images captured by the sensor are an orthographic projection of the ground plane. The images (obtained without rotating the robot) are a 360° view of the environment and therefore are not sensitive to wheel slippage or small vibrations. This low-cost sensing device provides enough information for our navigation system. Although it is not easy to obtain distance estimations from an omnidirectional image due to the shape of the mirror, the apparent angles of objects around the robot are relatively accurate and easy to derive from the image (Imou et al., 2008). We proposed this system as a potential substitute for the GPS function for localization using landmarks in the working environment.

1.4 CONCLUSIONS

This chapter provided a brief review of the research on guidance system technologies in agricultural vehicles over the past 20 years. Although the research developments are abundant, there are some shortcomings (e.g., low robustness of versatility and dependability of technologies) that are delaying the improvements required for commercialization of the guidance systems. We can conclude that either GPS and machine vision technologies will be

'fused' together or one of them will be 'fused' with another technology (e.g., laser radar) as the trend development for agricultural vehicle guidance systems. The application of new popular robotic technologies for agricultural guidance systems will augment the realization of agricultural vehicle automation in the future.

2 PROBLEM DESCRIPTION, OBJECTIVES AND OUTLINE

2.1 PROBLEM DESCRIPTION

This dissertation gives a partial solution to a problem that can be considered at three factors. First, the farming labor force is dwindling that is a common problem in the world. We also can recognize that this problem is a social complicated problem. It can be solved only by taking a set of integrated measures such as increasing production efficiency, decreasing labor intensity, improving labor condition and increasing labor incoming to absorb laborers and increasing laborer numbers. Automation guidance systems for agricultural vehicles can be regarded as one promising alternative to help solve the problem and satisfies with the precision agriculture. GPS has been as a better alternative technology to implement automation guidance systems. In section 2.1.2, there are three sub-problems to restrict developing in agricultural vehicle. Third, as stated in the Chapter 1, until today for already 50 years since the first 'driverless tractor' prototype was created (Morgan, 1958), however, except GPS, vision sensors, laser ranger, gyroscope, GDS and some sensors, there are some prototype in the laboratory, the commercialization about agricultural guidance systems is very lower really.

2.1.1 DWINDLING IN NUMBERS OF FARMING LABOR FORCE AND PRECISION AGRICULTURE NECESSARY

Usually, with the development of industry in any country, the farming labor force is dwindling less and less because the farming is not better job comparatively. This results in that the elder and women are occupying the large-scale of farming labor force. This is a common problem in the world. Just there being the problem, the agricultural vehicle manipulation should become more safety and simpler. Automation is an effective measurement to solve the problem. Additionally, the less farming labor force must complete the more farming work. Automation is one way to improve production rate and solve the problem. Precision agriculture also needs agricultural vehicle automation as one of first

requirements. Autonomous navigation is the precondition of agricultural vehicle automation. Therefore, the development of autonomous navigation systems for agricultural vehicles is regarded as an important advance in precision agriculture and a promising alternative to the dwindling farming labor force, in addition to satisfying the quest for higher production efficiency and safe operation (Murakami et al., 2006).

Problem 1: the less farming labor force and precision agriculture cause the necessary development of autonomous navigation for agricultural vehicle.

2.1.2 LIMITATIONS OF GPS FOR AGRICULTURAL VEHICLE NAVIGATION

In previous studies of navigation systems for agricultural vehicles, the most popular method has been GPS (Nagasaka et al, 2008). Differential GPS can provide accuracy within 50 cm, and real-time kinematic (RTK) GPS can deliver centimeter accuracy consistent with guidance applications. Nevertheless, this sensor also has three limitations. First, its accuracy depends on the position of the satellites. In rural environments, especially in valley, hills or trees can obscure the microwave beams from satellites, resulting in a considerable drop in accuracy. To overcome this problem, the GPS sensor must be fused with other sensors, such as dead-reckoning sensors and machine vision sensors. Second, kinematic GPS for agricultural application is very expensive.

Problem 2: Limitations of GPS for agricultural vehicle causes the necessary of developing a more effective agricultural vehicle autonomous navigation as a compensation or substitution for GPS.

2.1.3 SHORTCOMINGS OF GUIDANCE SYSTEM PROTOTYPE IN THE LABORATORY

As stated in the introduction, since the first 'driverless tractor' prototype was created (Morgan, 1958), a long history of research into automatic guidance has been progressed, and especially, a number of guidance system technologies have developed improvement in recent two decades as above. Except GPS, although there are some guidance system prototypes in the research laboratory, the commercialization about them is lower. The general conclusions can be drawn regarding the failure of many prototype 'service robots' to reach commercial viability to date.

The discussion gets that different prototypes in the laboratory using guidance technologies are some shortcomings to retard commercialization in Chapter 1.3 GPS and machine vision will 'fuse' together or one of them will be 'fused' with another technologies will be the trend development for agricultural vehicle guidance system. Application of new popular robotic technologies for agricultural guidance system will be an augments for realize agricultural vehicle guidance system in future.

Problem 3: Shortcomings of guidance system prototypes in the laboratory calls up us to apply popular robotic technologies and fuse with the advantages of GPS and (or) machine vision for the future agricultural vehicle guidance system.

2.2 STATUS QUO ANALYSIS

As stated in the Chapter 1, the hottest topics of researching on agricultural vehicle guidance system are machine vision and GPS. They have their advantages and disadvantages, respectively.

Machine vision is a relative position and heading sensor with the image sensor mounted on the vehicle. One of the most commonly used machine vision methods is for detecting a guidance directrix on row crops, soil tillage, and the edges along harvested crops.

GPS-based navigation systems are the only navigation technologies that have become commercially available for navigation of agricultural vehicles. GPS guidance systems provide an absolute guidance system based on GPS base station on the ground and require that a GPS base station is located within approximately 10 km of the RTK GPS guided tractor.

Machine vision is cheaper and passive sensor, which has some excellent computer algorithm to support and matured success researches (Subramanian, et al., 2006; Han, et al., 2004). But it also has difficult to deal with changing light conditions, shadows, direct sunlight and other difficulties with extracting guidelines from images captured in the working environment. Although most problems can be solved with electronic shutters, automatic diaphragm, color differences and the right position and adjustment of the camera, a row of plants or a furrow is needed to guide a vehicle with image processing, tasks like spraying or fertilizing on uncultivated fields need another strategy. GPS is different with machine vision,

which is not affected by environment varying and Real-Time Kinematic (RTK) GPS can provide with better accuracy. Since they don't depend upon the visual appearance of the crop, they are not adversely affected by weed density, shadows, missing plants or other conditions that degrade the performance of machine vision guidance systems. Another advantage of GPS guidance systems is that they can be easily programmed to follow curved rows (Slaughter et al., 2008). However, GPS has some limitations for agricultural vehicle application.

The best solution on technology is a guidance system fusing with the technologies of GPS and machine vision.

Localization is a fundamental problem in mobile robotics or autonomous vehicle navigation. **Most autonomous vehicles must be able to locate themselves in their environment as a prerequisite to implementing their tasks.** A great deal of work has recently been disclosed on the topic of autonomous robot navigation in various work areas using different sensors and methods (Duckett and Nehmzow, 1998; Menegatti et al., 2004; Cobano et al., 2008; Subramanian et al., 2006). Localization methods can be classified as geometric localization and topological localization. Geometric localization tries to estimate the position of the robot as accurately as possible, while topological localization needs a topological mapping and gives a more abstract position estimate. GPS is a typical geometric localization. For agricultural vehicle working environments, the guidance lines are changing frequency with the different crops are planting in different seasons. The variety crops express variety colors and different planting methods, **the topological mapping is impossible to make it in practice easily and effectively.**

Recently, omnidirectional vision sensors are very attractive for autonomous navigation system. An omnidirectional vision sensor is cheap and simply composed of a digital camera aiming at a catadioptric mirror (Aihara et al, 1998; Winters and Santos-Victor, 1999). The camera and the mirror are mounted on the top of the mobile robot's platform. The images grabbed from the sensor are orthographic projections of the ground plane. The images (obtained without rotating the robot) are 360° view of the environment and therefore are not sensitive to wheel slippage and small vibrations. This low cost sensing device provides

enough information for our navigation system. **Although it is not straightforward to obtain distance estimations from an omnidirectional image due to shape of the mirror, the apparent angles of objects from the robot are relatively accurate and easy to derive from the image.**

There are many approaches about localization based on omnidirectional vision sensors in robot. The key advantage of these approaches is that the robot has a panoramic view of its environment, which makes it possible to create features that are invariant to the robot's orientation. Iwasa et al. (2003) proposed a memory-based self-localization method. Tamimi et al. (2006) improved the Scale Invariant Features Transform and applied Particle Filter to localize mobile robot. Spacek and Burbridge (2007) researched localization by trilateration. Marques and Lima (2001) detected field lines using the Hough transform and correlated them with the field model to estimate the robot position. Motomura et al. (2003) localized their robots using dead-reckoning and angle measurements between two landmarks. Briggs et al (2000) used self-similar gray pattern landmarks to navigation and localization aids. Jang et al (2002) presented a simple artificial landmark model and a tracking algorithm for indoor mobile robots. However, there have been few studies on agriculture and the application of the apparent angles of objects from the robot being relatively accurate and easy to derive from the image. We utilize the omnidirectional vision sensor to provide the panoramic view of landmarks around the camera and relatively accurate and easy to estimate the directional angles of landmarks via image processing, and then calculate the position of the camera based on the directional angles of landmarks. The agricultural working areas generally do not change; landmarks can be easily set up around the corners of a field and be taken as a stationary environment. The crops are always at the same places and colored landmarks can be easily distinguished from the environments. Compared with common vision method, this method is not limited to straightaway farming tasks. Compared with dead-reckoning method, this method does not accumulate errors. This method is a different new method to augment GPS based solutions or substitute for GPS to localize agricultural vehicle.

2.3 OBJECTIVES

This research develops a simple localization system using a low-cost omnidirectional camera and four artificial landmarks (named as OLS) for the following three objectives (as shown in Table 2-1).

Table 2-1 Objectives and application property

Objective	Function	Application area	Accuracy requirement (cm)	Application mode	Vehicle operation mode
1	Compensation GPS for navigation	The accuracy of GPS is worse, e.g. in the valley	50	GPS+OLS	Automatic
2	Automatic navigation	Forage production operation	50	Only OLS	Automatic
3	Localization	Precision agriculture, e.g. fertilization and spraying	100	Only OLS	Manual acting

First, in order to make advance of autonomous navigation for agricultural vehicle and develop a simple localization system to compensate for GPS that can use in the places where hills or trees obscure the microwave beams from satellites, resulting in a considerable drop in accuracy.

Second, the operations of forage production, for example harvesting, seeding, fertilization, tedding and transportation, high-speed working is required rather than accurate positioning by autonomous tractor for saving laboring because of the workload in broad area and sometimes the bad weather (Nishimura et al. 1996; Ishida et al. 1998). The location accuracy is feasible on about 50 cm. Besides, it is very difficult to control the position of agricultural vehicle and implement operations smoothly in forage production because there is no obvious objects for the localization of vehicle on the grassland even the operation worked by man. Therefore, it is necessary to develop a localization system for autonomous tractor in the forage production.

Third, the localization will apply for precision agriculture. In precision farming, there are tasks that are necessary to know the position of working in detail. One example is field mapping. In the process of making map in the field, when we use sensors to measure soil properties and crop production status, it is also necessary to know the real time position of the measurement spot to create database. And when the variable operation is done based on the

field mapping, the operation also needs to know its position firstly, and then executes its job (e.g. fertilizing or spraying medicine) appropriately according with the information of map. For the precision agriculture, the localization is necessary by a simple tool but the accuracy does not require too much and the location accuracy is feasible below 100 cm.

The proposed localization system will use machine vision to extract local information to detect the landmarks and utilize the omnidirectional vision image to calculate absolute position relative to the landmark-based coordinate system on the ground similar to substitute for the function of GPS by geometrical localization. Especially, the system would work indoor and outdoor environments although depending on building artificial landmarks by man to waste some time. And more, the system would have the function avoiding obstacles. The agricultural vehicles with the system would possibly carry out navigation by their “eyes” entirely like mammal move in the world.

In the dissertation, a new localization system for agricultural vehicle navigation with its program software will be developed successfully. The system will be cheaper than GPS, simply and effective application in practice. The system mainly adopts the advantages of omnidirectional vision system and artificial landmarks. Four landmarks will be set on the corners of a rectangular around a working area. In order to make the crops environments to be easily detected as an image spot, the artificial landmark model and its algorithm will be considered. Because the application area of agricultural field is general broader, but the omnidirectional vision should take the landmark to extract the landmark features in the image to go forward the next step for localization, the landmark size in the image will become smaller. The relationship between landmark specific size and landmark image size will be grasped. The localization algorithm program software will be the most important task to be developed to realize the localization system. The computational burden of the algorithms will be limited and running speed should be faster, at least ten images must be processed every second to allow stable control at high operational speed in future. The software should include four landmarks, three landmarks and even two landmarks computational program, also include the smoothness program to eliminate the image noise. We will use it to calculate results and analyze the process of calculating perfectly. As a common vision system, it is

necessary to calibrate intrinsic and extrinsic parameters to adjust the imaging distortion. For the localization system, the calibration will be considered and we obtain the parameters. However, the omnidirectional vision is consisted of hyperbolic mirror and orthographic camera. Besides dealing with the camera calibration, because the mirror rotational axis and camera optical axis maybe be misalign, which causes distortion will be considered. The popular calibration pattern will be planned to use. If the agricultural vehicle guides him completely by himself, the road navigation in the field should be considered. A road localization system will be developed. An experimental test procedure will be proposed to evaluate the performance of localization system.

2.4 OUTLINE

In the remainder of the dissertation, first, introduces the localization system generally. Then studies the algorithms to realize the localization function and calibrate the omnidirectional vision system. Next, about the landmark imaging is analyzed. The field localization experiments are done to prove the localization system feasibility. In order to enlarge the application, we develop it to use for field road localization and also create its algorithm and do experiments to test it. The last chapter, general conclusions are drawn and future works are considered.

Chapter 3 introduces the localization system architecture and features. Section 3.1 concludes previous studies on outdoor and indoor localization systems. Section 3.2 discusses the principle of localization in landmark-based methods. Section 3.3 explains the architecture of our system and in section 3.4, features of the system is discussed. Finally, we present conclusions.

Chapter 4 is about the important algorithms. Section 4.1 generally summarizes algorithms of landmark tracking extraction, position estimation and smoothness for eliminating image noise. Section 4.2 introduces our proposed algorithms and calculation methods in detail. Section 4.3 presents the results of program running. Finally, a simple analysis of the performance and robustness of the program and our conclusions are drawn.

Chapter 5 develops a fast and practical method for calibration of omnidirectional vision system. Section 5.1 reviews on the central catadioptric camera calibration. Two requirements of calibrating for our system are analyzed in section 5.2. The calibration method includes section 5.3 catadioptric camera projection model and section 5.4 calibration algorithms. Section 5.5 introduces the experimental results to prove the calibration. Section 5.6 summarizes.

Chapter 6 is about landmark imaging influence analysis. Section 6.2 discusses the existed two key problems in our study. In section 6.3, theoretical analysis of the necessary to balance camera height and landmark height to enlarge application area has done. In section 6.4, experimental results of our proposed landmark model and application area are described. Finally, we conclude the work.

Chapter 7 is the evaluation of the localization system by experiments. The experimental devices and scenes are introduced in section 7.1. Indoor experiment, outdoor experiment and camera tilt experiment are introduced in section 7.2, section 7.3 and section 7.4, respectively. Section 7.5 concludes the experimental results and discusses.

Chapter 8 proposes to use two simple artificial landmarks and utilize omnidirectional vision to realize self-localization for agricultural vehicle field road navigation. Section 8.2 describes the artificial landmark model and tracking algorithm simply. In section 8.3, we confirm the distance computation model and algorithm for position estimation. Section 8.4 presents the experimental results. Finally, our conclusions are drawn and future works are considered.

Chapter 9 is the general conclusions and future work.

3 FIELD LOCALIZATION SYSTEM ARCHITECTURE AND FEATURE

The development of autonomous navigation systems for agricultural vehicles is an important endeavor. We propose a localization system based on artificial landmarks and omnidirectional vision for agricultural vehicle navigation in both indoor and outdoor environments, and we also propose a landmark model. The system consists of four artificial landmarks, an omnidirectional vision sensor, PC and operating vehicle. The system sets four red artificial landmarks as a rectangle in the corners of an operating spot and estimates an absolute position similar to GPS. Based on our analysis of system features, we conclude that agricultural vehicles equipped with our system will likely carry out navigation using their “eyes” in the same way that mammals move around in the world.

3.1 INTRODUCTION

Previous studies on navigation systems for agricultural vehicles in field applied various methods such as radar positioning (Subramanian et al., 2006), laser positioning (Matsuo et al., 1997), ultrasound Doppler sensor (Imou et al., 2001a, 2001b) and machine vision (Marchant et al., 1995), with the most popular method being GPS (Nagasaka et al., 2008). However, those sensors also have some limitations. Machine vision is cheaper and passive sensor, which has some excellent computer algorithm to support and matured success researches (Han, et al., 2004) and GPS-based navigation systems are the only navigation technologies that have become commercially available for navigation of agricultural vehicles. The position information from GPS can be used for both guidance and other applications such as seed mapping, traffic control, and tillage control. GPS is different with machine vision, which provides an absolute guidance system based on GPS base station on the ground and is not affected by environment varying. Real-Time Kinematic (RTK) GPS can provide with better accuracy. Since they don't depend upon the visual appearance of the crop, they are not

adversely affected by weed density, shadows, missing plants or other conditions that degrade the performance of machine vision guidance systems. Another advantage of GPS guidance systems is that they can be easily programmed to follow curved rows (Slaughter et al., 2008). However, GPS has some obvious limitations for agricultural vehicle (as stated in 2.1.2).

In investigating indoor localization for autonomous navigation, a variety of sensors have been used, including vision (Mehta et al., 2008), ultrasonic (Lawitzky et al., 1995), wireless Ethernet (Ladd et al., 2004), radio-frequency (Gezici et al., 2005) and GSM-based (Otason et al., 2005) sensors. To the best of our knowledge, a method similar to GPS that can be used for robot localization indoors has not been developed until now.

Localization of agricultural vehicles is very different from common indoor and outdoor navigation. The agricultural environments offer an unstable (ground soil materials and structure are different) and unconstrained (weather changing) conditions. This inspires us to use the advantage of GPS which provides an absolute guidance system based on GPS base station on the ground and is not affected by environment varying. Omnidirectional vision sensors are very attractive for autonomous navigation system with their cheaper price, panoramic view and easily obtain directional angle of objects around camera. Inspired by the two ideas, we developed a localization system for agricultural vehicle navigation which uses omnidirectional vision to extract local information to detect the landmarks and utilize the omnidirectional vision image to calculate absolute position based on landmarks coordinate system similar to substitute for the function of GPS by geometrical localization.

Section 3.2 discusses the principle of localization in landmark-based methods. Section 3.3 explains the architecture of system and in section 3.4, features of the system is discussed. Finally, we present our conclusions on this chapter.

3.2 LANDMARKS BASED METHODS PRINCIPLE

Localization methods can be classified as geometric localization and topological localization. Geometric localization attempts to estimate the position of the robot as accurately as possible, e.g., by calculating a pose estimate (x, y, θ) , while topological localization gives a more abstract position estimate, e.g., "I'm in the coffee room". We use geometric localization

based on landmark detection. Landmarks are divided into two kinds: natural and artificial. Natural landmarks must be easily detected from the image signal and be locally characterized to distinguish them from other objects. Methods using natural landmarks employ a more general approach compared to those using artificial landmarks. Natural landmarks are chosen in consideration of their particular characteristics in the image. However, extraction of natural landmarks is a difficult task. Artificial landmarks are simple and powerful self-localization aids that can provide very accurate and robust performance even in complex environments. Generally, more than three landmarks are used to compute the bearing or metric distance to achieve localization (Briechle and Hanebeck, 2004; Shimshoni, 2002).

Landmarks can be geometric shapes (e.g., rectangles, lines, circles) and they may include additional information (e.g., in the form of bar codes). In general, landmarks have a fixed known position, relative to which a system can localize itself. The input data for position estimation in landmark-based systems may be of a range or bearing type, which leads to two different techniques, trilateration and triangulation. Trilateration is the determination of a robot's position based on distance measurement to known landmarks, whereas triangulation uses the bearing to different landmarks in the environment (Borenstein et al., 1996).

Fig. 3-1 (a) shows the case of identifying a landmark, I_1 , and measuring the distance, r_1 . This constrains the position to a circle. Similarly, if two landmarks, I_1 and I_2 , are detected at the same time at measured distance r_1 and r_2 , the position will be determined as the intersection of two circles, I_1 or I_2 , as shown in Fig. 3-1 (b).

Fig. 3-2 (a) illustrates another case in which the system measures the angle, θ_1 , between two landmarks, I_1 and I_2 . According to the angle θ_1 , two circular arcs, C_1 and C_2 , are drawn and the position will be on circular arc C_1 or C_2 (Sutherland and Thompson, 1993; Abdul and Robert, 2006). In this case, there are an infinite number of possible positions and the system must detect a third landmark point. Fig. 3-2 (b) illustrates the system identifying three landmarks and the position is on intersection I_1 or I_2 or I_3 . If using four landmarks, as shown in Fig. 3-2 (c), four circular arcs are obtained and the position will be on intersection I_1 or I_2 or I_3 or I_4 based on the principle of one intersection formed by two circular arcs. If there is no error, the four intersections should converge at the same point.

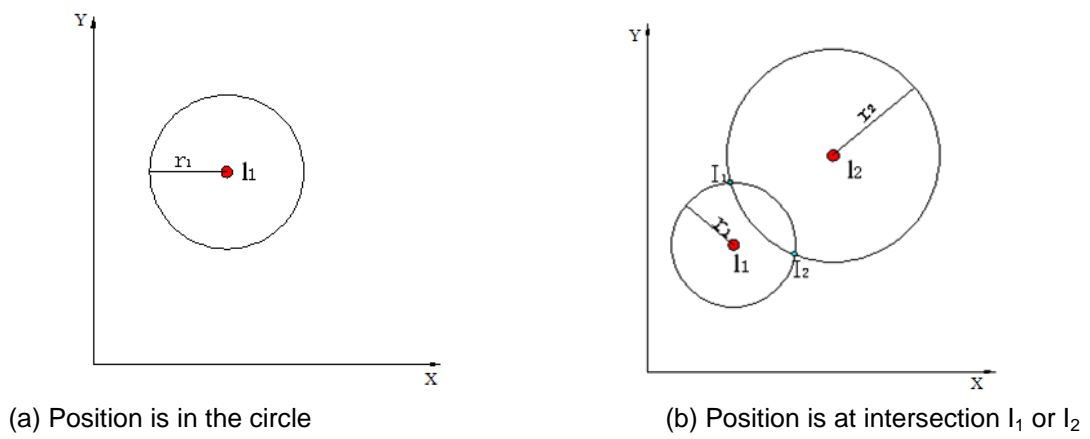


Fig. 3-1 Position constrained by landmarks and distances

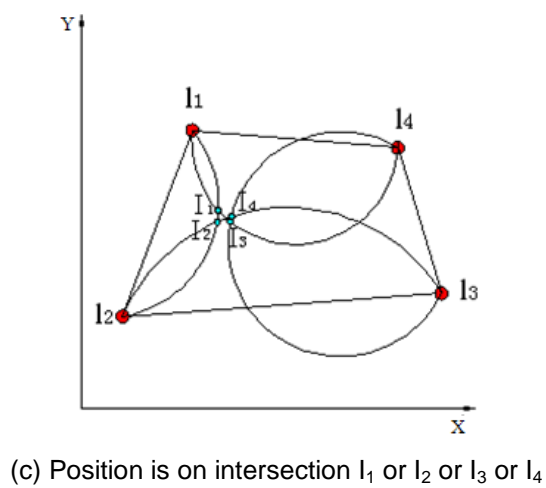
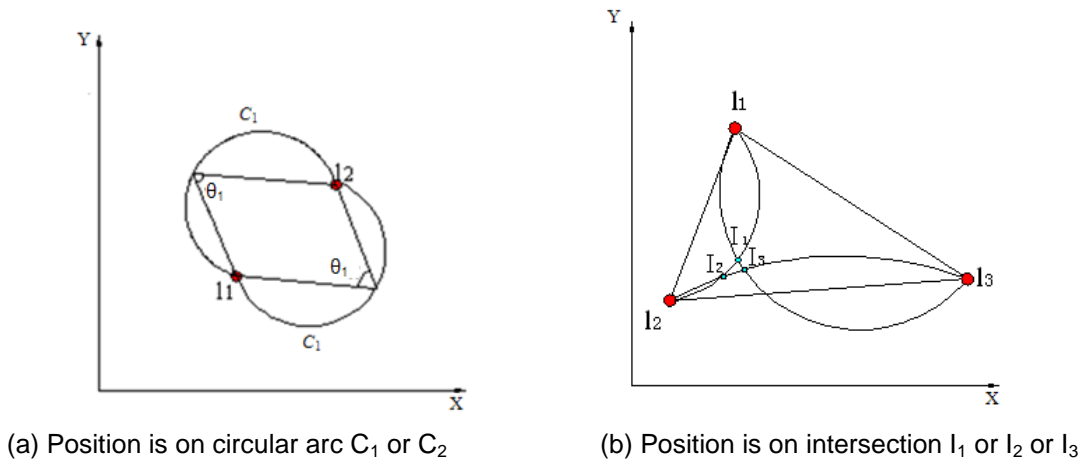


Fig. 3-2 Position constrained by landmarks and angles

Landmark methods will result in perfect localization in a flat field if there is no measurement error. However, measurements are never perfect and errors in distance or angle estimation vary significantly (Makadia and Daniilidis, 2003). In addition to measurement errors, there could be an error in landmark identification or matching with the world map using image processing. For identification errors, some landmarks may not be detected, and some spurious landmarks may be detected. Hence, it is necessary to consider landmark properties and ensure that the sensor can capture the features of the landmarks and collect sufficient landmarks to achieve a satisfactory estimation of the position. Our system uses artificial landmarks to reduce problems and errors, and applies the principle as shown in Fig. 3-2 (c), as well as the principle shown in Fig. 3-2 (b) if the camera only finds three landmarks in a particular environment.

3.3 ARCHITECTURE OF SYSTEM

3.3.1 SYSTEM ARCHITECTURE

The proposed localization system architecture is shown in Fig. 3-3. The system is built with an omnidirectional vision sensor, image processor, four landmarks, and PC and operating vehicle. We set four landmarks, one on each corner, to form a rectangle inside a greenhouse or outside in a field. In a case where the shape is erratic, such as the field shown in Fig. 3-3, the landmarks were set on four corners to create a rectangle on the field by plotting the dimensions beforehand. The omnidirectional vision sensor installed on the vehicle collects information on the four landmarks, and the PC software calculates the absolute camera position. In the process of calculating the camera position, firstly, the landmark position is detected from the image and the directional angles between landmarks are obtained. Then, the program can estimate the absolute position relative to the landmark-based coordinate system on the ground through the geometric relationship.

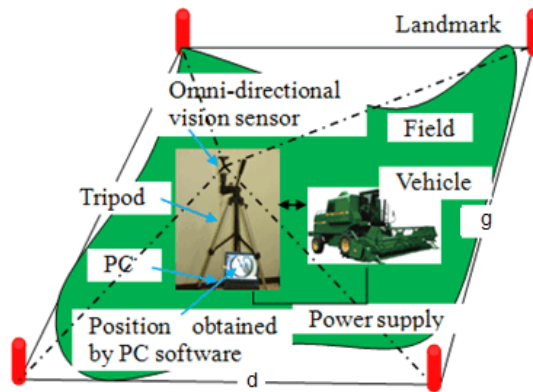


Fig. 3-3 System architecture

Fig. 3-4 shows a diagram of signal processing in the system. The algorithm mainly includes features extraction, noise elimination and position estimation. In this process, we utilized the low-pass filter to eliminate the omnidirectional images noise at first; then the red pixels intensity were calculated and red pixels were extracted as a small area; the center of gravity was calculated for the extracted small area representing the position of one landmark; when the process detected the positions of all the landmarks in the image, the directional angles of landmarks based on the principal point of camera were obtained. At last, the camera position was estimated using the center of gravity of the four intersections formed by four arcs according to the geometric transformation based on the directional angles of landmarks.

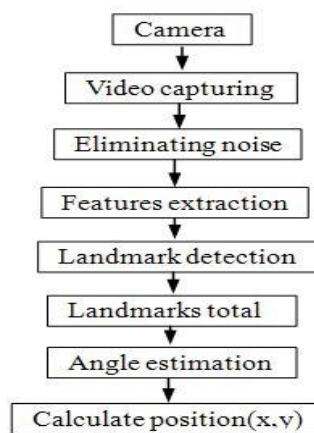


Fig. 3-4 Signal processing diagram

The system combines colored artificial landmarks with an angulation method that utilizes the advantages of omnidirectional vision to define the camera position based on landmarks easily constructed around the working field. The computational program and process is simple. And the omnidirectional camera is low-cost. On the whole, the method is low-cost and simple.

3.3.2 OMNIDIRECTIONAL VISION SYSTEM

As shown in Fig. 3-5, an omnidirectional image is a 360° projection of the world on a single image plane, and can be obtained with different catadioptric vision systems. Catadioptric systems are simple and compact. They combine a camera and a convex mirror. A desirable property of these systems is the single viewpoint that easily allows the transformation of omnidirectional images to perspective images. This property is present in the combination of an orthographic camera and parabolic mirror or a conventional camera and hyperbolic mirror. The latter system, shown in Fig. 3-6, was selected for this study. We used an integrated-type omnidirectional camera (Vstone, VS-C-300-TK), with resolution reaching 2048(H) ×1536(V), frame rate 2048×1536 (6 fps) / 640×480 (20 fps), ½-inch color image sensor connected with USB 2.0 and image format RGB24. Although it is not straightforward to obtain distance estimations from an omnidirectional image due to shape of the mirror, the apparent angles of objects from the robot are relatively accurate and easy to derive from the image (Imou et al., 2008; Li et al., 2009).



Fig. 3-5 Panoramic view



Fig. 3-6 Omnidirectional vision system structure

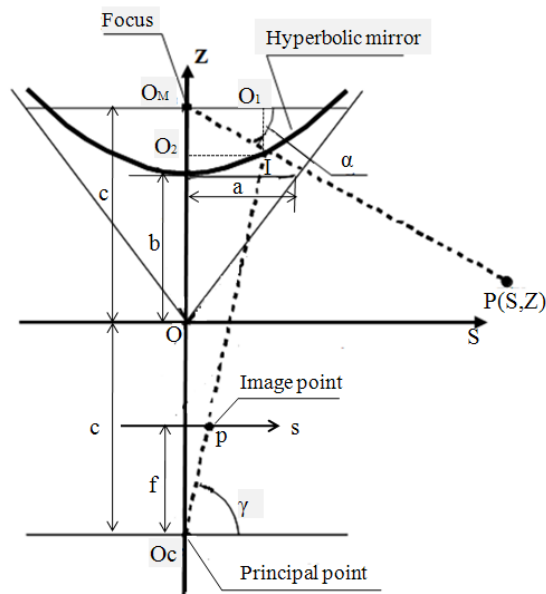


Fig. 3-7 Omnidirectional vision system cross section and its point imaging

The omnidirectional image is symmetrical in all directions. Fig. 3-7 shows a cross section of the omnidirectional vision system (S, Z) , where the plane $S = \sqrt{X^2 + Y^2}$, and a, b and c are the structural parameters for the hyperbolic mirror surface. $c = \sqrt{a^2 + b^2}$. $O_M(0, +c)$ is the focus of the hyperbolic mirror and $O_C(0, -c)$ is the principal point of the camera lens. A

hyperbolic curve is expressed by $\frac{S^2}{a^2} - \frac{Z^2}{b^2} = -1$ ($Z > 0$), thus, the hyperbolic mirror is expressed

by the following equation:

$$\frac{X^2 + Y^2}{a^2} - \frac{Z^2}{b^2} = -1 \quad (Z > 0) \quad (3-1)$$

The image plane $s = \sqrt{x^2 + y^2}$ is parallel to the coordinate system S plane. P(S, Z) is a random point in space and p is the image point of P in the image plane s. We can obtain the following correlations:

$$Z = S \tan \alpha + c = \sqrt{X^2 + Y^2} \tan \alpha + c \quad (3-2)$$

$$\gamma = \tan^{-1} \frac{f}{s} = \tan^{-1} \frac{f}{\sqrt{x^2 + y^2}} \quad (3-3)$$

Here, f is the focus of the camera, and α and γ are geometrical angles as defined in Fig. 3-7.

According to Eqs. (3-2) and (3-3) and the trigonometric relationship between $\Delta O_c I O_2$ and $\Delta O_M I O_1$, we can obtain α :

$$\alpha = \tan^{-1} \frac{(b^2 + c^2) \sin \gamma - 2bc}{(b^2 - c^2) \cos \gamma} \quad (3-4)$$

From the top view of the imaging (Fig. 3-8), we can obtain the relationship for the direction angle, θ , of point P:

$$\tan \theta = Y/X = y/x \quad (3-5)$$

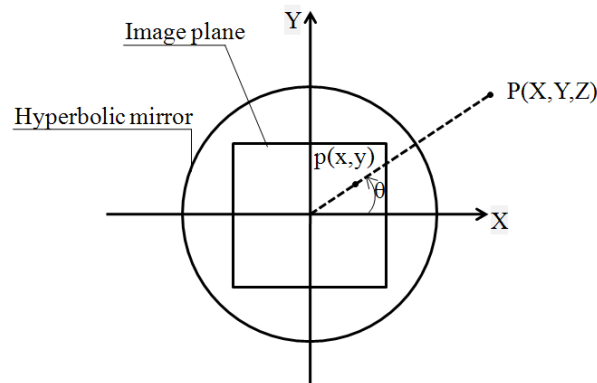


Fig. 3-8 Top view of imaging

We can deduce the following correlation between the space point $P(X, Y, Z)$ and relative image point $p(x, y)$ from Eqs. (3-2) through (3-5). We can then conveniently use it for calculating the transformation of $P(X, Y, Z)$ in the space and $p(x, y)$ produced in the image by the omnidirectional camera.

$$\begin{aligned} x &= \frac{(b^2 - c^2)Xf}{(b^2 + c^2)Z - 2bc\sqrt{X^2 + Y^2 + Z^2}} \\ y &= \frac{(b^2 - c^2)Yf}{(b^2 + c^2)Z - 2bc\sqrt{X^2 + Y^2 + Z^2}} \end{aligned} \quad (3-6)$$

The optical system is usually set at a specific height from the ground to facilitate image capturing in the application; thus, the coordinate system is changed as shown in Fig. 3-9. Based on the above Eq. (3-6), the correlation becomes Eq. (3-7) and is applied to the space point coordinate and image point coordinate in order to determine the position of each landmark in the spatial coordinate system.

$$\begin{bmatrix} x \\ y \end{bmatrix} = \frac{f \cdot (b^2 - c^2)}{(b^2 + c^2)(Z + c - H) - 2bc\sqrt{X^2 + Y^2 + (Z + c - H)^2}} \begin{bmatrix} X \\ Y \end{bmatrix} \quad (3-7)$$

where a, b, c and f are the same representation as above, and H is the height of the camera from the ground.

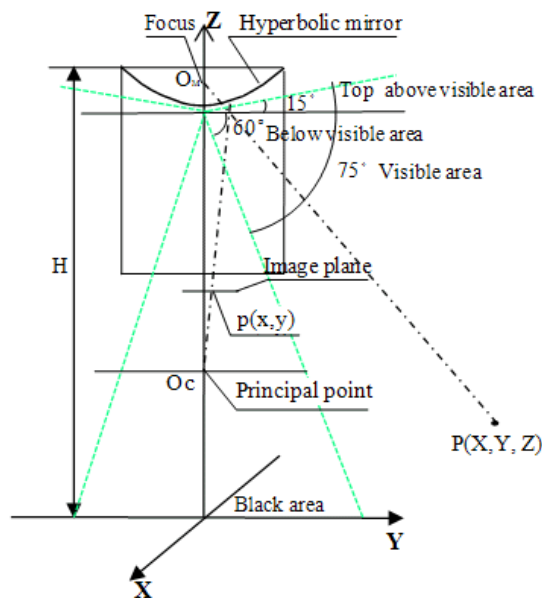


Fig. 3-9 Illustration of vision area

Fig. 3-9 shows that the hyperbolic mirror system has a wide visual area of about 75° including at the top above the visual area and below the visual area. The black area cannot be used, so care should be taken to avoid landmarks standing in the black area. Also, if a landmark is outside the visual area, the camera will not capture its image.

3.3.3 LANDMARK MODEL

In this study, the recognition of landmarks and extraction of features is pivotal to realizing localization. In farm fields, the same crop usually shows a homologous color pattern, which makes it very difficult to utilize natural crop landmarks as features for processing images. Omnidirectional vision having a 360° view can capture landmark images in different directions. In order to ensure that images are captured in all directions and provide the same results, the landmarks are designed as a right circular cylinder. Furthermore, to distinguish the landmarks from environmental interferences, we propose a color model. Fig. 3-10 shows the appearance of a complete landmark. The color pattern is divided into two kinds. One is made up of two red and blue or green adjacent color patches, which is used to avoid interference from similar red objects as the vision sensor easily captures everything within a small area. The red patch covers the top part of the landmark as the detection area. The blue or green patch covers the bottom part of the landmark to further distinguish it from other objects in a complex environment. The other color pattern is pure red and is used when there is no need to avoid red color interference, which eliminates some troublesome tasks, such as landmark and computer calculation.

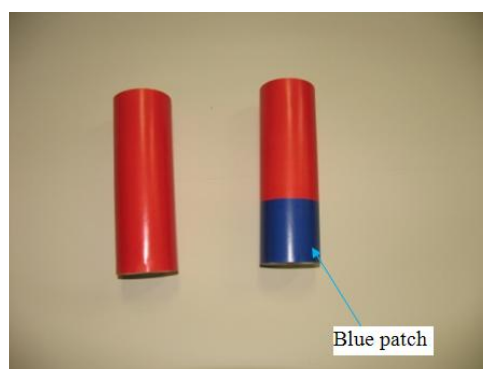


Fig. 3-10 Landmark models

3.4 FEATURES ABOUT SYSTEM

3.4.1 LOCALIZATION ROLE

The system is mainly applied to achieve localization for agricultural vehicle navigation in both indoor and outdoor environments. As described above, the architecture of the system is simple, although it takes some time to set up the artificial landmarks. The main advantage of this system is that the less expensive omnidirectional vision sensor decreases the total cost compared to the GPS guidance system for agricultural vehicle navigation. The system was faced with the same problems as other vision applications, such as difficulty dealing with changing light conditions, shadows, direct sunlight and other issues in the working environment. However, we adopted characteristic artificial landmarks to improve the extraction features and our system only needs to obtain landmark information rather than having to connect with the entire background environment, which makes system performance easy and feasible.

3.4.2 COMPUTER VISION ROLE

It has been reported that GPS and computer vision will inevitably be 'fused' together (e.g., Zhang et al., 1999) or one of them will be 'fused' with another technology such as gyroscope (Morimoto, 2005; Nagasaka, 2004), GDC (Benson et al. 1998), laser radar (Subramanian, 2006), etc. to realize autonomous vehicles in agriculture, allowing real-time image processing with a digital controller on a simple PC, precision positioning with a RTK DGPS system, or heading computation with a traditional gyroscope.

Machine vision has some excellent computer algorithms to support and advance successful research on localization in the agricultural field (e.g., Subramanian et al., 2006; Han et al., 2004). However, most studies require a row of plants or a furrow to guide the image processing vehicle, and tasks such as spraying or fertilizing on uncultivated fields require another strategy. In our system, the omnidirectional vision sensor depends on landmarks as the measurement base for calculating directional angles, similar to the way in which navigation satellites depend on GPS ground receivers to measure distance for determining absolute position. Our system is not only a potential substitute for the GPS

guidance system to localize agricultural vehicles, but it can also operate common computer vision functions to support localization and obstacle avoidance with the combination of computer vision technologies similar to fusing GPS and computer vision, which would make its application possible for any work area and would satisfactorily accomplish path planning with obstacle avoidance. Agricultural vehicles equipped with our system will likely carry out navigation using their “eyes” in the same way that mammals move around in the world.

3.5 CONCLUSIONS

In this chapter, we introduced a new localization system based on artificial landmarks and omnidirectional vision for agricultural vehicle navigation in both indoor and outdoor environments. This is a simple system consisting of four artificial landmarks, an omnidirectional vision sensor, PC and operating vehicle. The principle of localization is that the omnidirectional vision sensor depends on the landmarks as a measurement base for calculating the directional angle and determining the absolute position. The system not only can as a potential substitution for the GPS guidance system to localize agricultural vehicles, but also it can operate common computer vision functions to support localization and obstacle avoidance. Agricultural vehicles equipped with this system will likely carry out navigation using their “eyes” in the same way that mammals move around in the world. In next work, we intend to research the algorithm for landmark feature extraction and localization in detail and examine the correlation between camera height, landmark size and landmark image size to achieve effective and feasible landmark feature extraction.

4 ALGORITHMS AND PROGRAM

In order to make the localization system effective, the algorithms are very important. The algorithms mainly include landmark tracking extraction and position estimation. Similar to common image processing, image noise elimination should be considered. This chapter introduced them in detail.

4.1 INTRODUCTION

This chapter introduces two algorithms and one image processing. One algorithm is about landmark tracking extraction in which red landmark pixels beyond the threshold were extracted as a small area and the center of gravity was calculated for the extracted small area representing the candidate of one landmark. Generally, providing the blue patch as compensation to further distinguish the landmark from other objects in a complex environment, blue patch pixels beyond the threshold were extracted as a small area and the center of gravity was calculated and judged the candidate of landmark by the distance between the two centers of gravity. Then the positions of four representative landmarks were obtained.

One image processing is about noise smoothness, which the classic low-pass filter (LPF) is employed to remove high spatial frequency noise from digital images. We multiplied convolution kernel elements by the least common multiple to compute the weighted sum and then divide the summation with the least common multiple to obtain the real results to improve computational speed.

Then, the second algorithm is about estimation of the position of vehicle installed with camera. Based on the obtained positions of four landmarks via the landmark tracking extraction algorithm, and then estimated the four directional angles of the landmarks centered by camera principal point using only one omnidirectional image. Vehicle location was estimated using the center of gravity of the four intersections formed by four arcs according to

geometric transformation based on the four directional angles of the landmarks. If only find three landmarks, we also utilize the directional angles to estimate the vehicle location.

In this chapter, Section 4.2 introduces our proposed algorithms and calculation methods in detail. Section 4.3 presents the results of program running. Finally, A simply analysis of the performance and robustness of the program and our conclusions are drawn.

4.2 PROPOSED ALGORITHM

4.2.1 LANDMARK TRACKING ALGORITHM

Landmark tracking is very important for the following task of calculating the bearing and distance. Our proposed algorithm is used to determine the landmark position using the center of gravity of the red pixels or providing the blue patch as compensation to further distinguish the landmark from other objects in a complex environment. Firstly, to find the red pixels and extract the red intensity pixels in the image that are not less than the threshold (e.g., maximum red intensity minus 50) as a small area, the center of gravity (RCG) is calculated as one landmark position candidate. If using pure red landmarks, this process can obtain the landmark position. To avoid possible interference from other impurities in the image, the algorithm is used to find the blue pixels and calculate the center of gravity (BCG), if the pixel distance value between the two centers of gravity, RCG and BCG, is less than the distance threshold (e.g., 0.1 times the image height), which is taken as one landmark position candidate.

The extracted red intensity is defined as re , extracted blue intensity as be . Here, re and be are estimated for every pixel in the image by using Eq. (4-1) (Imou et al., 2008).

$$[re, be] = [R - (B + G)/2 - |B - G|, B - (R + G)/2 - |R - G|] \quad (4-1)$$

where R represents red intensity, G represents green intensity and B represents blue intensity. The colors that are isolated in the chromaticity space are selected as the landmark. Both the average value and absolute value are used to increase the distinguishing effect.

The re of pixels that is not less than the threshold and the distance between two random adjacent pixels that is less than the distance threshold (e.g., 0.1 times the image height) is

assigned as R_i ($i = 1, 2, 3, \dots, n$) to form a small area. In the small area, the center of gravity is calculated to represent the landmark position candidate (X_{re}, Y_{re}) using Eq. (4-2):

$$[X_{re}, Y_{re}] = \left[\frac{\sum_{i=1}^n R_{ix}}{n}, \frac{\sum_{i=1}^n R_{iy}}{n} \right] \quad (4-2)$$

Also, the be of pixels that is not less than the threshold and the distance between two random adjacent pixels that is less than the distance threshold is assigned as B_i ($i = 1, 2, 3, \dots, n$) to form a small area. In the small area, the center of gravity is calculated to represent the landmark position candidate (X_{be}, Y_{be}) using Eq. (4-3):

$$[X_{be}, Y_{be}] = \left[\frac{\sum_{i=1}^n B_{ix}}{n}, \frac{\sum_{i=1}^n B_{iy}}{n} \right] \quad (4-3)$$

Then, the distance between the center of gravity of the red patch and the center of gravity of the blue patch is calculated in order to judge whether or not it is an appropriate landmark representation.

Fig. 4-1 and Fig. 4-2 show red landmark and combined red and blue landmark tracking program flow chart, respectively.

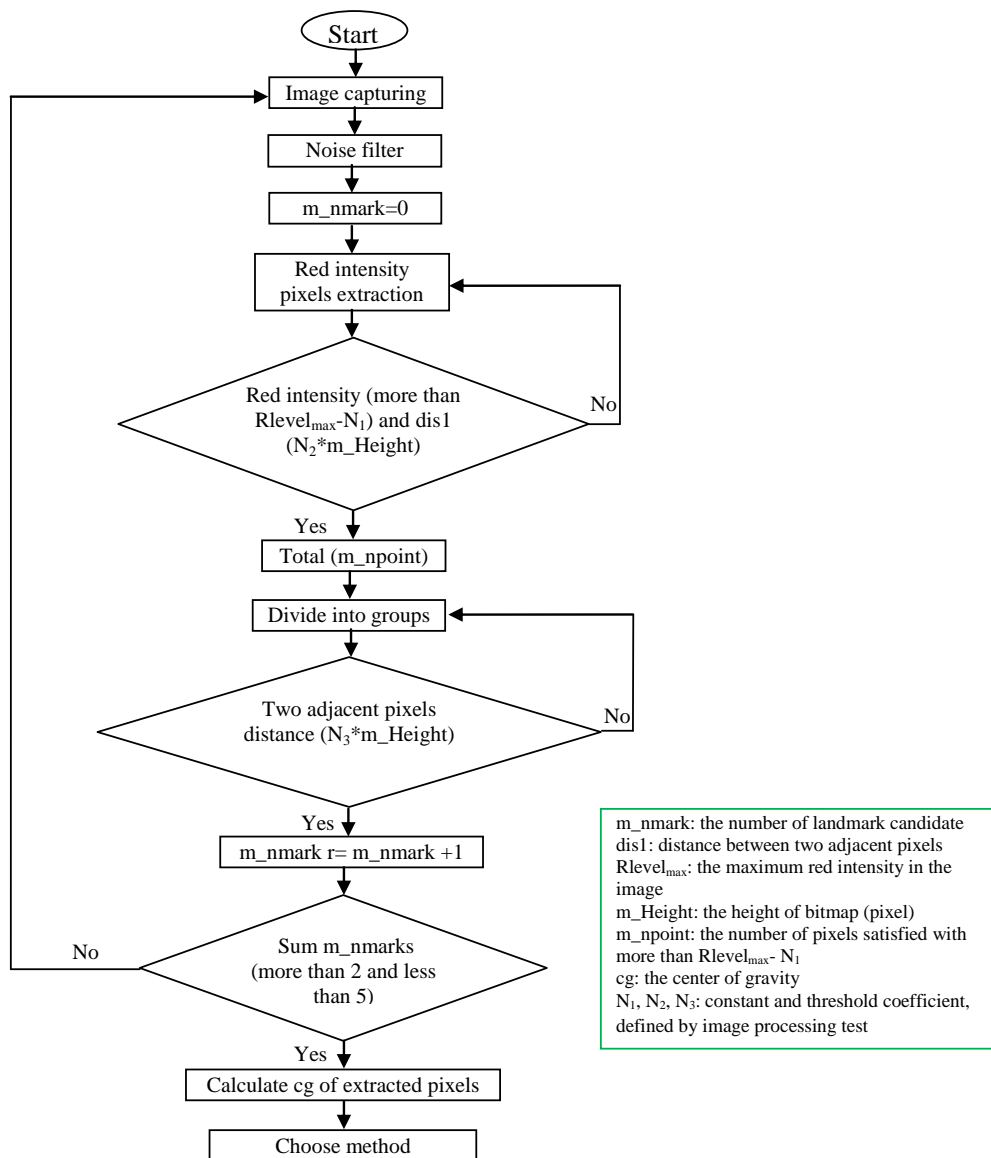


Fig. 4-1 Red landmark model tracking flow chart

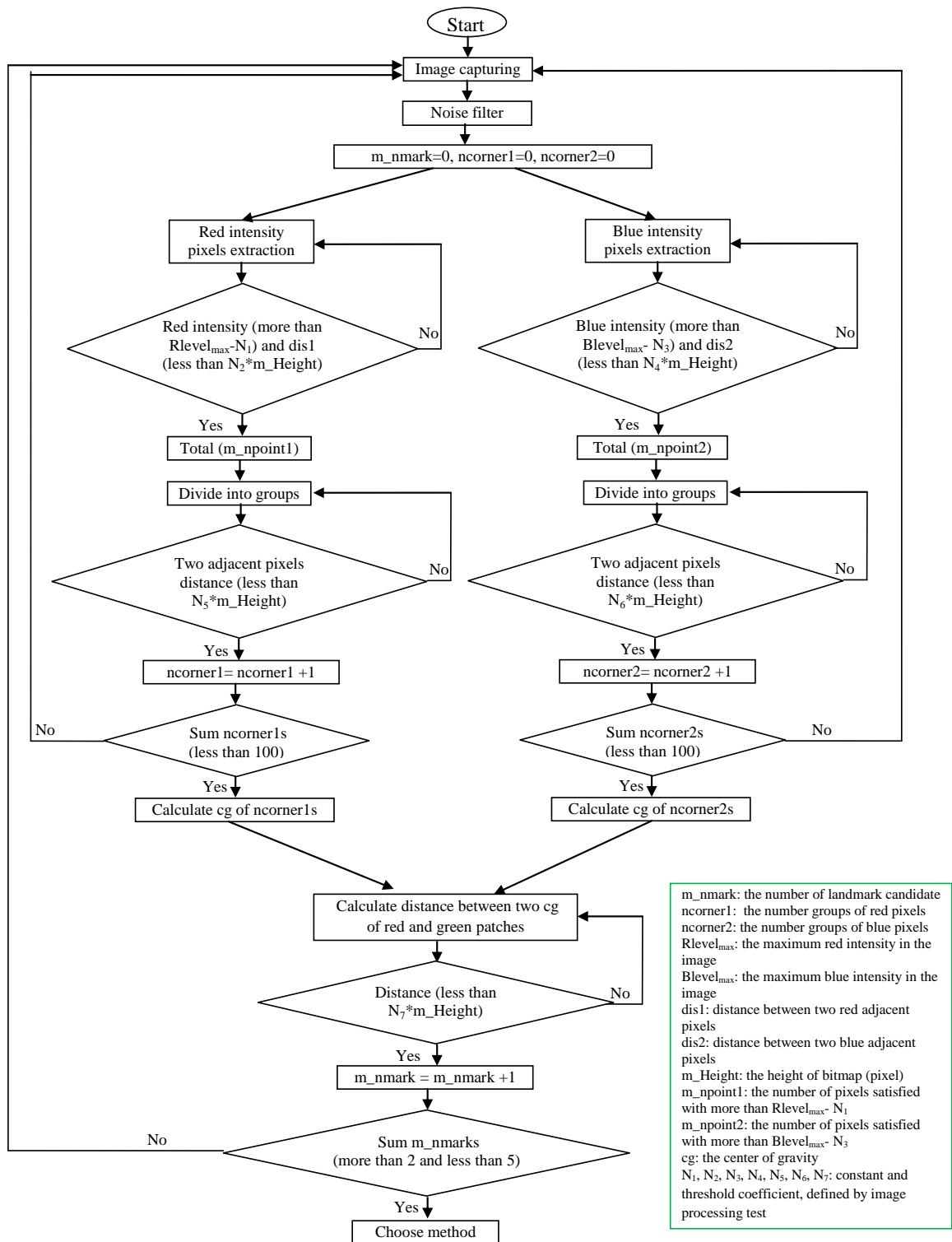


Fig. 4-2 Red and blue combined landmark model tracking flow chart

4.2.2 SMOOTHNESS

When our system is used to capture images, the distance between omnidirectional camera and landmark is different, and thus the imaging is a difference in landmark image size and color value. Sometimes, the natural scenery also interferes with the image characteristics. In our algorithm, threshold coefficients N_1 and N_3 (constant, defined by image processing test, e.g. 50, as shown in Fig. 4-2) control the decomposition of red and blue pixels from the original image, so the standard value (selected threshold value) is very important. Generally, we define the value as being in the range of 10 to 50, but if the original image is disordered, the landmark might not be detected or too many false landmarks might be detected as candidates, making the system ineffective. We utilize the classic low-pass filter (LPF), which is employed to remove high spatial frequency noise from digital images. The advantages of LPF include its ability to provide a smooth appearance and suppress unwanted noise or disturbance and its disadvantages are blurring of edges and the presence of ripples near edges. We simply utilize its advantages as we do not need to consider the edges of images. We use the following convolution kernel:

$$K = \begin{bmatrix} 1/16 & 1/8 & 1/16 \\ 1/8 & 1/4 & 1/8 \\ 1/16 & 1/8 & 1/16 \end{bmatrix}.$$

If we use the kernel for directly calculating the weighted sum, the computation is very large and time-consuming. Therefore, we multiply the convolution kernel elements by the least common multiple ($m = 16$) and change the kernel as follows:

$$K = \begin{bmatrix} 1 & 2 & 1 \\ 2 & 4 & 2 \\ 1 & 2 & 1 \end{bmatrix}.$$

We use this kernel to compute the weighted sum and then divide the summation with the least common multiple ($m = 16$) to obtain the real results.

4.2.3 ESTIMATING POSITION

4.2.3.1 Four landmarks extraction

The method involves setting up four red artificial landmarks as a rectangle with known width (d) and length (g) on the corners of a farm field. Distortions due to the mirror reflection

cause nonlinear changes on the projected image, which cannot be appropriately handled by linear calculation methods (Makadia and Daniilidis, 2003). Hence, only the information on the direction of the landmarks is used to estimate the location of the camera. Vehicle location is estimated using the center of gravity of the four intersections formed by four arcs according to the geometric transformation based on the four directional angles of the four landmarks, using the camera. Since the number of landmarks detected could be less than four due to changes in light intensity, tree shadows and overlong distance, our system is designed to deal with four or three landmarks.

The vehicle position was determined from the directional angles of the landmarks using the method shown in Fig. 4-3, where θ_1 through θ_4 indicate the angles of the direction between neighboring landmarks in the captured image. For example, θ_1 is the angle of the direction between landmarks L_1 and L_2 , giving the circular arc S_1 in the ground coordinate system. We can draw the circular arcs S_i ($i = 1,2,3,4$) based on the directional angles. If there is no error, all four arcs should intersect at one point, but under practical conditions, several different intersections could be produced due to measurement errors. In our system, the estimated position $P(x_1, y_1)$ is determined by the center of gravity of the four intersections I_i ($i = 1,2,3,4$), in which I_i ($i = 1-3$) are intersected by arcs S_i and S_{i+1} , respectively, and I_4 is intersected by arcs S_1 and S_4 . We assume the coordinate system of the farm field is represented by the x- and y-axis. According to the geometric relationship, we obtain Eq. (4-4):

$$\begin{cases} \tan\theta_1 = \frac{gx_{ii}}{(x_{ii}^2 + y_{ii}^2 - gy_{ii})} \\ \tan\theta_2 = \frac{dy_{ii}}{(x_{ii}^2 + y_{ii}^2 - dx_{ii})} \end{cases} \quad (4-4)$$

The following result (5) is obtained:

$$\begin{cases} x_{ii} = \frac{g\left(c + \frac{1}{\tan\theta_1}\right)}{1 + c^2} \\ y_{ii} = cx_{ii} = \frac{gc\left(c + \frac{1}{\tan\theta_1}\right)}{1 + c^2} \end{cases} \quad (4-5)$$

Here, $c = \frac{g / \tan \theta_1 - d}{d / \tan \theta_2 - g}$.

Similarly, we can obtain the x-axis and y-axis absolute values for the four intersections I_i ($i = 1, 2, 3, 4$). Then, the absolute coordinate value of the estimated position is calculated using Eq. (4-6):

$$\begin{cases} x_1 = (x_{I1} + x_{I2} + x_{I3} + x_{I4}) / 4 \\ y_1 = (y_{I1} + y_{I2} + y_{I3} + y_{I4}) / 4 \end{cases} \quad (4-6)$$

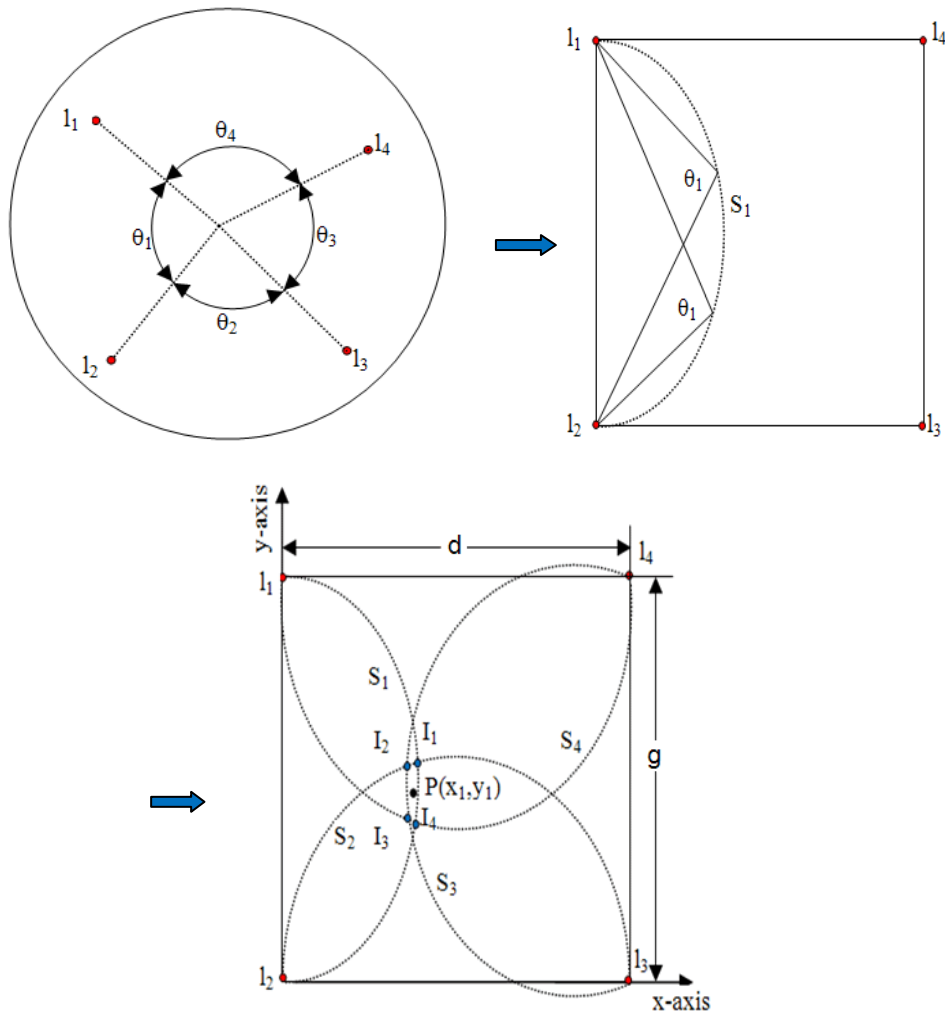


Fig. 4-3 Position determination from four landmarks

4.2.3.2 Three landmarks extraction

If the system only detects three landmarks as shown in Fig. 4-4, the analysis adds a diagonal and an included angle different from the state of four landmarks detection. Using the above referred four landmarks method to extract pixel features and define landmark representation, we can get the directional angles. Under this condition, we use the Eq. (4-7) transformed by Eq. (3-7) to get the spatial coordinate of image points [X, Y].

$$\begin{bmatrix} X \\ Y \end{bmatrix} = \frac{\{f(b^4 - c^4)(Z + c - H) + \sqrt{4b^2c^2(b^2 - c^2)^2(Z + c - H)^2(f^2 + x^2 + y^2)}\}}{f^2(b^2 - c^2)^2 - 4b^2c^2(x^2 + y^2)} \begin{bmatrix} x \\ y \end{bmatrix} \quad (4-7)$$

Then calculate to obtain three distances among three landmarks by two points distance formula. Comparing with the distance length, we judge the diagonal and corresponded included angle. Similar to four landmarks method, the system can obtain the estimated position.

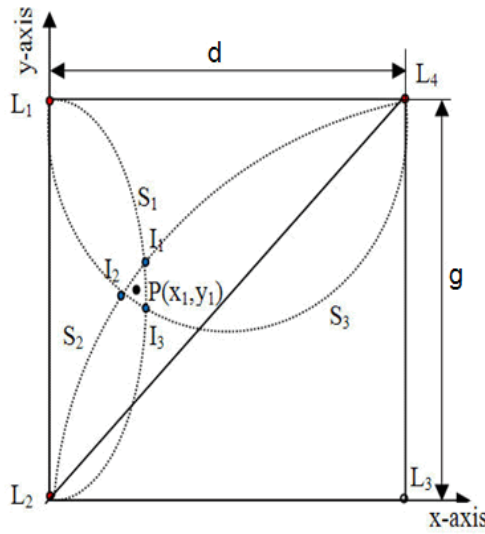


Fig. 4-4 Position determination from three landmarks

4.3 RESULTS OF PROGRAM RUNNING

4.3.1 LANDMARK EXTRACTION

Fig. 4-5(a) an original example of images with combined with red and blue landmarks captured by omnidirectional camera. There are four landmarks and six other red interferences. Fig. 4-5(b) shows the result of landmark extraction after image processing, which includes

four landmarks and eight red interferences. The landmarks are represented by a black block and the symbol (✖) and interferences are represented by a black block only.

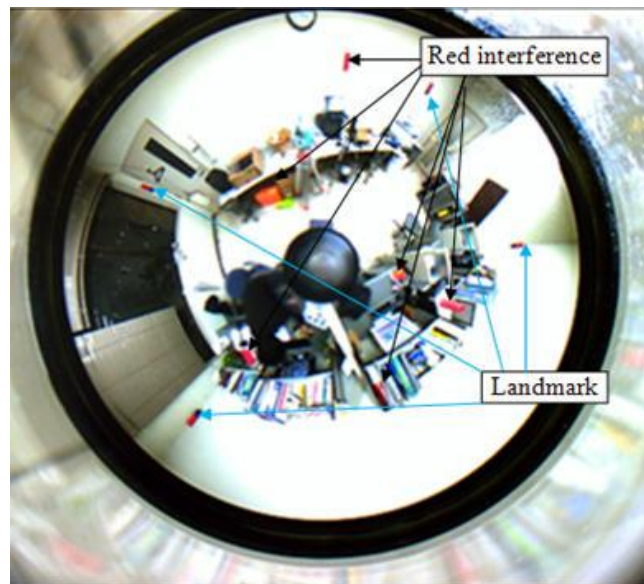


Fig. 4-5(a) Original image with landmark and interference

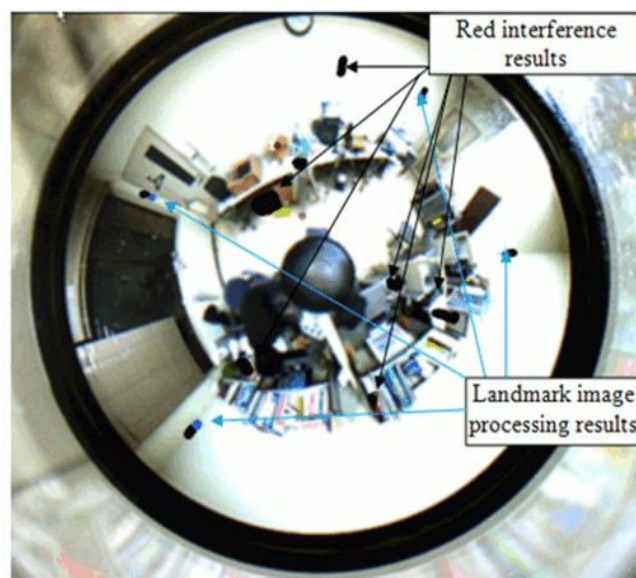


Fig. 4-5(b) Landmarks extraction

4.3.2 SMOOTHNESS RESULT

In order to verify the result of smooth process, we laid only one landmark far away from camera at a distance 50 m. The result is clear only one landmark or no. Because the number

of landmarks is less than three, our running program shows the message “Error”. The following figures show the results via smoothness. In Fig. 4-6, (a1) the original image. (b1) the histogram of R, G, B and (c1) the landmark detection result with original image. The detection result message (as shown in Fig. 4-6 (c1)) was “no landmark” because there were too much noise or interference in the image where red landmark pixel intensity was not enough strong to extract by our threshold. In Fig. 4-6, (a2) the smoothness image, (b2) the histogram of R, G, B and (c2) the landmark detection result with smoothed image. If compared (a2) with (b2), we know that the R wave crest became lower obviously in the image (b2). This showed that the smoothness eliminated some high spatial frequency noise. In Fig. 4-6(c2), the result showed that “only one landmark” was found successfully.



Fig. 4-6(a1) Original image (only one landmark)



Fig. 4-6(b1) Smoothed image

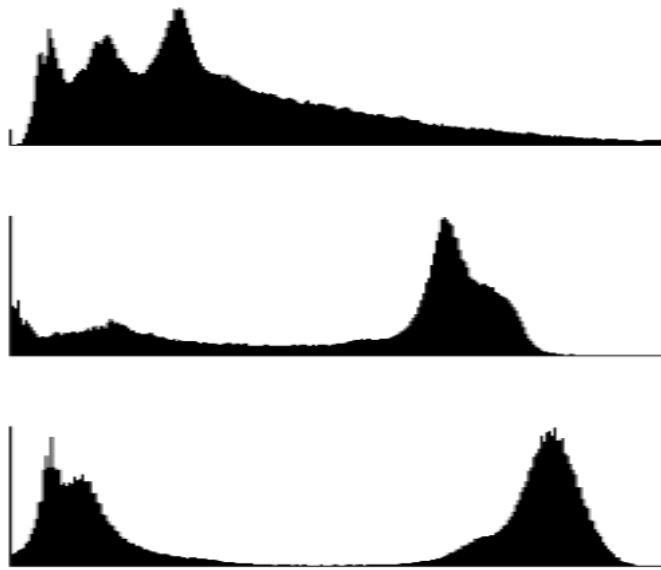


Fig. 4-6(a2) Histogram of R, G and B before smoothness

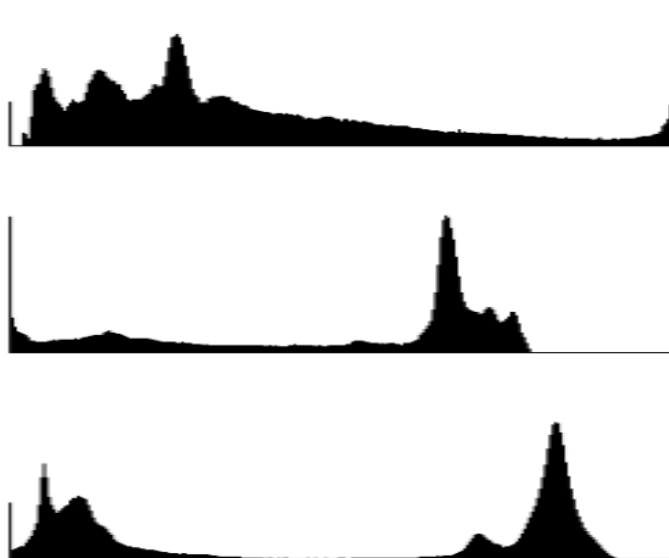


Fig. 4-6(b2) Histogram of R, G and B after smoothness



Fig. 4-6(a3) Results of landmark extraction before smoothness

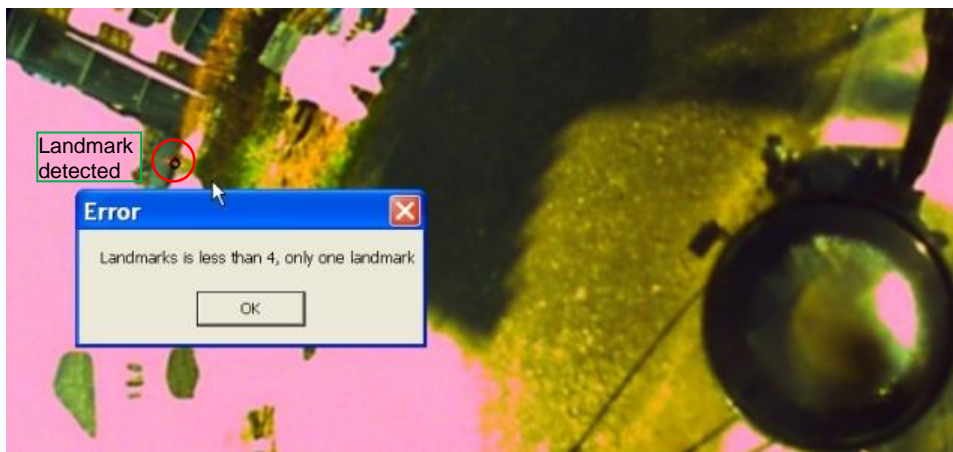


Fig. 4-6(b3) Results of landmark extraction after smoothness

4.3.3 POSITION ESTIMATION RESULT

Fig. 4-7 shows an example of program running for four landmarks, and the calculated results are including angles value, e.g. "Angle1: 123.765 degrees", illustration and intersections of arcs, the landmark information, e.g. "Number of points in final 4 red groups" represent 4 landmarks extracted, the intersections and camera position coordinate value in the end.

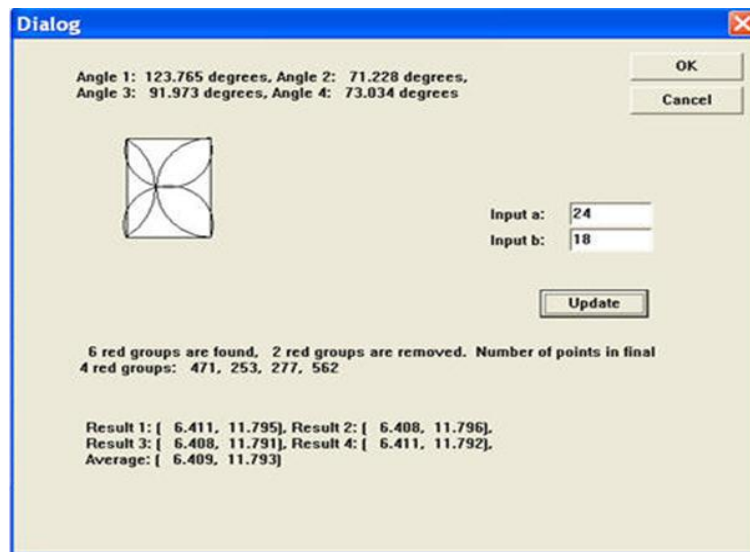


Fig. 4-7 Program interface for four landmarks extraction

4.4 CONCLUSIONS

This chapter introduced two algorithms and one image processing. Landmark tracking extraction algorithm mainly used color threshold to extract red and blue features and based pixels distance to decide the landmark; blue pitch is applied for complex environments. Position estimation algorithm was with the use of directional angles of landmarks to estimate vehicle position successfully. The use of LPF smoothness was also effective.

In the test, if we used PC (Intel Core 2, 2.33GHz) to process a piece of image resolution 1024×768, it took about 100~200 ms. If the landmarks are apparent, the smoothness is not necessary, and the landmark tracking extraction and position estimation algorithms are robustness because our algorithm can treat with four or three landmarks. If the image noise is enough to need eliminate, the LPF smoothness image processing is used to keep the robustness.

Next work, we will calibrate the omnidirectional vision system to find out the camera principal point and vision system parameters to improve the image distortion.

5 OMNIDIRECTIONAL VISION CAMERA CALIBRATION

In our localization system for agricultural vehicle, omnidirectional camera was used. This study developed a fast and practical method for calibration of omnidirectional vision system. In our system localization algorithm, the principal point in the image is pivotal position and other calibration parameters are useful for improving the accuracy of locating. The calibration method utilized a 2D calibration pattern that can be freely moved. Without a priori knowledge of the motion, the boundary ellipse of the catadioptric image and field of view (FOV) were used to obtain principal point and focal length. Then, the explicit homography between the calibration pattern and its virtual image was used to initialize the extrinsic parameters. Last, the intrinsic and extrinsic parameters are refined by nonlinear optimization. Experimental results show that the calibration method is feasible and effective. The application experimental results show that calibration can provide with the principal point value and improve the accuracy of localization about 1.6 cm in a 1.8 m×0.9 m area.

5.1 INTRODUCTION

Accurate calibration of a vision system is necessary for any computer vision task requiring extracting metric information of the environment from 2D images, like in ego-motion estimation and structure from motion. In our localization system for agricultural vehicle, omnidirectional camera was used to collect landmarks information to estimate the directional angles, therefore, which is very important to obtain accurate landmarks information in 2D images. The advantages of catadioptric cameras are that can provide 360 degree panoramic view of the scene and such imaging systems have a single viewpoint (Nayar, 1997). However, the disadvantage of catadioptric cameras is that the alignment between the mirror and camera must be exact. If there is misalignment, the camera cannot maintain desired optical characteristics such as a single viewpoint (Baker, 1999; Micusik, 2004). The misalignment problem causes different errors in systems using catadioptric cameras.

Therefore, the mirror alignment is absolutely essential for a catadioptric camera. But it is very difficult to align the mirror and camera positions because alignment correlates with the camera intrinsic parameters and manufacture. Therefore, catadioptric camera calibration is as important as conventional camera calibration. However, the catadioptric camera calibration is more complicated and difficult to obtain the calibration results, because it includes conventional camera calibration and mirror posture estimation, and the methods for catadioptric calibration differ according to the mirrors, reflection, and camera models that are used.

The previous calibration methods for the central catadioptric cameras could be classified into the following five categories (Deng, 2007):

(1) Self-calibration or auto-calibration. Kang (2000) used the consistency of pair-wise tracked point features for calibration and the mirror boundary. The method is only suitable for catadioptric cameras with a paraboloidal mirror. Micusik and Pajdla (2004) proposed auto-calibration and 3D reconstruction methods by using mirror boundary and an epipolar geometry approach.

(2) Sphere based calibration. Ying and Hu (2004) analyzed the relation of the camera intrinsic parameters and the sphere imaged contour. Then, they applied the relation to calibrating central catadioptric cameras.

(3) Line based calibration. Geyer and Daniilidis (2002) calibrated a catadioptric camera system consisted by a paraboloidal mirror and an orthographic lens from at least three line images. Barreto and Araujo (2005) studied the geometric properties of line images under the central catadioptric model, and gave a calibration method for all kinds of central catadioptric cameras. All these methods involved conic fitting, an error-prone process when only partial contour is available.

(4) Point based calibration. From known 3D space points, Aliaga (2001) proposed a paracatadioptric camera calibration method, which relaxed the assumption of the perfect orthographic projection and placement. Vasseur and Mouaddib (2004) calculated intrinsic parameters by a nonlinear method with 3D space points.

(5) 2D calibration method. Scaramuzza et al. (2006) proposed a 2D calibration method for catadioptric cameras. Since the images of 2D pattern can easily cover the whole catadioptric image, their methods are capable of accurate calibration. Mei and Rivers (2007) also proposed a 2D calibration method for catadioptric cameras based on the unified model of Geyer (2000). Deng et al. (2007) used the bounding of ellipse of the catadioptric image and field of view (FOV) to obtain the initial estimation of the intrinsic parameters. The method was easier.

This study will satisfy for agricultural vehicle working in the field, the camera system calibration is to improve the accuracy of localization. For the real-time working in the field, the calibration process requires to be as fast and simple as possible. Self-calibration or auto-calibration doesn't need scene information, but the method is not stable in practice or there are limitations (Deng, 2007). 2D calibration method is easy and our work is inspired by the researches of Kang (200), Deng (2007), Scaramuzza (2006) and Mei (2007). We propose a fast and practical method for calibration of the omnidirectional camera for our localization system. We programmed using Matlab 6.5.

5.2 CALIBRATION REQUIREMENTS

5.2.1 PRINCIPAL POINT

As shown in Fig. 4-3 (Chapter 4), our localization system decides the directional angles between landmarks θ_1 to θ_4 , and then estimate the camera position based on them. If we need to estimate the directional angles between landmarks, we must know the principal point of camera lens in the image firstly.

As shown in Fig. 5-1, we can know that principal point of camera is different from image center usually. We should know the position of principal point in the image before we estimate directional angles of landmarks. But it is very difficult or no way to find out the principal point of camera in the image directly.

As shown in Fig. 5-2, we can know, if the position of principal point is changed, the directional angles between landmarks will be following changed obviously.

Therefore, the principal point is very pivotal. We should decide the position of principal point of camera lens in the image accurately before the process of estimation of camera position.

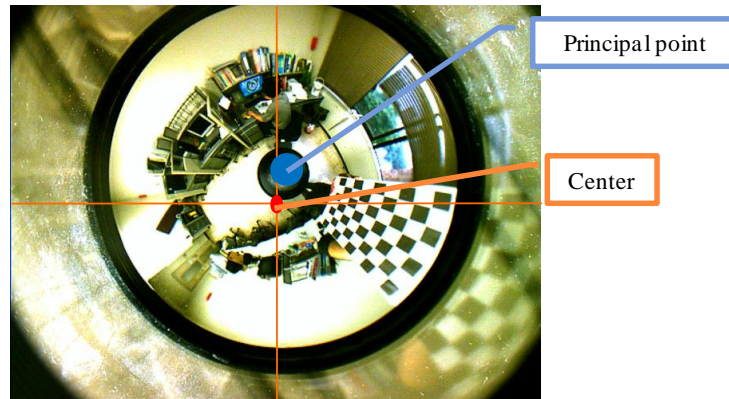


Fig. 5-1 Principal point of camera different from image center

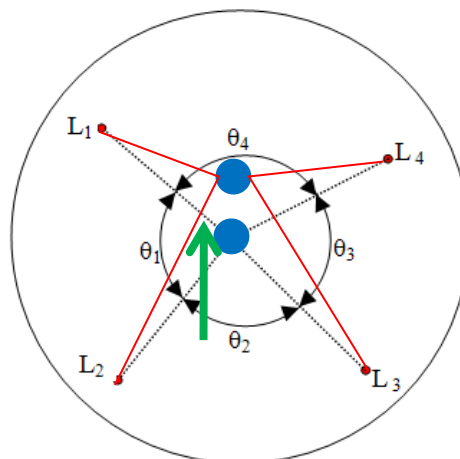


Fig. 5-2 Directional angles changing with principal point

5.2.2 OMNIDIRECTIONAL VISION SYSTEM DISTORTION

As this sensor has the same optical characteristic of a single viewpoint, which can generalize correct perspective images geometrically from the pictures captured by the omnidirectional camera easily (as shown in Fig. 3-7, Chapter 3). If the mirror is misaligned, the single viewpoint does not exist and the image is distorted. We can correct the some

image distortion by adjusting the focal f . However, we can't promise the accuracy and accord with the geometrical transformation.

Based on the above two considerations, the calibration is very necessary.

5.3 CATADIOPTRIC CAMERA PROJECTION MODELS

5.3.1 PINHOLE CAMERA MODEL

We denote a 2D point in the image coordinate system as $\mathbf{p} = (x, y)^T$ and a 3D point in the camera coordinate system as $\mathbf{P} = (X, Y, Z)^T$. The relation between a 3D point \mathbf{P} and its image projection \mathbf{p} is expressed by the following equations.

$$\begin{bmatrix} \mathbf{p} \\ 1 \end{bmatrix} \approx \mathbf{K} \begin{bmatrix} \hat{\mathbf{R}} & \mathbf{t} \end{bmatrix} \begin{bmatrix} \mathbf{P} \\ 1 \end{bmatrix}, \quad \mathbf{K} = \begin{bmatrix} \lambda f & s & u_0 \\ 0 & f & v_0 \\ 0 & 0 & 1 \end{bmatrix} \quad (5-1)$$

Where $\hat{\mathbf{R}} = [r_1, r_2, r_3]$ is the rotation matrix and \mathbf{t} is the translation 3-vector, \mathbf{K} is the matrix of camera intrinsic parameters, with λ the aspect ratio, f the focus, $[u_0, v_0]$ the principal point and s is the skewness of x and y axes.

5.3.2 CENTRAL CATADIOPTRIC CAMERA MODEL

Baker (1999) and Geyer (2000) respectively studied the image formation and projective geometry in a catadioptric vision system. They showed that a central catadioptric projection is equivalent to a two-step mapping via the sphere (as shown in Fig.5-3). In our system, an incident ray from a 3D point \mathbf{P} is reflected by a hyperbolic mirror, and then the reflected ray is refracted through the perspective camera onto the image plane. Based on the project model of Geyer (2002) and Brrreto (2001, 2005) for central catadioptric cameras, the projection of 3D point can be done in the following steps.

A 3D point \mathbf{P} is projected to a point \mathbf{P}_u on a unit sphere centered at the viewpoint \mathbf{O} , and then projected to a point \mathbf{p} on the image plane by a virtual pinhole camera through the principal point \mathbf{O}_c . The camera optical axis is line \mathbf{OO}_c . The catadioptric image plane Π is vertical to the line \mathbf{OO}_c . The principle point $\mathbf{C} = [u_0, v_0, 1]^T$ is the intersection of the line

$\mathbf{O}\mathbf{O}_c$ with the image plane. $\xi = \|\mathbf{O} - \mathbf{O}_c\|$, which is the mirror parameter. The process can be explicitly expressed as:

$$\mathbf{p} \approx \mathbf{K} \left(\frac{\hat{\mathbf{R}}\mathbf{P} + \mathbf{t}}{\|\hat{\mathbf{R}}\mathbf{P} + \mathbf{t}\|} + [0, 0, \xi]^T \right) \quad (5-2)$$

where \mathbf{K} , \mathbf{R} and \mathbf{t} are as (5-1). $\|\cdot\|$ denotes the norm of vector in it. Our system using hyperbolic mirror, $0 < \xi < 1$.

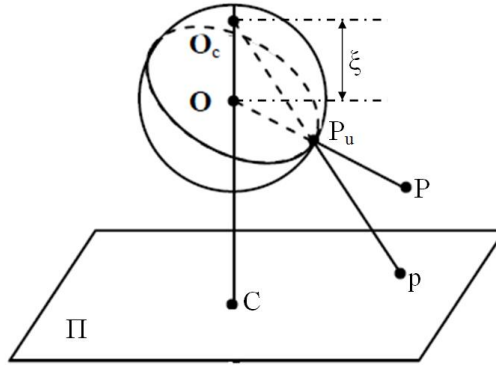


Fig. 5-3 Unified image formation

5.3.3 DISTORTION

We considered two main sources of distortion (Heikillä, 1997): imperfection of the lens shape that is modeled by radial distortion and improper lens and camera assembly including misalignment between the camera optical axis and the mirror rotational axis that generate both radial and tangential errors.

Five parameters can be used to model the distortion. A three parameters model was chosen for the radial distortion. The radial distortion $\delta^{(r)}$ can be approximated using in the following expression (Heikillä, 1997):

$$\begin{bmatrix} \delta_x^{(r)} \\ \delta_y^{(r)} \end{bmatrix} = \begin{bmatrix} x(k_1\rho^2 + k_2\rho^4 + k_3\rho^6) \\ y(k_1\rho^2 + k_2\rho^4 + k_3\rho^6) \end{bmatrix} \quad (5-3)$$

$$\rho = \sqrt{x^2 + y^2}$$

Different models can be used for the tangential distortion according to the relative importance of the alignment and angular errors. We added two extra variables to model the tangential distortion $\delta^{(t)}$ in the following form (Mei, 2007):

$$\begin{bmatrix} \delta_x^{(t)} \\ \delta_y^{(t)} \end{bmatrix} = \begin{bmatrix} 2k_3xy + k_4(\rho^2 + 2x^2) \\ k_3(\rho^2 + 2y^2) + 2k_4xy \end{bmatrix} \quad (5-4)$$

We note $\zeta = [k_1, k_2, k_3, k_4, k_5]$ the parameters.

5.4 CALIBRATION ALGORITHM

In our method, we initialize the intrinsic and extrinsic parameters firstly, and then use a Levenberg-Marquardt approach to solve the nonlinear minimization problem of an algebraic distance.

By assuming that the errors from the theoretical model are small, we suppose that $k_1 \approx k_2 \approx k_3 \approx k_4 \approx k_5 \approx s \approx 0$ and $\lambda = 1$. Based on the common experience, we can suppose $\xi = 0.8$ for hyperbolic mirror.

Next, we need to initialize the extrinsic parameters of grids and values for principal point (u_0, v_0) and focal length f .

5.4.1 MIRROR BOUNDARY EXTRACTION FOR PRINCIPAL POINT ESTIMATION

Our method used an ellipse in the image made from mirror boundary (Gander, 1994; Deng, 2007; Mei, 2007). The mirror boundary is projected to an omnidirectional image as an ellipse (conic) curve, and if the equation of the fitted boundary is represented as the following equation:

$$ax^2 + by^2 + 2cx + 2dy + 2exy + g = 0 \quad (5-5)$$

Where a, b, c, d, e and g are constant, (x, y) is in the image coordinate system, we can get the principal point (u_0, v_0) as:

$$u_0 = \frac{ed - bc}{ab - e^2}, v_0 = \frac{ec - ad}{ae - e^2} \quad (5-6)$$

Because the density of information around the mirror edge is heavy, hyperbolic mirror boundary extraction is not straight forward. We adopt the following steps to extract boundary points and estimate the principal point.

Using a predefined threshold, remove the area that is too far from the given circle and between the center and the edge points. From the remaining points, create many possible ellipses and use the Eq. (5-5) and (5-6); the median value of the estimated principal points is as the principal point.

5.4.2 INITIALIZATION OF FOCAL LENGTH

In our system, we know the field of view (FOV) about 105° of the omnidirectional vision sensor. Based on the Kang (2000) and Deng (2007), as shown in Fig. 5-4, the camera coordinate system 3D point P was projected P_u on the unit sphere, the refracted to p on the image plane. We define the \varnothing as the angle of FOV.

We can obtain the following relation via the triangular geometry relations (Appendix B).

$$\omega = \frac{2\xi \cos\varphi + \xi^2 + 1}{(\cos\varphi + \xi)^2} \quad (5-7)$$

The focal length f :

$$f = \sqrt{\frac{(x - u_0)^2 + (y - v_0)^2}{\omega - 1}} \quad (5-8)$$

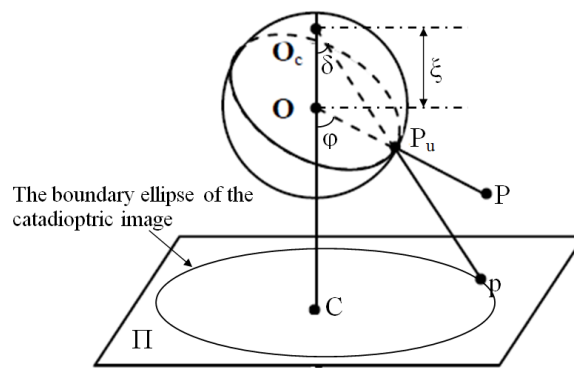


Fig. 5-4 Unified image formation with FOV

We let get $\varphi = 50^\circ$, and then estimate f as the initialization value.

5.4.3 HOMOGRAPHY BETWEEN THE CALIBRATION PATTERN AND ITS VIRTUAL IMAGE

During the calibration procedure, a calibration pattern of known geometry is shown at different unknown positions, which are related to the sensor coordinate system by a rotation matrix $\hat{\mathbf{R}} = [r_1, r_2, r_3]$ and a translation 3-vector \mathbf{t} , called the extrinsic parameters. $\mathbf{P} = [X, Y, Z]^T$ is the 3D coordinate of the calibration pattern points in the pattern coordinate system. $\mathbf{p} = [x, y]^T$ is the correspondent pixel coordinates in the image plane. Without loss of generality, we suppose that the calibration pattern is on $Z=0$ of the world coordinate system. By abuse of notation, we still define $\mathbf{P} = [X, Y, 0]^T$ to denote a point on the calibration pattern and $\tilde{\mathbf{P}} = [X, Y, 1]^T$.

Because a 3D point \mathbf{P} is projected on the image plane via the sphere, we can't map homography (\mathbf{H}) between the \mathbf{p} and \mathbf{P} straightly. We need to initialize the extrinsic parameters ($\mathbf{R} \mathbf{t}$) via the homography \mathbf{H} from the calibration pattern to a virtual image plane. The following transformations help to estimate \mathbf{H} .

From Eq. (5-2), we can obtain the following relation:

$$\mu \mathbf{p} = \mathbf{K} \left(\frac{\hat{\mathbf{R}}\mathbf{P} + \mathbf{t}}{\|\hat{\mathbf{R}}\mathbf{P} + \mathbf{t}\|} + [0, 0, \xi]^T \right) \quad (5-9)$$

where μ is a nonzero scalar related to \mathbf{p} . The principle point is $\mathbf{C} = [u_0, v_0, 1]^T$. We can get:

$$\mu \mathbf{p} - \xi \mathbf{C} = \mathbf{K} \left(\frac{\hat{\mathbf{R}}\mathbf{P} + \mathbf{t}}{\|\hat{\mathbf{R}}\mathbf{P} + \mathbf{t}\|} \right) \approx \mathbf{K}(\hat{\mathbf{R}}\mathbf{P} + \mathbf{t}) \quad (5-10)$$

then,

$$\mathbf{K}(\hat{\mathbf{R}}\mathbf{P} + \mathbf{t}) = \mathbf{K} [r_1, r_2, r_3, \mathbf{t}] \begin{bmatrix} X \\ Y \\ 0 \\ 1 \end{bmatrix} = \mathbf{K} [r_1, r_2, \mathbf{t}] \begin{bmatrix} X \\ Y \\ 1 \end{bmatrix} \quad (5-11)$$

Define $\tilde{\mathbf{p}} = \mu \mathbf{p} - \xi \mathbf{C}$ and we know $\tilde{\mathbf{p}}$ is just an image point of the corresponding \mathbf{P} under perspective camera. $\tilde{\mathbf{P}}_\mu = \mathbf{K}^{-1} \tilde{\mathbf{p}}$. $\tilde{\mathbf{P}}_\mu$ is the corresponding point of \mathbf{p} on the unit sphere.

Since $\tilde{\mathbf{P}}_\mu^T \tilde{\mathbf{P}}_\mu = 1$,

$$(\mu\mathbf{p} - \xi\mathbf{C})^T \mathbf{K}^T \mathbf{K}^{-1} (\mu\mathbf{p} - \xi\mathbf{C}) = 1 \quad (5-12)$$

Solving μ and simplifying the result by $\mathbf{K}^{-1}\mathbf{C} = (0, 0, 1)^T$, $\mathbf{C}^T \mathbf{K}^T \mathbf{K}^{-1} \mathbf{C} = 1$ and $\mathbf{p}^T \mathbf{K}^T \mathbf{K}^{-1} \mathbf{C} = 1$.

We can get:

$$\mu = \frac{\xi \pm \sqrt{\xi^2 - \mathbf{p}^T \mathbf{K}^{-T} \mathbf{K}^{-1} \mathbf{p} (\xi^2 - 1)}}{\mathbf{p}^T \mathbf{K}^{-T} \mathbf{K}^{-1} \mathbf{p}} \quad (5-13)$$

From Eq. (5-11), we denote $\mathbf{H} = \mathbf{K}[r_1, r_2, t]$.

$$\tilde{\mathbf{p}} \approx \mathbf{H}\tilde{\mathbf{P}} \quad (5-14)$$

where $\tilde{\mathbf{p}} = \mu\mathbf{p} - \xi\mathbf{C}$, we know μ , ξ and \mathbf{C} , so we can get the homography between $\tilde{\mathbf{P}}$ and \mathbf{p} via virtual image.

We denote it by $\mathbf{H} = [h_1, h_2, h_3]$.

$$[h_1, h_2, h_3] = \beta \mathbf{K}[r_1, r_2, t] \quad (5-15)$$

where β is an arbitrary scalar. Given the homography and intrinsic parameters for each image, we can obtain

$$\mathbf{r}_1 = \beta \mathbf{K}^{-1} \mathbf{h}_1, \quad \mathbf{r}_2 = \beta \mathbf{K}^{-1} \mathbf{h}_2, \quad \mathbf{r}_3 = \mathbf{r}_1 \times \mathbf{r}_2, \quad \mathbf{t} = \beta \mathbf{K}^{-1} \mathbf{h}_3 \quad (5-16)$$

with $\beta = 1/\|\mathbf{K}^{-1} \mathbf{h}_1\| = 1/\|\mathbf{K}^{-1} \mathbf{h}_2\|$.

5.4.4 NONLINEAR OPTIMIZATION

Assuming that n is the image number of 2D calibration pattern in different directions and p_i is the image point number in the i -th image of the calibration pattern; the solution of the calibration problem can be simplified to minimizing the function:

$$\min_{\mathbf{K}, \mathbf{R}_i, \mathbf{t}_i, \zeta_i} \sum_{i=1}^n \sum_{j=1}^{B_i} \|\mathbf{p}_{ij} - \hat{\mathbf{p}}(\mathbf{K}, \mathbf{R}_i, \mathbf{t}_i, \zeta_i, \mathbf{P}_j)\|^2 \quad (5-17)$$

where $\hat{\mathbf{p}}(\mathbf{K}, \mathbf{R}_i, \mathbf{t}_i, \zeta_i, \mathbf{P}_j)$ is the projection of point \mathbf{P}_j in the i -th image with the initialization of extrinsic and intrinsic parameters. Minimizing (5-17) is a non-linear minimization problem, which we can solve it by the Levenberg-Marquardt method.

5.4.5 CALIBRATION STEPS

1. Print a pattern and attach it to a planar surface.

2. Take a few images of the calibration pattern in different orientations by moving either the plane or the camera.
3. Process the image to use the boundary ellipse to estimate the principal point and FOV to initialize the intrinsic parameters.
4. Estimate all the extrinsic parameters.
5. Refine all parameters, including lens distortion parameters, by minimizing (5-17).

5.5 CALIBRATION EXPERIMENTS

In order to verify the feasibility of our calibration method and prove its effect, we have done calibration experiment for calibration errors analysis and obtaining camera calibration parameters.

5.5.1 MATERIALS AND METHODS

Calibration pattern composes of grid size 7×9 with squares of 23 cm. We have done them in our laboratory in the daylight lamp environment. We first set up the red cylinders landmarks on the four wall corners lift from ground 150 cm in a 5.8 m \times 3.53 m rectangular area, the diameter of which was about 6.6 cm and the height is 20 cm. Height of omnidirectional camera was adjusted to 130 cm and the image resolution was chose to 1024 \times 768. We selected 10 positions in the rectangle area and adjusted the calibration pattern to take 10 images at different orientations, then calibrated and estimated the intersections and the estimated positions by image processing one by one.

5.5.2 EXPERIMENTAL PROCESS

(1) Taking images, one example as Fig. 5-5. The images include calibration pattern and red landmarks which is convenient for camera calibrating and estimating the position of camera.

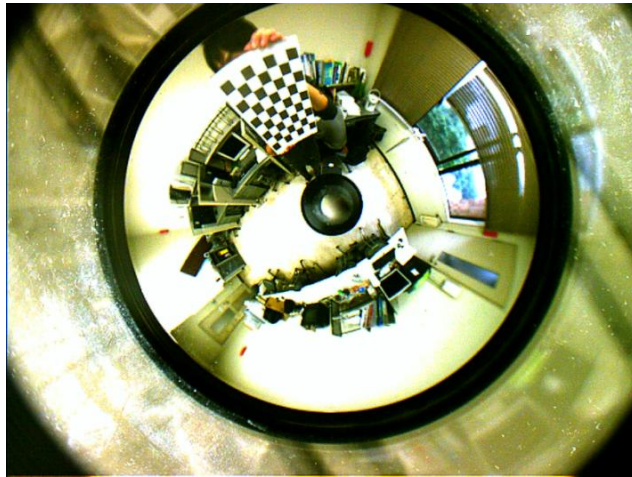


Fig. 5-5 One example of image

(2) Loading images.



Fig. 5-6 Loading images

(3) Estimating the principal point with the mirror boundary. Then, we will estimate focal length.



Fig. 5-7 Extraction of the mirror boundary and estimation of the principle point

(4) Extract four grid corners to initialize extrinsic parameters for every image. We will denote the x and y axis, as Fig. 5-8.

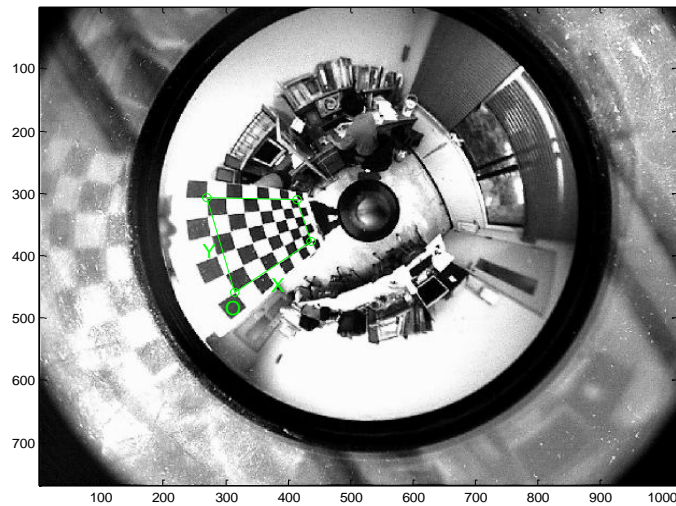


Fig. 5-8 Grids four corners extraction and coordinate

Then, re-projecting the grid pattern and sub-pixel point extraction, one example result is shown in Fig.5-9.

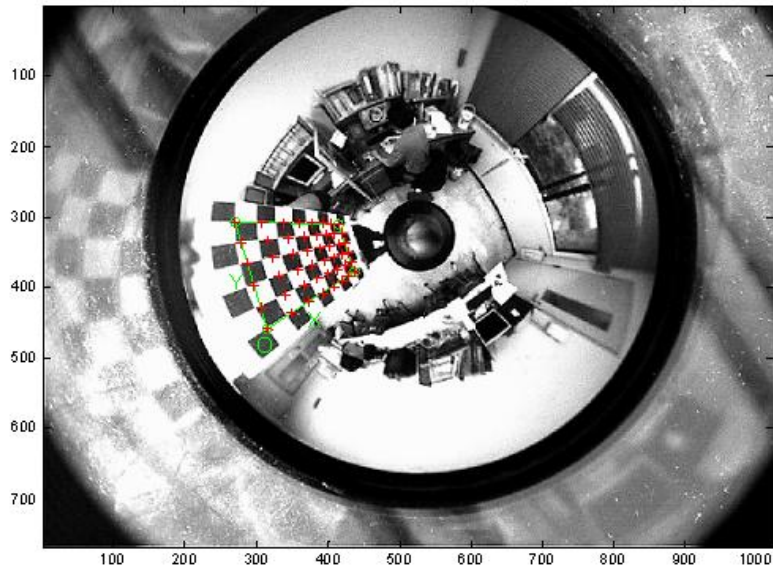


Fig. 5-9 Sub-pixel extraction of the corners

Finally, perform the minimization and optimization.

5.5.3 RESULTS

5.5.3.1 Analysis of errors

As shown in Fig.5-10, distribution of the reprojection errors of grid points for the entire calibration pattern. Colors refer to the different images of the calibration pattern. We can find the pixel errors are less than 2 pixels, which can prove our calibration method is feasible.

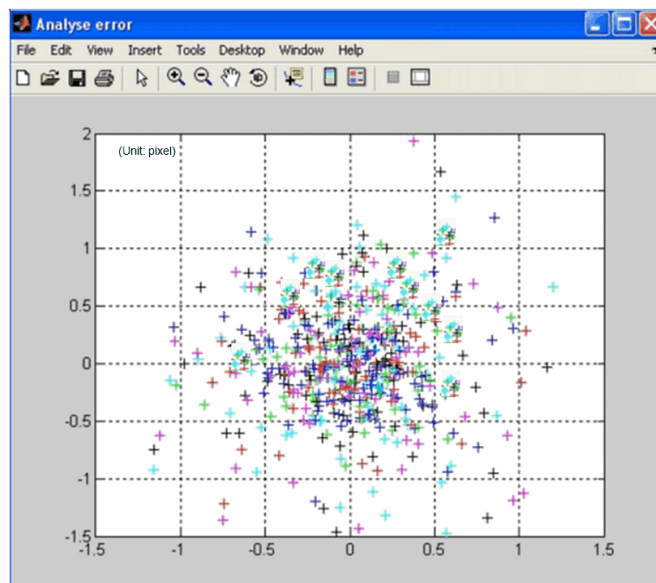


Fig. 5-10 Errors distribution

5.5.3.2 Calibration results

Focal Length: $f_c = [1959.91654] \pm [10.35813]$

Principal point: $cc = [534.69713 \ 320.19981] \pm [11.41115 \ 11.11700]$

Aspect ratio: $\text{gama}_c = [1.16175] \pm [0.01026]$

Skewness: $\text{alpha}_c = [0.23198] \pm [0.05247]$

Mirror parameter: $\xi = [0.75654] \pm [0.348725]$

Distortion: $kc = [-0.03631 \ 0.00339 \ 0.02093 \ 0.00077 \ 0.00000] \pm [0.02779$
 $0.00309 \ 0.01381 \ 0.01161 \ 0.00000]$

Pixel error: $\text{err} = [1.82613 \ 1.95621]$

Translation vector: $Tc_{\text{ext}} = [98.351723 \ -274.904117 \ 275.419452]$

Rotation vector: $omc_{\text{ext}} = [-0.980861 \ -1.362173 \ -0.535005]$

Rotation matrix: $Rc_{\text{ext}} = [0.178990 \ 0.810331 \ -0.557966$
 $0.214024 \ 0.521473 \ 0.825990$
 $0.960290 \ -0.267262 \ -0.080092]$

Pixel error: $\text{err} = [0.70261 \ 0.87714]$

5.6 APPLICATION EXPERIMENTS

Then, we have done experiments to prove the calibration effect for our localization system. We compared the directional angle error, x and y errors, the distance error between estimation position and original position coming from not calibration image with calibrated image. Here, original position is the measurement point and estimation position is the estimated position from the omnidirectional image.

5.6.1 MATERIALS AND METHODS

In our laboratory, in order to ensure to set up landmark and camera position accurately, we set four landmarks on the corners of a small 1.8 m×0.9 m rectangular area. The omnidirectional camera resolution was set at 640×480. For the landmark, we used the red cylinder, the diameter of which was about 6.6 cm and were on the plane ground. We selected 8 original positions ((0, 60)、(30, 60)、(60, 60)、(90, 60)、(0, 120)、(30, 120)、(60, 120)、(30, 120)) to test (red dots as shown in Fig. 5-11). In order to set omnidirectional camera on

the accurate point, the height of camera system directly installed on the ground not lending to support.

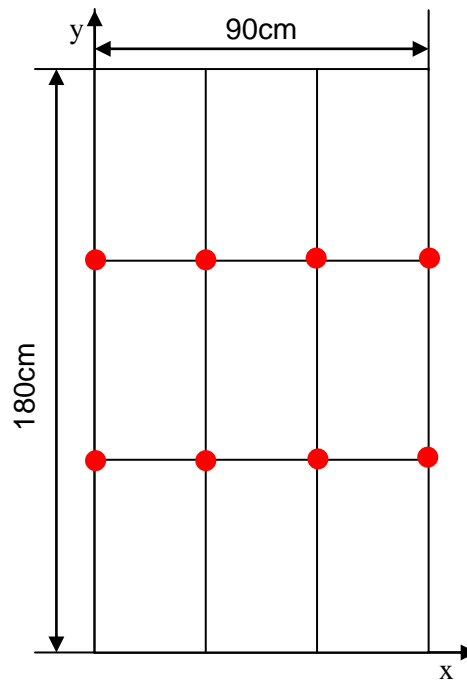


Fig. 5-11 Experimental setting

5.6.2 RESULTS

The experimental results are shown in Table 5-1~5-3. From Table 5-1 the errors of directional angle (Here, original image is one without calibration and rectification image is one calibrated image.), we can know that the errors of directional angles from rectification images are lower obviously than from original images. For example, the RMS error of θ_2 is 2.35° from original images but only 1.6° from rectification images. Just about there are the directional angle errors difference, Table 5-2 and Table 5-3 show that the RMS and mean absolute error (MAE) of x axis, y axis and distance are all less obviously from rectification images. The RMS difference values are about 1.34 cm, 1.18 cm and 1.74 cm in x axis, y axis and distance, respectively. The distance of MAE and RMS error falls down from 4.06 cm to 2.46 cm, 4.25 cm to 2.51 cm, respectively. The role of calibration is very effective because the error decreases essentially. Also, we can find that the errors of directional angle from rectification

images are not less than from original images, which result from the images transformation. Anyhow, the calibration effect is very obvious for our system.

Table 5-1 Absolute errors ($\Delta\theta$) of directional angle

Position (cm)	Original image (°)				Rectification image (°)			
	$\Delta\theta_1$	$\Delta\theta_2$	$\Delta\theta_3$	$\Delta\theta_4$	$\Delta\theta_1$	$\Delta\theta_2$	$\Delta\theta_3$	$\Delta\theta_4$
(0, 60)	2.28	1.13	0.28	3.13	0.81	1.52	0.42	1.13
(30, 60)	3.25	1.64	0.78	4.11	0.95	1.99	0.34	1.38
(60, 60)	1.63	2.04	1.09	2.58	1.42	1.89	0.54	1.01
(90, 60)	0.21	0.94	0.23	0.92	1.20	2.72	0.21	1.30
(0, 120)	0.95	2.76	0.82	2.89	1.08	1.72	1.06	0.43
(30, 120)	1.35	3.57	3.05	1.88	0.98	0.08	1.75	0.85
(60, 120)	1.54	3.15	1.22	3.47	1.07	0.11	1.15	0.20
(30, 120)	1.59	2.20	0.67	3.12	0.88	0.62	1.15	0.89
MAE	1.60	2.18	1.02	2.76	1.05	1.33	0.83	0.90
RMS error	1.81	2.35	1.32	2.91	1.06	1.60	0.97	0.98

Table 5-2 Errors of x, y and distance (D) by original images.

	RMS error (cm)	MAE (cm)	Max. error (cm)	Min. error (cm)
x	2.68	2.54	4.05	0.95
y	3.30	3.06	5.42	0.90
D	4.25	4.06	5.72	1.31

Table 5-3 Errors of x, y and distance (D) by rectification images.

	RMS error (cm)	MAE (cm)	Max. error (cm)	Min. error (cm)
x	1.34	1.16	2.11	0.31
y	2.12	1.93	3.25	0.27
D	2.51	2.46	3.58	2.04

5.7 CONCLUSIONS

This chapter introduced a calibration method for our localization system using 2D calibration pattern. Calibration experimental results showed that the calibration method is feasible and effective. The localization application experimental results showed that

calibration can provide with the principal point value and improve the accuracy about 1.6 cm in our experiments. The role of calibration is very obvious.

In the future, we should improve the calibration method real-time performance. When the agricultural vehicles are working in the fields, the environmental backgrounds often do a harmful effect on the vision system, adjusting the focus is a usual easy method to conquer the problem. Like our using omnidirectional camera, if you adjust the focus, intrinsic and extrinsic parameters will change and need calibrate.

6 LANDMARK IMAGING INFLUENCE ANALYSIS

For the fast and accurate localization applying for agriculture vehicle localization, artificial landmarks can be used very efficiently in the natural environment. Based on the proposed artificial color landmark model in the Chapter 3.3, this Chapter continued to discuss the relations between landmark image size and distance (between landmark and camera), landmark height and camera height, respectively. We theoretically analyzed the method to adjust camera height and landmark height to enlarge application area. Experimental results show that we can obtain relation formulas which help to define the landmark size with application area, adjusting camera height and landmark size can adopt to enlarge application area for our agricultural vehicle localization.

6.1 INTRODUCTION

Our system uses machine vision to extract local information to detect the landmarks and utilize the omnidirectional vision image to calculate absolute position similar to substitute for the function of GPS. The detecting landmarks information is pivotal and difficult. In this chapter, we conclude two related problems for landmark requirements in section 6.2. In section 6.3, theoretical analysis of the necessary to balance camera height and landmark height to enlarge application area has done. In section 6.4, experimental results of landmark image size with different three factors are described. Finally we conclude that the results assist to decide landmark size in the application area.

6.2 TWO RELATED PROBLEMS

6.2.1 LANDMARK DETECTION

Landmark detection is that the landmark features are extracted in the omnidirectional image by image processing. Landmarks are divided into two kinds: natural landmarks and artificial landmarks, which have to be easily detected in the image signal and be locally characterized to distinguish them from others. Those methods using natural landmarks are

more general approaches than those using artificial landmarks. Natural landmarks are chosen in consideration of their particular characteristics in the image. However, extraction of natural landmarks is a difficult task. Artificial landmarks are very simple and powerful for self-localization, which can provide very accurate and robust performance even in the complex environments. In farm fields, the same crop shows the homologous color, so we almost can't use natural landmarks; while we can take the farm field as a stationary environment since the area doesn't change for many years though the crop may be changed usually. Henceforth, we propose using artificial simple color landmarks in a stationary field environment. We have discussed landmark model in Chapter 3 and their algorithm in Chapter 4.

6.2.2 APPLICATION AREA

About this research, we use the system in agricultural field and the agricultural vehicle doesn't only go forward and back like the robot walks on the road. The agricultural vehicle works in a specified area field and executes one task for one time usually. We call the environment as a stationary environment. The area of the stationary environment is named as application area. Application area for common robot navigation indoor and outdoor doesn't investigate because a lot of methods with topological localization just only know mapping (Andreasson, 2007; Cassandra, 1996; Duckett, 1998). Some geometrical localization methods are also just talking about the feasibility but don't make research about application area (Bais, 2006). For our proposed system, we must investigate the application area to testify the research practical application capability. We should prove the camera vision can take image for landmarks clearly. Henceforth, we consider about the two problems and find out its solutions.

6.3 ENLARGING APPLICATION AREA ANALYSIS

In this research, we took the height (width) of landmark size in image (landmark image size) as the standard to consider the capability for application area. For example, if the landmark image height is 10 pixels size, which will be applied wider area than the landmark image height only 5 pixels size. The reason is that if the landmark image height has 10 pixels size, we can enlarge the application area and the landmark image height will become 5 pixels size.

6.3.1 LANDMARK IMAGING

The omnidirectional image is symmetrical in all of directions. Fig.6-1 shows the cross-section of the omnidirectional vision system with landmark imaging.

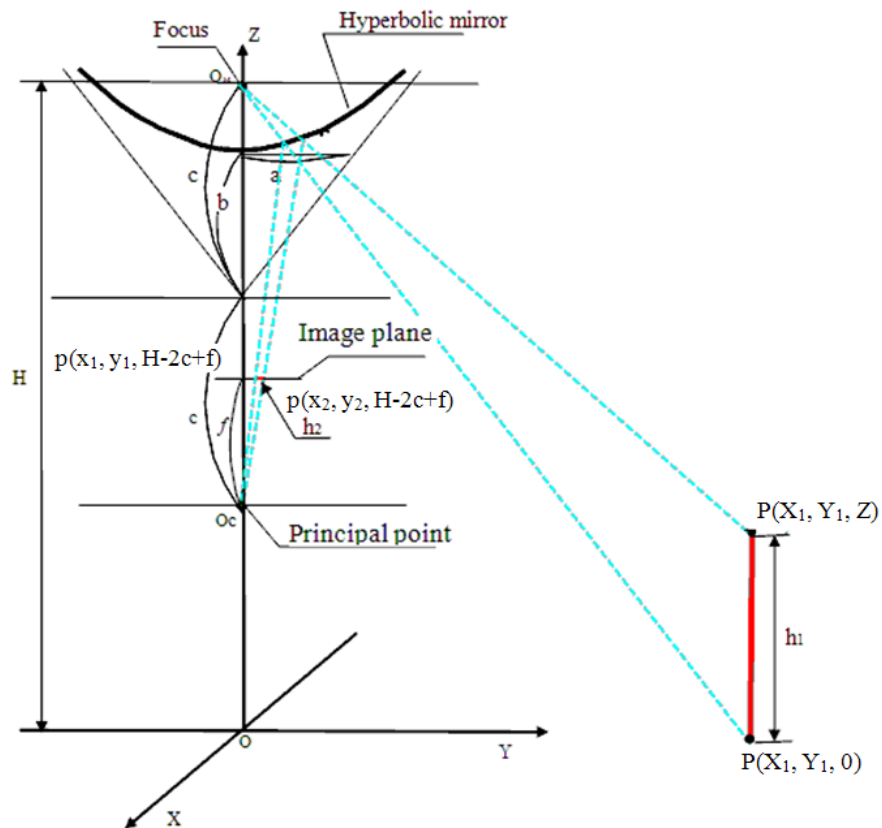


Fig. 6-1 Omnidirectional vision sensor with landmark imaging

The parameters, a and b define the shape of the hyperbolic mirror and $c = \sqrt{a^2 + b^2}$; f is the focus length of camera; H define the camera height off ground. h_1 is the height of landmark; h_2 is the height of landmark image; $P(X_1, Y_1, 0)$ and $P(X_2, Y_2, Z)$ are the top point and the bottom point of landmark, and $p(x_1, y_1, H-2c+f)$ and $p(x_2, y_2, H-2c+f)$ are corresponding point in the image plane, respectively.

We can get the following correlations (6-1) based on the Eq. (3-7) and two points distance Equation.

$$h_2 = fa \sqrt{\left(\frac{X}{(b^2 + c^2)(c - H) - 2bc\sqrt{X^2 + Y^2 + (c - H)^2}} - \frac{X}{(b^2 + c^2)(c - H + h_1) - 2bc\sqrt{X^2 + Y^2 + (c - H + h_1)^2}} \right)^2 + \left(\frac{Y}{(b^2 + c^2)(c - H) - 2bc\sqrt{X^2 + Y^2 + (c - H)^2}} - \frac{Y}{(b^2 + c^2)(c - H + h_1) - 2bc\sqrt{X^2 + Y^2 + (c - H + h_1)^2}} \right)^2}$$

(6-1)

In the correlation, b , c , H and h_1 are constant. The landmark imaging length h_2 is proportional to focus length f .

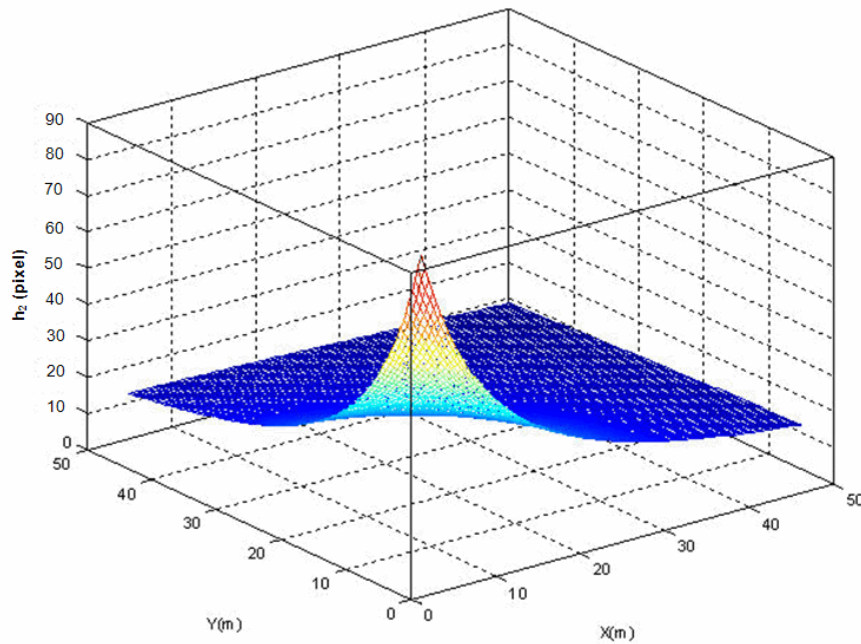


Fig. 6-2 Relation between height of landmark image and X, Y value

We use Matlab 6.5 to simulate the relation between landmark height and landmark image height. In the graph, $b=5$ cm, $c=9.43$ cm, $f=2400$ pixel size, $H=3$ m and $h_1=1$ m. The height of landmark imaging height is almost more than 10 pixels to extract when it is used in the 50 m x 50 m area. If landmark is far away from camera over 30 m, the change of height of landmark image becomes very less. But, we can know, the height of landmark image has about 10 pixels to extract even in the distance about 70 m in the diagonal of the graph. Therefore, the camera and landmark under those conditions are enough to take landmark

features for landmark detection if the environmental conditions (light and air) and camera resolution are enough to take clear image even in a wider 100 m×100 m theoretically.

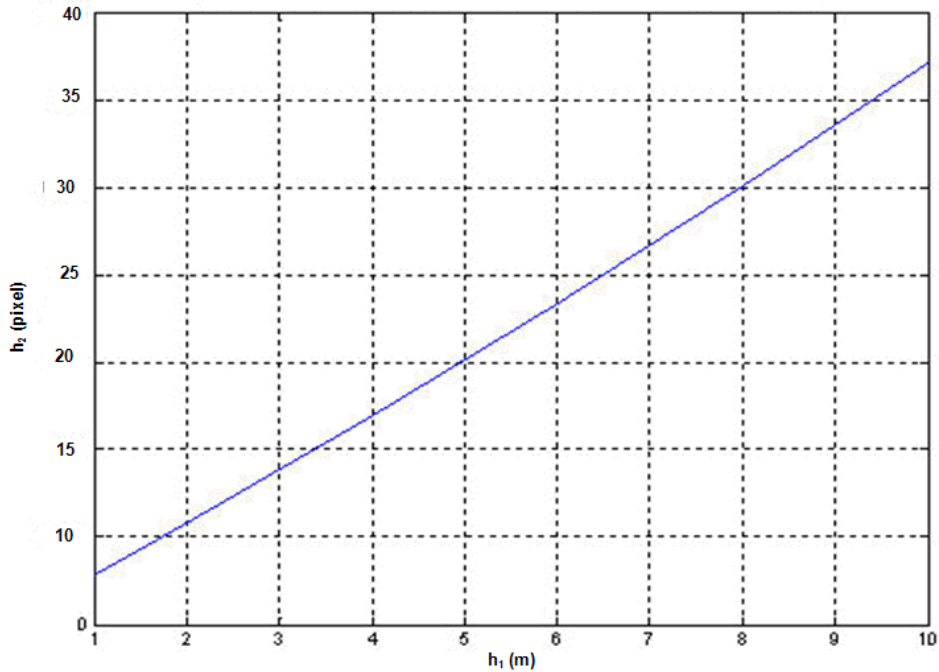


Fig. 6-3 Relation between height of landmark (h_1) and height of landmark image (h_2)

In Fig. 6-3, b , c , f and H are the same parameters as referred above. Supposed the landmark position ($x=50$ m and $y=50$ m). The shape of curve between height of landmark (h_1) and height of landmark image (h_2) is approximate to an increasing line, which expresses that there is a proximate proportional correlation between height of landmark image and landmark height. If lengthen landmark, the height of landmark image will increase. Therefore, one method is that we can adopt to add landmark size (height and width) to enlarge working area.

In Fig. 6-4, b , c and f are the same parameters as referred above and $h_1=2$ m. Also, supposed the landmark position ($x=50$ m and $y=50$ m). The shape of curve between height of landmark image (h_2) and height of camera is approximate to a descending line, which expresses that there is a proximate inverse proportional correlation between height of landmark image and camera height. Therefore, another method is that we can consider adjusting down the height of camera some extent to increase landmark size in the image.

In theory, the omnidirectional camera is enough to apply for 50 m×50 m area under the conditions, e.g. height of landmark 2 m, focus length 10 cm. We can also adopt to add landmark size and adjust down the height of camera to enlarge application area.

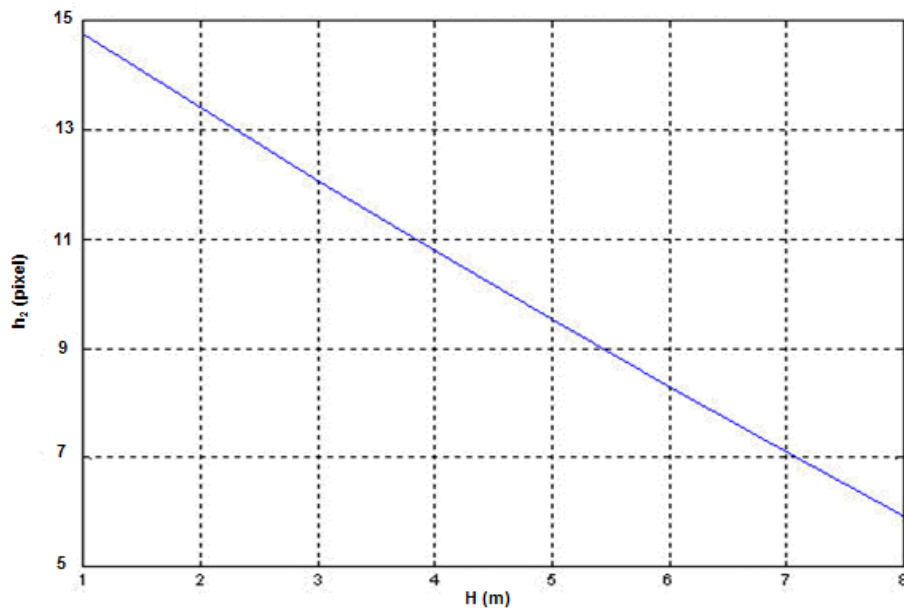


Fig. 6-4 Relation between height of camera (H) and height of landmark image (h₂)

6.4 EXPERIMENTS

6.4.1 MATERIALS AND METHODS

We have done three experiments on the horizontal asphaltic ground in the sun. We used tripod to support camera and landmark to adjust their height expediently. The image resolution was set at 2048(H) ×1536(V); image format 24 bit RGB. Landmark was formed by cylinder part (Diameter 20 cm) and road cone part (bottom diameter about 25 cm) which kept the landmark steady with the landmark height increasing. Using the maximum measurement values (Unit, pixel) for our proposed estimation values, measurement software is Cam View2.5 (Cam View2.5 Information). In order to improve the definition of landmark image and measurement accuracy, we didn't move too long distance. But the result can enough explain the variation trend of size of landmark image. About the three experiments:

(1) Change the distance (L) between landmark and camera. Height of camera (H=1.45 m) and Height of landmark (h₁=2 m) are constant.

(2) Change the landmark setting height. The distance between landmark and camera (50 m) and camera height ($H=1.45$ m) are constant. Landmark setting height is the height of landmark from the ground level.

(3) Change the camera height (H). The distance between landmark and camera (50 m) and landmark height ($h_1=2$ m) are constant.

6.4.2 RESULTS AND ANALYSIS

6.4.2.1 Relation of size of landmark image and distance between landmark and camera

Fig. 6-5 shows relation of size (height and width) of landmark image and distance between landmark and camera. With the distance increasing, the size of landmark image decreases speedy first and then the shape of curve becomes approximate to a line with a constant. For enlarging application area, it is necessary to define the constant to satisfy image processing detecting landmark features. From Fig. 6-5, we can find the landmark image height experimental curve is approximate theory curve simulated by Eq. (6-1).

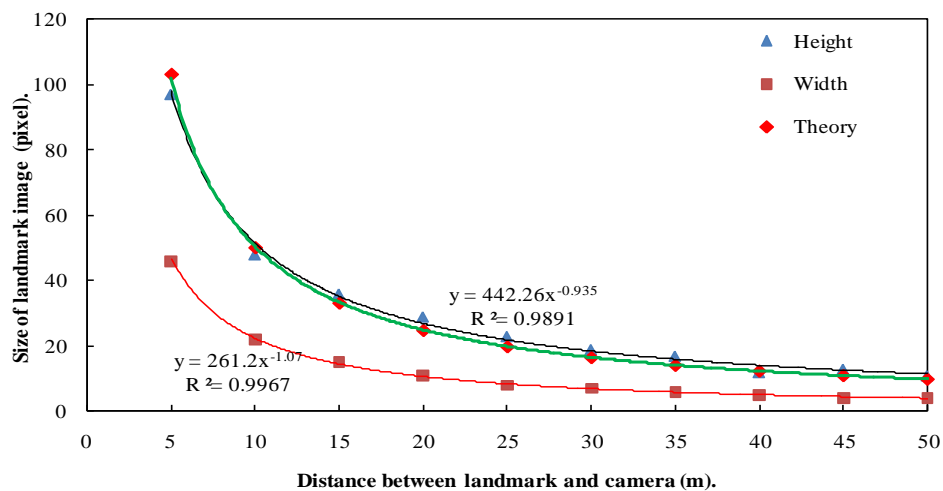


Fig. 6-5 Relation of size (height and width) of landmark image and distance between landmark and camera

We can obtain the following Least Square Fit relation between height of landmark image (y) and the distance (x) between landmark and camera.

$$y = 442.26x^{-0.935} (R^2 = 0.9891) \quad (6-2)$$

And obtain the following Least Square Fit relation between width of landmark image (y) and the distance (x) between landmark and camera.

$$y = 261.2x^{-1.07} (R^2 = 0.9967) \quad (6-3)$$

According with the relations, we can decide landmark size with application area size.

6.4.2.2 Relation of size of landmark image and landmark setting height

Fig. 6-6 shows relation of size (height and width) of landmark image and height of landmark. We can know that the size of landmark image increased with the height of landmark increasing, but the change is not very obvious. In the results, the curves of width and height of landmark image are close approximation to two increasing lines. Experimental results showed that we can increase the landmark setting height to increase the height of landmark image. We also deduced that we can adopt to add landmark size (height and width) to add size of landmark image, which verified the above theoretical analysis (as shown in Fig. 6-3).

We can obtain the following Least Square Fit relation between height of landmark image (y) and landmark setting height (x) from the ground level.

$$y = 14.058x^{0.3072} (R^2 = 0.91) \quad (6-4)$$

Also, obtain the following Least Square Fit relation between width of landmark image (y) and landmark setting height (x) from the ground level.

$$y = 6.944x^{0.4728} (R^2 = 0.943) \quad (6-5)$$

According with the experimental results, the landmark setting height is higher and the height of landmark image is higher. However, the visible area of omnidirectional camera limits the landmark height and setting height.

Our utilized omnidirectional camera illustration of landmark height was shown in Fig. 6-7. The visible area is about 75 degree. The top position of landmark limits to about $(H + L \tan 15^\circ)$.

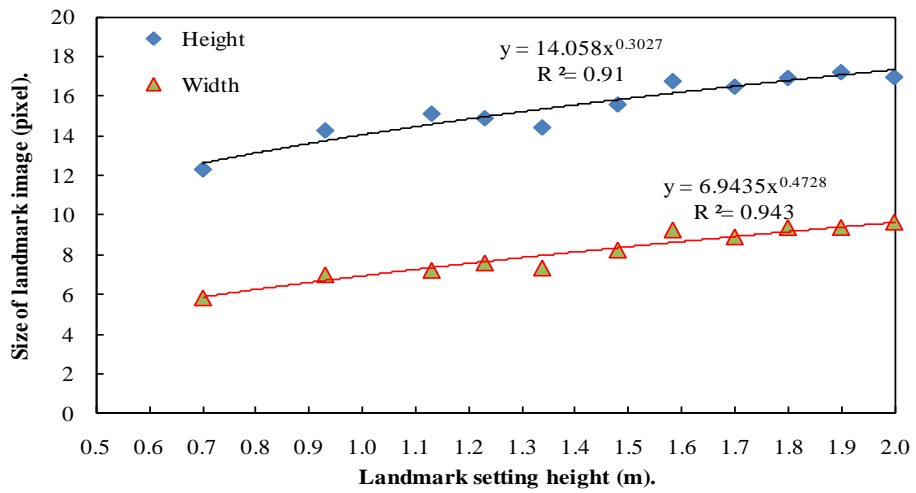


Fig. 6-6 Relation of size (height and width) of landmark image and height of landmark

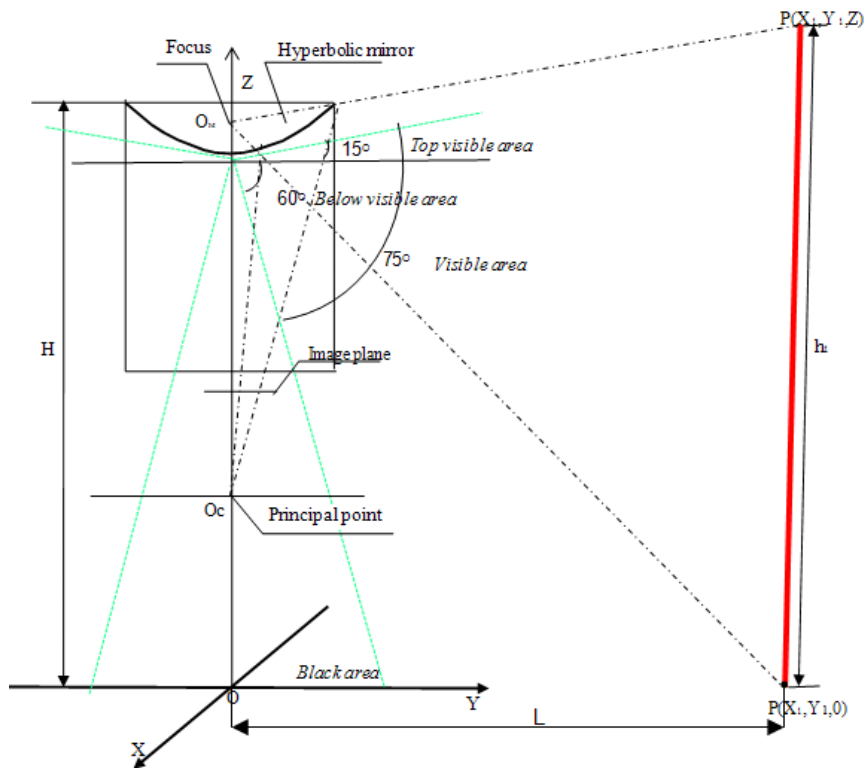


Fig. 6-7 Illustration of landmark height

The omnidirectional sensor has black area and visible area. Black area refers to the area that hyperbolic mirror can't absorb reflection lights of object decided by structure design. Visible area for our system is about 75 degree including top visible area and below visible

area. For example, if the height of landmark is over h_1 in this figure, it can't also result in increasing height of landmark image. We also can find that it is feasible and effective to obtain the maximum height of landmark that is higher than height of camera based on maximum distance between landmark and camera.

6.4.2.3 Relation of size of landmark image and height of camera

Fig. 6-8 shows relation of size (height and width) of landmark image and height of camera.

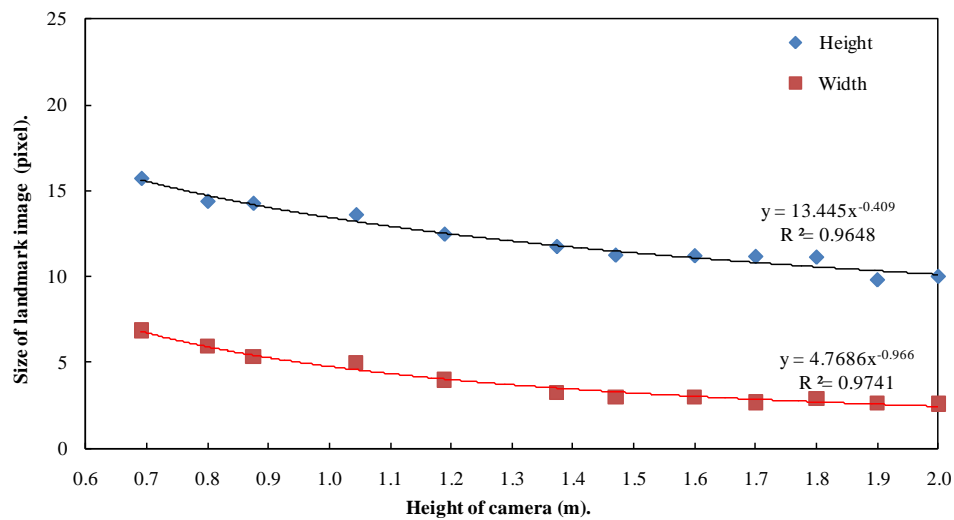


Fig. 6-8 Relation of size (height and width) of landmark image and height of camera

We can know the size of landmark image decreases with the height of camera increasing, which verified the above theoretical analysis as shown in Fig. 6-4. Although, if the size of landmark image is too small to detect features, adjusting low the height of camera is a measurement, it is necessary to guarantee to the lowest height for taking the image including landmarks.

Via the experimental results, we can obtain the following Least Square Fit relation between height of landmark image (y) and height of camera (x) from the ground level.

$$y = 13.332x^{-0.407} (R^2 = 0.9511) \quad (6-6)$$

Also, obtain the following Least Square Fit relation between width of landmark image (y) and height of camera (x) from the ground level.

$$y = 4.724x^{-0.979} (R^2 = 0.9604)$$

(6-7)

6.5 CONCLUSIONS

We can conclude that there are correlations about size of landmark image with distance between camera and landmark, landmark setting height and height of camera, respectively. Experimental results showed that (1) with the distance between landmark and camera increasing, the size of landmark image decreases speedy first and then the shape of curve becomes approximate to a line with a constant; (2) with the landmark setting height increasing, the size of landmark image increases; and (3) with the height of camera increasing, the size of landmark image decreases. In order to enlarge application working area, it is necessary to consider the size of landmark image constant decided by distance between landmark and camera, balancing height of camera and landmark to satisfy with the basic requirement for detecting landmark features in image.

7 EVALUATION OF THE SYSTEM

In order to prove the localization system, we have done indoor experiments and outdoor experiments to verify the feasibility and effectiveness for indoor and outdoor field. The agricultural vehicle system is operated on uneven ground usually, camera tilt experiments also have done to test the errors caused by tilt angle. Indoor experiments were conducted under daylight lamps in a 5.8 m×3.53 m rectangular area of the laboratory, and outdoor experiments were conducted under natural sunlight in a 50 m×50 m square area to verify the system. Indoor experimental results showed that all the errors were less than 8 cm in an illuminated and small environment. Outdoor experimental results showed that the maximum and RMS distance errors were about 46.96 and 34.24 cm, respectively; camera tilt experiments showed that the tilt angle had some effect on errors, but not to an obvious level, and it was not necessary to compensate for the errors caused by camera tilt. In conclusion, this system is a potential substitute for GPS in agricultural vehicle navigation required for indoor and outdoor environments in the future.

In this Chapter, section 7.1 introduces experimental main devices and scenes. In section 7.2 to 7.4, indoor experiment, outdoor experiment and camera tilt experiment are represented the methods, results and discussion in detail. Finally, conclusion is drawn.

7.1 EXPERIMENTAL DEVICES AND SCENES

7.1.1 DEVICES

7.1.1.1 *Camera system*

The omnidirectional camera system is introduced in Chapter 3.3.2. The experimental device is shown as in Fig. 7-1.



Fig. 7-1 Experimental device

7.1.1.2 Measurement

Nikon laser distance measurement (left) and common measurement (right) (as shown in Fig. 7-2).



Fig. 7-2 Distance measurement tools

The laser distance measurements can provide with directional angle and distance data.

7.1.1.3 Landmark

Landmark is divided into two kinds. The shape is column form (Fig. 7-3). Landmark (1) is used indoor small area, which the diameter is about 6.6 cm and the height about 20 cm. The second is used outdoor about 50 m×50 m area, which the diameter is about 25 cm and the height about 100 cm.



Fig. 7-3 Landmark (1)



Fig. 7-3 Landmark (2)

7.1.2 SCENES

7.1.2.1 Indoor scene



Fig. 7-4 One indoor scene

7.1.2.2 Outdoor scene



Fig. 7-5 One outdoor scene

7.2 INDOOR EXPERIMENT

7.2.1 METHODS

The indoor experiment was conducted in our laboratory under a daylight lamp environment to simulate greenhouse conditions. For the landmarks, we used the red and blue patches

combination cylinder, the diameter of which was about 6.6 cm and the height 20 cm. Landmarks were installed at a height of 150 cm at the four corners of a 5.8 m×3.53 m rectangular area. The height of the camera was adjusted to 130 cm and the image resolution was set at 1028×768. We selected 10 positions within the rectangular area and calculated the intersections and estimated position of each landmark by image processing.

7.2.2 RESULTS AND DISCUSSION

Fig. 7-6 shows the comprehensive results for the intersections and estimated positions. The estimated positions are shown by the symbol (*) (center of gravity of four intersections) and they almost cover the original positions, which are shown by the symbol (+). The intersections are shown by the symbol (x) with some of them deviating slightly from the original position due to measurement error and landmark feature pixel extraction error.

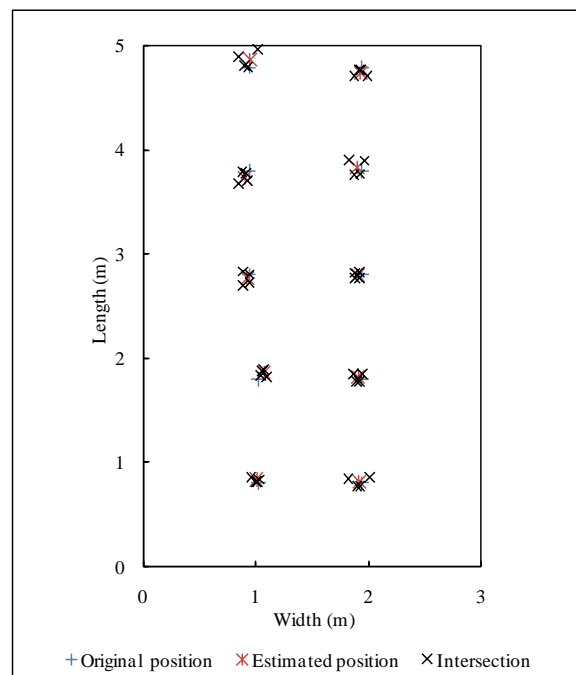


Fig. 7-6 Experimental results depicted on a map

Table 7-1 shows that the maximum error in the x-axis and y-axis is 4.85 and 6.99 cm, respectively. The maximum error in distance between original points and estimated points is 7.8 cm. All errors are less than 8 cm and distance RMS error is 5.3 cm. The accuracy is very

good in the small area and the experimental results prove that the proposed system adapts to working indoors in an illuminated environment.

Table 7-1 Errors in x, y and distance (D) in indoor experiment

	RMS error (cm)	MAE (cm)	Max. error (cm)	Min. error (cm)
x	2.94	2.59	4.85	0.55
y	4.40	3.84	6.99	0.19
D	5.30	4.98	7.80	2.43

7.3 OUTDOOR EXPERIMENT

7.3.1 METHODS

The outdoor experiment was conducted on flat ground under natural sunlight. We used the red cylinders combined with red road cones as the landmarks and set them up at the four corners of a 50 m×50 m square area, the bottom diameter of which was about 25 cm and the height about 100 cm. The height of the camera was adjusted to 186 cm and the image resolution was set at 2048×1536 because of the wide area. We selected 16 positions to test the estimated positions and original positions.

7.3.2 RESULTS AND DISCUSSION

Fig. 7-7 shows the experimental results. The original positions are represented by circle symbols (o); the estimated positions are represented by intersection symbols (×).

Table 7-2 shows that the MAE in the x-axis is 25.47 cm and the MAE in the y-axis is 14.53 cm. The MAE in distance between original positions and estimated positions is 31.99 cm. The RMS error of x-axis, y-axis and distance are 29.75 cm, 17.32 cm and 34.24 cm. The maximum error in the x-axis is 45.60 cm and the maximum error in the y-axis is 35.40 cm. The maximum error in distance (D) between the original positions and estimated positions is 46.96 cm, respectively. The maximum error in distance shows that the results are not very good. This research proposed accuracy is about 50 cm to 100 cm for the agricultural application purposes, so the accuracy is also adaptive and feasible. One of the main reasons is the landmarks and camera positions measurement errors when we set up them in the 50 m

× 50 m square area by measure manually. Second, there is error about the recognition of landmarks.

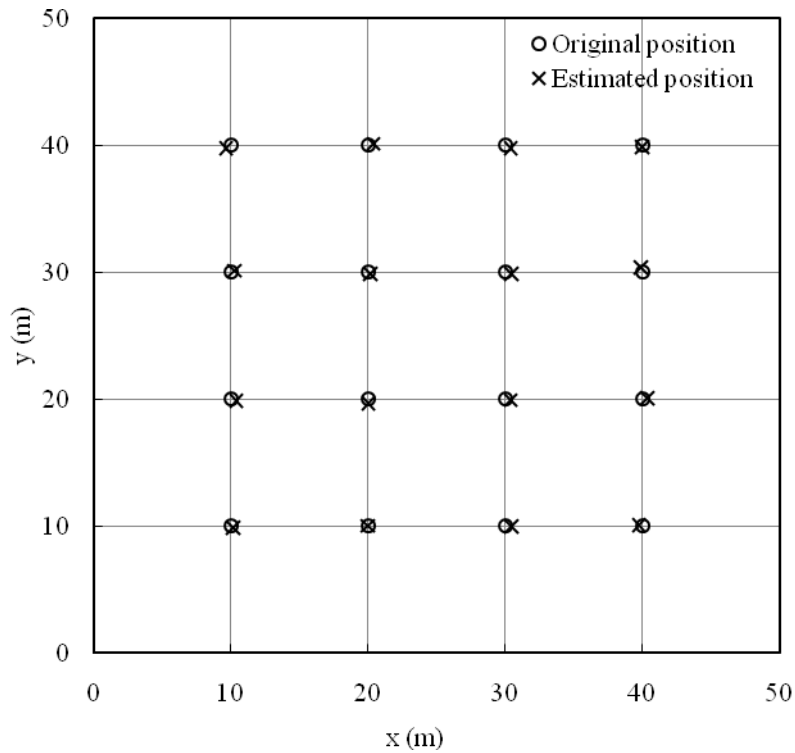


Fig. 7-7 Experimental results for original and estimated positions

Table 7-2 Errors in x, y and distance (D) in outdoor experiment

	RMS error (cm)	MAE (cm)	Max. error (cm)	Min. error (cm)
x	29.57	25.47	45.60	0.20
y	17.32	14.53	35.40	1.40
D	34.24	31.99	46.96	2.05

7.4 CAMERA TILT EXPERIMENT

7.4.1 METHODS

Since agricultural vehicles often operate on uneven ground and there is vibration caused by engine, they are easy to cause camera tilt. Imou et al. (1997) concluded that the tilt angle caused by above referred two factors was usual about less than 5° based on agricultural vehicle practical experiments in the field. According the tilt angle standard (5°), we have

conducted a tilt experiment to determine the level of accuracy influenced by the camera tilt angle.

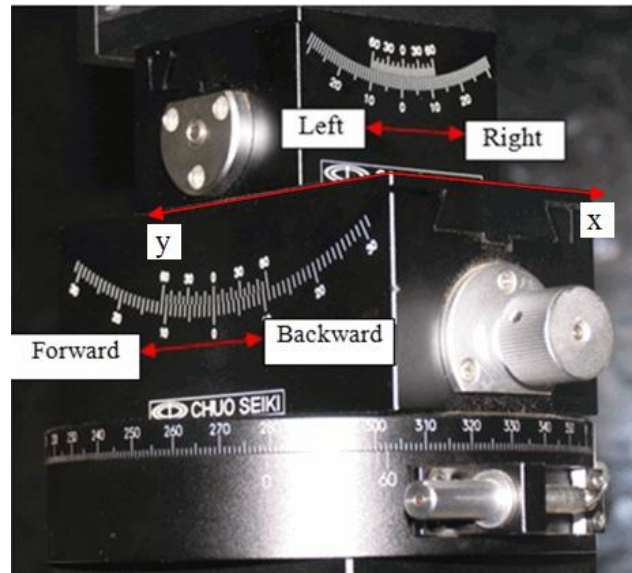


Fig. 7-8 Equipment for adjusting camera angle

We conducted the camera tilt experiment immediately after the outdoor position tracking experiment, using the same setup: red cylinders combined with red road cones as landmarks set up at the four corners of a 50 m × 50 m square area, bottom diameter about 25 cm, height about 100 cm, camera height 186 cm and image resolution 2048×1536. As shown in Fig. 7-8, we used Chuo Seiki precision equipment for adjusting the camera angle by hand. The equipment has two functions for changing the tilt angle: one for tilting right or left in x direction, and the other for tilting forward or backward perpendicular to the direction of tilting right or left as y direction. We defined the right tilt or forward tilt as a positive tilt angle and set the right or left tilt parallel to the x-axis and the forward or backward tilt parallel to the y-axis on the ground coordinate system. We selected 6 positions $(x, y) = (1000, 250), (2000, 250), (3000, 250), (1000, 3000), (2000, 3000),$ and $(3000, 3000)$ (unit: cm) near the edge and in the middle of the square area. At every position, all images were taken by adjusting the camera tilt one degree and 11 images were taken from -5° to $+5^\circ$ in one direction. We selected 4 combinations of angle tilt direction: right and left, forward and backward, combined right and

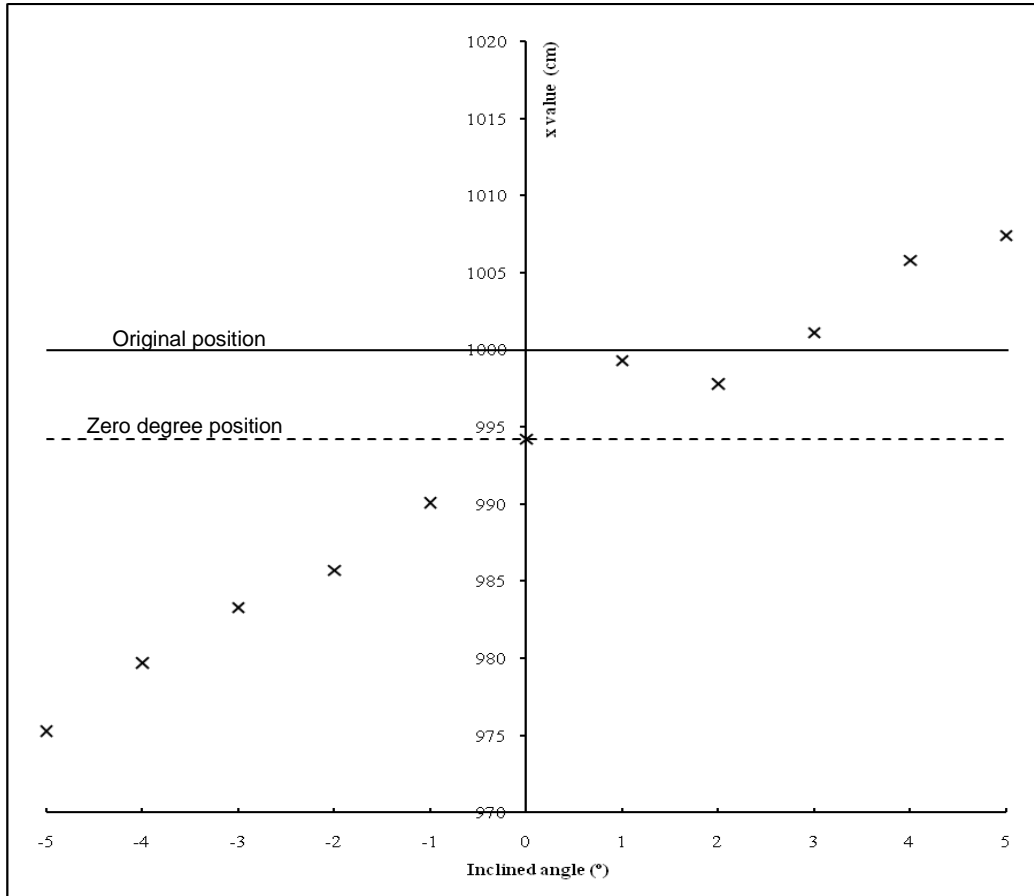
left with forward and backward, combined right and left with backward and forward. Thus, for each different position, a total of 41 images were taken. Then, the x- and y-axis coordinate values of every estimated position were obtained. We defined the selected positions in the ground coordinate system as the original positions; when the tilt angle of the camera was zero degrees, we defined the position as the zero degree position. We then calculated the distance between estimated position and zero degree position, and the distance between estimated position and original position, respectively.

7.4.2 RESULTS AND DISCUSSION

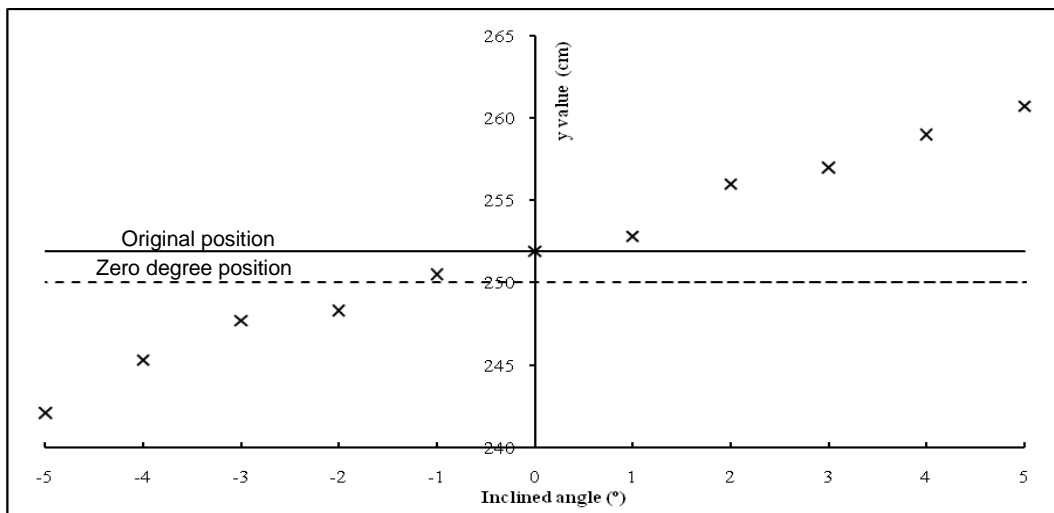
Fig. 7-9 shows an example of the experimental results. The original position (1000, 250) was determined through measurement, where we adjusted the camera to tilt in the direction of combined right and left with forward and backward, which caused the maximum possible errors in the tilt direction. We used our system to estimate the zero degree position (994.28, 251.96); thus the errors in x and y values were 5.72 and 1.96 cm, respectively. In Fig. 7-9 (a) and (b), the x and y of the original position are represented by a line, the x and y of the zero position are represented by broken lines and the estimated positions are represented by the symbol (\times). When the camera was tilted to the right and forward simultaneously, x and y values increased and deviated farther from the zero degree position with increasing tilt angle. On the contrary, when the camera was tilted to the left and backward simultaneously, x and y values decreased and also deviated farther from the zero degree position with increasing tilt angle. For example, in Fig. 7-9 (a), with the increasing tilt angle, the estimated position is close to the x value of the original position (1000) at the first stage due to the error in estimating the zero degree position. The varying trend in x and y values was correct. Fig. 7-9 (c) shows the x, y and distance errors relative to the zero degree position. These errors increase with increasing tilt angle. The maximum error in distance, x and y is 21.29 cm, 9.8 cm and 18.9 cm, respectively, when the tilt angle is -5° . Fig. 7-9 (d) shows the x, y and distance errors relative to the original position. These errors also increase with increasing tilt angle. The maximum distance error and y error are 25.93 and 24.7 cm, respectively, when the tilt angle is -5° ; the maximum x error is 10.7 cm when the tilt angle is 5° . Combined with all experimental results, there are varying trends in x and y values with the change in tilt angle

and its direction. All maximum errors show the same trend when the tilt angle is $+5^\circ$ or -5° .

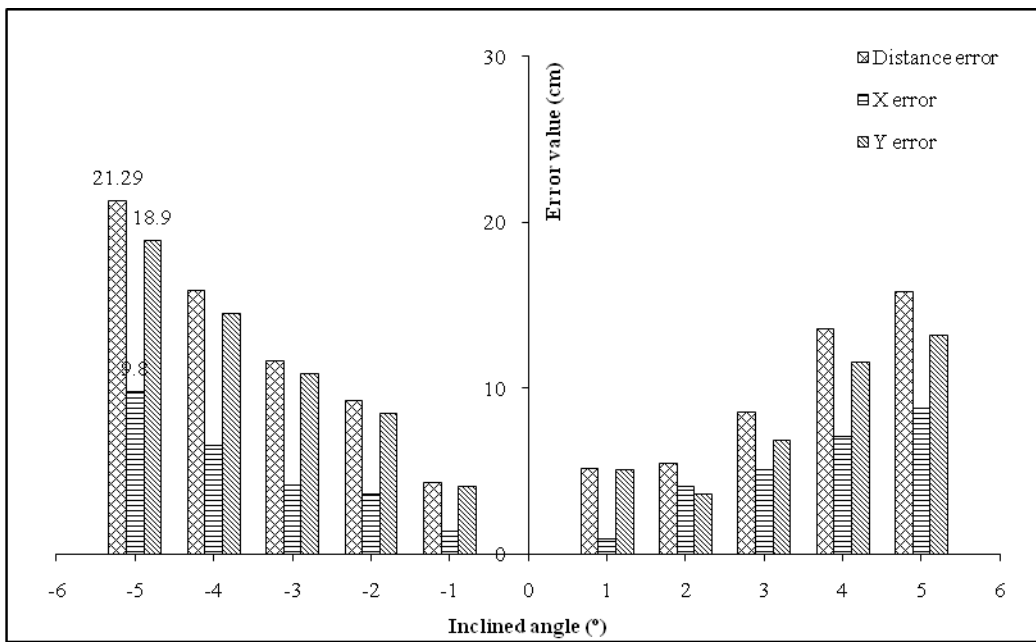
We can conclude that the errors will increase when the camera is tilted.



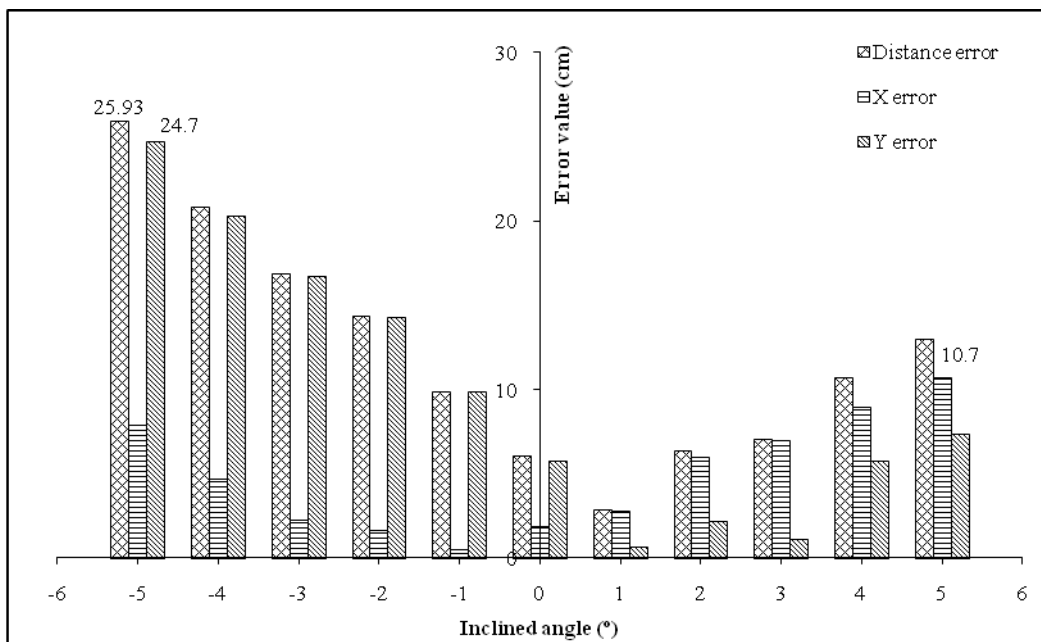
(a) Variation in x values



(b) Variation in y values



(c) Errors relative to zero degree position



(d) Errors relative to original position

Fig. 7-9 Example of x and y values and errors varying with tilt angle

Table 7-3 shows the error results relative to the zero degree position. The MAE in x, y and distance is 8.08 cm, 12.61 cm and 17.01 cm, respectively, which shows that the tilt angle has an influence on the level of accuracy, but the maximum error is less than 25 cm.

Table 7-4 shows the distance errors relative to the zero degree position with the tilt angle varying for the 6 positions. With increasing tilt angle, the error in distance becomes larger. When the tilt angle reaches $\pm 5^\circ$, the RMS, MAE, maximum and minimum errors in distance are 18.65 cm, 17.16 cm, 21.77 cm and 12.99 cm, respectively. Therefore, we consider that the accuracy influenced by the camera tilt angle is not significant. Our system does not require compensation for errors caused by the camera tilt angle.

Table 7-3 Errors in x, y and distance (D) relative to zero degree position

	RMS error (cm)	MAE (cm)	Max. error (cm)	Min. error (cm)
x	8.54	8.08	16.61	1.11
y	13.65	12.61	24.20	1.71
D	18.25	17.01	24.23	11.11

Table 7-4 Errors in distance (D) relative to zero degree position with varying tilt angle

Tilt angle ($^\circ$)	RMS error (cm)	MAE (cm)	Max. error (cm)	Min. error (cm)
± 1	10.89	8.77	16.95	4.75
± 2	12.46	11.59	15.54	7.33
± 3	13.56	13.06	17.54	10.12
± 4	16.60	14.90	18.11	10.32
± 5	18.65	17.16	21.77	12.99

7.4.3 POSITION ERRORS WITH CAMERA TILT

Table 7-4 shows the position error results with camera tilt. The RMS in x, y and distance are 32.23 cm, 20.15 cm and 40.12 cm; 52.36 cm, respectively. The maximum errors in x, y and distance are 52.36 cm, 50.45 cm and 54.65 cm, respectively. Compared with Table 7-2, the distance RMS and maximum errors increase about 6 cm and 5 cm, respectively. The error increases but not very obvious with camera tilt. For this research objects proposed accuracy about 50 cm to 100 cm, the accuracy is adaptive and feasible.

Table 7-5 Errors in x, y and distance (D) with camera tilt

	RMS error (cm)	MAE (cm)	Max. error (cm)	Min. error (cm)
x	32.23	29.65	52.36	1.12
y	20.15	18.96	50.45	1.40
D	40.12	38.46	54.65	10.23

7.5 CONCLUSIONS AND FUTURE WORK

We can conclude that our proposed system is a feasible application for agricultural vehicle navigation. The system can successfully estimate absolute camera localization using the proposed methods and algorithms. Indoor experimental results show that the MAE in x, y and distance are less than 8 cm in a small area and illuminated environment. The accuracy is very good. The outdoor experimental results show that the maximum and MAE position errors are about 46.96 and 31.99 cm, respectively, in a 50 m×50 m square area. The errors are a little big, but for this research objects proposed accuracy about 50 cm to 100 cm, which is adaptive and feasible. The results of the camera tilt experiment show that the tilt angle has some effect on errors, but it is not obvious; the maximum error in distance is 21.77 cm relative to the zero degree position when the tilt angle is $\pm 5^\circ$. We need not compensate for errors caused by camera tilt. Combined with camera tilt, the position distance RMS error is about 40 cm, although overall accuracy is a little lower, the localization can compensate for GPS utilizing in the valley, apply for the forage operation agricultural vehicle and improve the precision agriculture, e.g. mapping localization and mapping operation.

With the application area becoming wider, an increase in measurement errors in landmark setup is inevitable as is an increase in landmark position errors with increasing size for equipment installation. In future field applications, we can solve this problem by building a standard area with precise landmarks. However, a problem that cannot be ignored is that sunlight and a dark background can cause blurring of images and difficulty in detecting landmarks, which reduces the accuracy in outdoor experiments. In our next work, both camera and landmark performance will be considered in order to decrease the influence of outside environments. The landmark model in our system is feasible, but it cannot be adapted to adjust the intensity of reflected light, e.g., a dark background may lead to invisible landmark images and strong sunlight may lead to blurry landmark images. Now, when we used PC (Intel Core 2, 2.33GHz) to estimate a position via a piece of omnidirectional image resolution 2048×1536, it took about 0.1~0.2 s with our program. We should improve the program faster and develop it connecting with autonomous vehicle to practice. We have done the experiments on the even ground and the system is feasible. We should apply the system

working on the slope with considerations such as the landmarks and camera system setting. We also intend to consider countermeasures against camera vibrations when operating. To further advance our system, we intend to research localization and obstacle avoidance for path planning. In next chapter, we will introduce a new localization on road for agricultural field utilizing another omnidirectional camera advantage that there is a permanent correlation between image point and spatial point.

In conclusion, if omnidirectional vision is sufficient for capturing distinct images of landmarks, the proposed system would be a potential compensation or substitute for GPS to realize localization for agricultural vehicles in both indoor and outdoor environments. The system can also be applied for other robotic navigation in specified working areas.

8 FIELD ROAD LOCALIZATION

This chapter introduces an artificial landmark self-localization method using omnidirectional vision for agricultural vehicles field road navigation. We proposed the same landmark model and tracking algorithm to detect easily in different environments similar to field localization referred in the above chapter. We used only two landmarks. The algorithm extracted landmark candidate in the image and estimated the distance between landmark and camera. The self-localization algorithm estimated the absolute location of vehicle relative to the landmark-based coordinate system on the ground. Experimental results show that the RMS distance error is about 15 cm on a 20 m distance experiment. We conclude that the proposed self-localization method is feasible and effective for agricultural vehicles field road navigation.

8.1 INTRODUCTION

In this work, we divide agricultural vehicles localization into two solutions to realize navigation: Field localization and Field road localization. Field localization refers to define a vehicle position in the working field. Field road localization refers to define a vehicle position on the road between the vehicle warehouse and the working field. The above research almost centered on the field localization.

In this paper, we propose to use two simple artificial landmarks and utilize omnidirectional vision to realize self-localization for agricultural vehicle field road navigation. Section 8.2 describes the artificial landmark model and tracking algorithm simply. In section 8.3, we confirm the distance computation model and algorithm for position estimation. Section 8.4 presents the experimental results. Finally, our conclusions are drawn and future works are considered.

8.2 LANDMARKS MODEL AND TRACKING ALGORITHM

On the sides of field road, there is nothing for asphalt/concrete road or just the same plants and grasses, which shows the homologous color, so we almost can't use natural landmarks.

omnidirectional vision can take 360° view image and take landmark image in different directions. In order to preserve the images are taken in all directions as the same result, we design the similar landmark model to the introduced model in Chapter 3.3.3. And the algorithm is the same referred in the Chapter 4.2.1.

8.3 DISTANCE COMPUTATION MODEL

We used the same omnidirectional vision system (Fig. 3-6).and have done the calibration referred in Chapter 5.

First, we analyzed the distance computation model between image distance and spatial distance. The cross-section of the omnidirectional vision system ground point imaging is shown in Fig.8-1(a). The omnidirectional image is symmetrical in all of directions. The coordinate system is represented by 2D X and Z axis. In Fig. 8-1, the incidence light i toward the focus of hyperbolic mirror $O_M(0, H)$ is reflected to converge into perspective camera principal point. As a property of hyperbolic curve, the following formula is given.

$$\frac{(z-H+c)^2}{b^2} - \frac{x^2}{a^2} = 1 \quad (z > 0); c = \sqrt{a^2 + b^2} \quad (8-1)$$

Where a , b and c are the hyperbolic mirror surface structure parameters; H determines the height of the system from the ground.

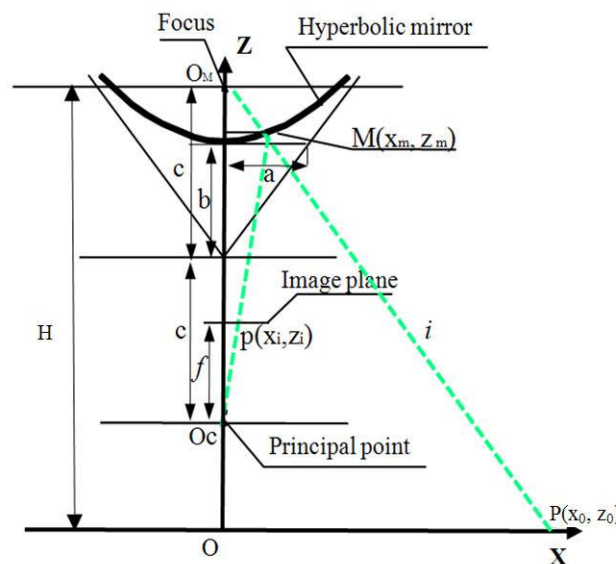


Fig. 8-1 (a) Omnidirectional vision with ground point imaging

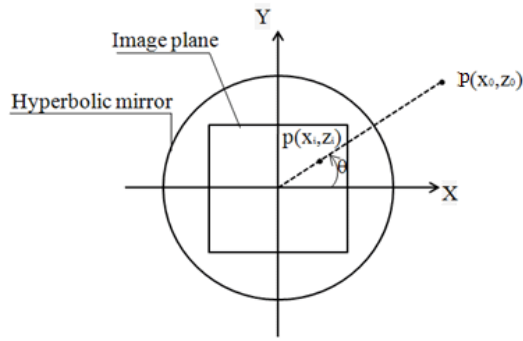


Fig. 8-1 (b) Top view of ground point imaging

A point of landmark $P(x_o, z_o)$ is reflected by point $M(x_m, z_m)$ on the hyperbolic mirror and corresponds to $p(x_i, z_i)$ on the image plane. That is, if there are different landmarks on the ground, it will gain a different point on the image. Fig.8-1(b) shows the omnidirectional vision with imaging top view. We can know that the directional angle θ of landmark and landmark image is same.

The equations for spatial real distance computation from the omnidirectional image are expressed as following processes. First, $M(x_m, z_m)$ is on the hyperbolic mirror, with Eq. (8-1), we can obtain:

$$\frac{(z_m - H + c)^2}{b^2} - \frac{x_m^2}{a^2} = 1 \quad (8-2)$$

$O_M(0, H)$, $M(x_m, z_m)$ and $p(x_o, z_o)$ on the same line, we can describe as Eq. (8-3)

$$z_m = \frac{-H}{x_o} x_m + H \quad (8-3)$$

From the similitude of the triangles, we can obtain

$$\frac{x_i}{x_m} = \frac{f}{z_m - H + 2c} \quad (8-4)$$

Eq. (8-4) can be transferred into Eq. (8-5)

$$x_m = \frac{2cx_o x_i}{x_o f + x_i H} \quad (8-5)$$

Substituting the x_m with Eq. (8-5) to Eq. (8-3), we can obtain the relationship z_m and x_i as Eq. (8-6)

$$z_m = \left(1 - \frac{2cx_i}{x_0f + x_iH}\right)H \quad (8-6)$$

Combining Eq. (8-3) and (8-5) with Eq. (8-2) will give a relationship between the real distance x_0 of landmark in the world and distance x_i on the image as Eq. (8-7)

$$\frac{\left(\frac{-2cx_i}{x_0f + x_iH} + c\right)^2}{b^2} - \frac{\left(\frac{2cx_0x_i}{x_0f + x_iH}\right)^2}{a^2} = 1 \quad (x_0, x_i > 0) \quad (8-7)$$

So, if we know the distance on the image, we can get the real distance in the world. Since the omnidirectional image preserves the directional angel θ of the landmark points about z axis as in Fig. 8-1(b), the relationship formula (8-7) is effective in all 360°directions for the desired distance measurement with a single image.

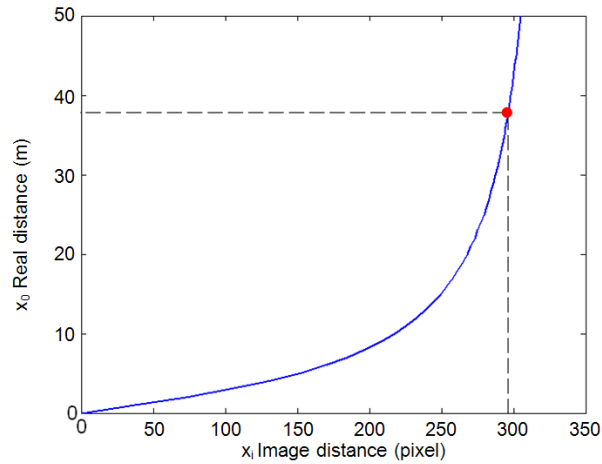


Fig. 8-2 Simulation on real distance (x_i) and image distance (x_0)

Fig. 8-2 shows a simulation relationship curve about image distance x_i and real distance x_0 by Matlab 6.5 when camera height is 145 cm, focal length is about 3 mm and mirror parameters $a=3.5$ cm, $b=5$ cm. The image distance has an apparent increasing when the real distance is less than about 40 m, which can explain the principle that we utilize the feature to implement measuring real distance based on image distance. We can apply it for about 40 m distance measurement.

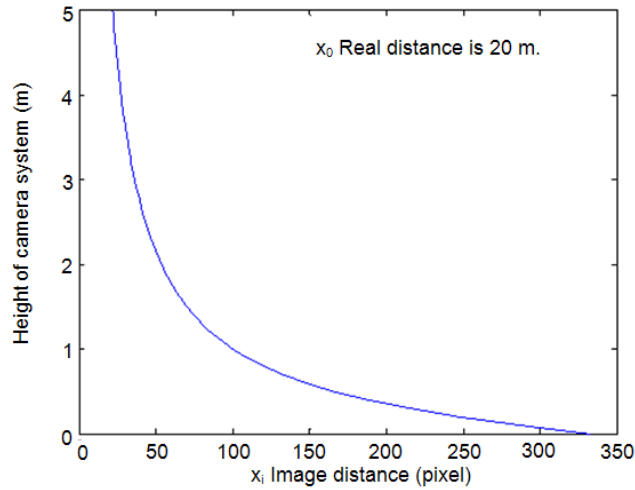


Fig. 8-3 Simulation on image distance (x_i) and height of system (H)

As shown in Fig.8-3, the image distance change value is becoming bigger with the height of H decreasing assuming the spatial real distance is a constant. We defined the sensitivity ($k = \frac{\Delta x_i}{\Delta x_0}$). one way to improve the sensitivity ($k = \frac{\Delta x_i}{\Delta x_0}$) is decreasing height of system. If the sensitivity increases, the image distance change is more and we can obtain the real distance more accurate from image distance. Hence, we should adjust lower of system as soon as possible for our system.

8.4 CAMERA POSITION ESTIMATION METHOD

Suppose two landmarks coordinate are $L_1(x_a, y_a)$ and $L_2(x_b, y_b)$, the distance (L), vehicle coordinate is $I(x, y)$ in the world coordinate system (as shown in Fig.8-4). Using the relationship formula (8-7), we can obtain the real distance between landmark and the vehicle, represented by r_1 and r_2 , respectively. The two circles at L_1 and L_2 can be described by (8-8) and (8-9) as followings.

$$\begin{cases} (x_{II} - x_a)^2 + (y_{II} - y_a)^2 = r_1^2 \\ (x_{II} - x_b)^2 + (y_{II} - y_b)^2 = r_2^2 \end{cases} \quad (8-8)$$

Because the landmarks coordinates $L_1(x_a, y_a)$ and $L_2(x_b, y_b)$ are known, the solutions of the two equations, which are the intersections of the two circles. We will obtain two possible positions in the world coordinate system. Because laid the landmarks on one side of field road

and utilized the boundary of road limiting the necessary position of vehicle, we can choose one right vehicle position candidate in the middle of field road.

Then, we can obtain the directional angle (θ_1) of landmarks utilized the omnidirectional image as referred in Chapter 4. As shown in Fig. 8-4, we define the xy coordinate system. Using the θ_1 and L_{12} can get the following relations and calculate position candidate (x_{12} , y_{12}).

$$X = r_1 \cos \theta_1 + \sqrt{(r_1 \cos \theta_1)^2 - r_1^2 + L_{12}^2} \quad (8-9)$$

$$\cos \theta = \frac{(r_1^2 + L_{12}^2 - X^2)}{2L_{12}r_1}, \sin \theta = \sqrt{1 - \cos^2 \theta} \quad (8-10)$$

We can obtain:

$$\begin{cases} x_{12} = L_{12} - r_1 \cos \theta \\ y_{12} = r_1 \sin \theta \end{cases} \quad (8-11)$$

Using the same method, we also obtain the position candidate $I_3(x_{13}, y_{13})$. The camera position is calculated by Eq. (8-12):

$$\begin{cases} x_1 = (x_{11} + x_{12} + x_{13})/3 \\ y_1 = (y_{11} + y_{12} + y_{13})/3 \end{cases} \quad (8-12)$$

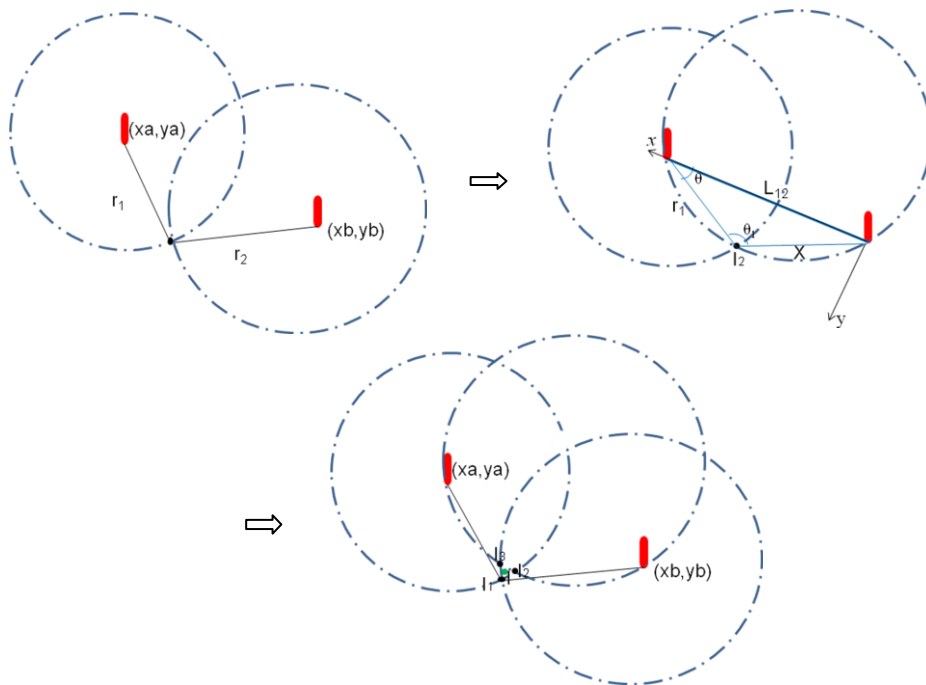


Fig. 8-4 Position candidate calculation method

8.5 EXPERIMENTS

The experiment was conducted on a flat asphalt road in the field under natural sunlight. We set two landmarks (L_1 and L_2) with 20 m distance linearly, then selected 20 positions (O_1 to O_{20}) to take images (as shown in Fig.8-5), the bottom diameter of landmark is about 23 cm and height is 71 cm. The height of the camera was adjusted to 145 cm and the image resolution was set at 1024×768.

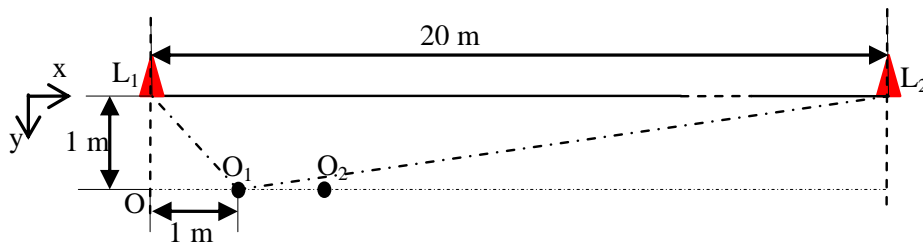


Fig. 8-5 Experimental illustration

8.5.1 RESULTS AND DISCUSSION

Fig. 8-6 shows the results of position tracking. Estimated positions deviate a little from original positions. From Table 8-1, the RMS errors in x , y and distance between original position and estimated position are 13.13 cm, 6.51 cm and 14.66 cm, respectively. The results are feasible for agricultural vehicle field road navigation. However, the maximum error reaches about 50 cm which is too bigger. In this experiment, we used the landmark with height about 70 cm, which affected estimating the distance between the landmark and camera in the image. Second, sunlight may cause image to intensity changing that lead to some error to extract landmark center. Finally, there are errors about parameters of hyperbolic mirror and landmarks installation.

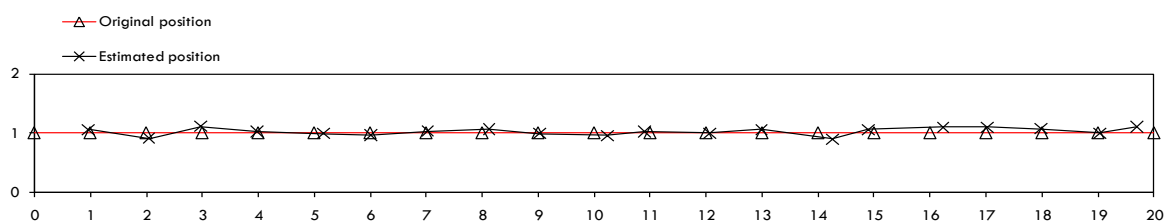


Fig. 8-6 Position tracking result

Table 8-1 Errors in x, y and distance (D) on 20 m distance road experiment

	RMS error (cm)	MAE (cm)	Max. error (cm)	Min. error (cm)
x	13.13	9.43	30.50	1.20
y	6.51	5.45	11.20	0.20
D	14.66	11.89	32.19	3.13

8.6 CONCLUSIONS

We proposed a new road localization method using omnidirectional camera and two landmarks. The experimental results showed that that our proposed artificial landmark self-localization method is a feasible application for agricultural vehicle field road navigation. In this work, the method was applied for about only 20 m distance. In our next work, we will study on for a longer distance application and consider applying this method for a curve path.

9 GENERAL CONCLUSIONS AND FUTURE WORK

9.1 GENERAL CONCLUSIONS

With the problem dwindling in numbers of farm labor force and satisfying with precision agriculture necessary, agricultural vehicle automation is becoming more important. GPS is the most popular method for agricultural vehicle navigation. However, there are some limitations for the future further development. Machine vision is also popular method and other methods like GDS are not matured for application.

In order to compensate for GPS that can use in the places where hills or trees obscure the microwave beams from satellites, resulting in a considerable drop in accuracy, and develop a localization substitute for GPS is used in the forage production and apply for precision agriculture. We develop a new localization system based on omnidirectional vision and artificial landmarks which estimates an absolute position relative to the landmark-based coordinate system on the ground.

The field localization system for agricultural vehicle indoor and outdoor environments consists of four artificial landmarks, an omnidirectional vision sensor, PC and operating vehicle. The system sets four red artificial landmarks as a rectangle in the corners of an operating spot and estimates an absolute position relative to the landmark-based coordinate system on the ground. The principle of localization is that the omnidirectional vision sensor takes the image of the landmarks and estimates the directional angles of landmarks in the image. Camera location was estimated using the center of gravity of the four intersections formed by four arcs according geometric transformation based on the directional angles. The system is not only a potential compensation or substitute for the GPS guidance system to localize agricultural vehicles, but it can also operate common computer vision functions to support localization and obstacle avoidance. Based on the analysis of system features, we know that agricultural vehicles equipped with the localization system will likely carry out navigation using their “eyes” in the same way that mammals move around in the world.

The recognition of landmarks and extraction of features is pivotal to realizing localization. In farm fields, the same crop usually shows a homologous color pattern, which makes it very difficult to utilize natural crop landmarks as features for processing images. Omnidirectional vision having a 360° view can capture landmark images in different directions. In order to ensure that images are captured in all directions and provide the same results, the landmarks are designed as a right circular red cone. Furthermore, to distinguish the landmarks from environmental interferences, we proposed a color model with red and blue pitches.

One algorithm is about landmark tracking extraction in which red landmark pixels beyond the threshold were extracted as a small area and the center of gravity was calculated for the extracted small area representing the candidate of one landmark. Generally, providing the blue patch as compensation to further distinguish the landmark from other objects in a complex environment, blue patch pixels beyond the threshold were extracted as a small area and the center of gravity was calculated and judged the candidate of landmark by the distance between the two centers of gravity. Then the positions of four representative landmarks were obtained.

One image processing is about noise smoothness, which the classic low-pass filter (LPF) is employed to remove high spatial frequency noise from digital images. We multiplied convolution kernel elements by the least common multiple to compute the weighted sum and then divide the summation with the least common multiple to obtain the real results to improve computational speed.

The second algorithm is about estimation of the position of vehicle installed with camera. Based on the obtained positions of four landmarks via the landmark tracking extraction algorithm, and then estimated the four directional angles of the landmarks centered by camera principal point using only one omnidirectional image. Vehicle location was estimated using the center of gravity of the four intersections formed by four arcs according to geometric transformation based on the four directional angles of the landmarks. If only find three landmarks, we also utilize the directional angles to estimate the vehicle location.

In the test, if we used PC (Intel Core 2, 2.33GHz) to process a piece of image resolution 1024×768 , it took only about 0.1~0.2 s. The tracking extraction, position estimation algorithms and image processing (LPF) are robustness.

In the localization algorithm, the principal point in the image is pivotal position and other calibration parameters are useful for improving the accuracy of locating. The calibration method utilized a 2D calibration pattern that can be freely moved. Without a priori knowledge of the motion, the boundary ellipse of the catadioptric image and field of view (FOV) were used to obtain principal point and focal length. Then, a polynomial approximation was used to initialize the extrinsic parameters. Last, the intrinsic and extrinsic parameters are refined by nonlinear optimization. Experimental results are proved to the calibration method which is feasible and effective and localization application experimental results show that calibration can provide with the principal point value and improve the accuracy about 1.6 cm in our experiments. The role of calibration is very obvious.

For the fast and accurate self-localization applying for agriculture, artificial landmarks can be used very efficiently in the natural environment. Based on the proposed artificial color landmark model, balancing landmark height and camera height to enlarge the application area was considered. We theoretically analyzed the necessary to balance camera height and landmark height to enlarge applying area. Experimental results show that adjusting camera height and landmark height can enough enlarge application area for agricultural vehicle localization.

In order to prove the localization system, we have done indoor experiments and outdoor experiments to verify the feasibility and effectiveness for indoor and outdoor field. The agricultural vehicle system is operated on uneven ground usually, camera tilt experiments also have done to test the errors caused by tilt angle. Indoor experiments were conducted under daylight lamps in a $5.8 \text{ m} \times 3.53 \text{ m}$ rectangular area of the laboratory, and outdoor experiments were conducted under natural sunlight in a $50 \text{ m} \times 50 \text{ m}$ square area to verify the system. Indoor experimental results showed that the maximum and RMS errors were less than 8 cm in an illuminated and small environment. Outdoor experimental results showed that the maximum and RMS distance errors were about 46.96 and 34.24 cm, respectively; camera

tilt experiments showed that the tilt angle had some effect on errors, but not to an obvious level, and it was not necessary to compensate for the errors caused by camera tilt. Combined with camera tilt, the position distance RMS error is about 40 cm, although overall accuracy is a little lower, the localization can compensate for GPS utilizing in the valley, apply for the forage operation agricultural vehicle navigation and improve the precision agriculture, e.g. mapping localization and mapping operation. In conclusion, this system is a potential substitute for GPS in agricultural vehicle navigation required for indoor and outdoor environments in the future.

We also introduced a new localization on road for agricultural field utilizing the directional angle and another omnidirectional camera advantage that there is a permanent correlation between the distances from image point to camera principal point on the image and from spatial point to the camera.

We used only two landmarks. The algorithm extracted landmark candidate in the image and estimated the distance between landmark and camera. The self-localization algorithm estimated the absolute location of vehicle. Experimental results show that the RMS distance error is about 15 cm on a 20 m distance experiment. We conclude that the proposed self-localization method is feasible and effective for agricultural vehicles field road navigation.

In a whole, we divide agricultural vehicles localization into two solutions to realize navigation: Field localization and Field road localization. The research mainly developed a localization system for agricultural vehicle in the indoor and outdoor field successfully. We also developed a localization system for agricultural vehicle in the field road. Both of them use the omnidirectional vision with artificial landmarks with simple construction and easy operation.

9.1.1 THE MAIN ORIGINAL CONTRIBUTIONS OF THIS WORK

(1) We proposed a localization system using omnidirectional vision and artificial landmarks, which can be used indoor and outdoor environments. Utilized the directional angle between landmarks to locate absolute position relative to the landmark-based coordinate system on the ground. Agricultural vehicles equipped with the system will likely carry out navigation using their “eyes” in the same way that mammals move around in the world.

(2) A color landmark model was proposed to distinguish even in the complicated natural environments. The Landmark tracking extraction algorithm mainly used color threshold to extract red and blue features and based pixels distance to decide the landmark. This method is simple but effective.

(3) Developed the position estimation algorithm.

(4) A fast and practical method for calibration of omnidirectional vision system was developed. The calibration method utilized a 2D calibration pattern that can be freely moved. Without a priori knowledge of the motion, the boundary ellipse of the catadioptric image and field of view were used to obtain principal point and focal length.

(5) Developed the field road localization system and its algorithm.

9.1.2 A FEW CRITICAL ASPECTS REQUIRING IMPROVEMENT

(1) Sunlight and a dark background can cause blurring of images and difficulty in detecting landmarks. Although the color pitch of landmark model used the stronger reflection performance material, but the problem still exists in the broader area.

(2) The color threshold for landmark extraction algorithm cannot adjust the value automatically. The adjustment by hand regulation makes the working efficiency lower and does not accord with practical application.

(3) There is a contradiction between calibration of omnidirectional vision system and omnidirectional vision system being used. Calibration of omnidirectional vision system is a very necessary work. But the omnidirectional vision system being used is often adjusted the focal length to adapt the environments varying to take images clearly. The calibration costs time and loads down with trivial details for computer.

(4) The application of localization system for field road navigation should prolong the distance and solve the curve road.

(5) The localization system should be installed on agricultural vehicle. Then integrating with all the programs into a set of commercial software to popularize its application.

(6) We should apply the system working on the slope with considerations such as the landmarks and camera system setting.

9.2 FUTURE WORK

The localization system for agricultural vehicle navigation using omnidirectional vision and artificial landmark is developed successfully in the previous theoretical and experimental period and we have done a lot of experiments indoor and outdoor simulated on field environments to prove the effective and feasibility of the system. The next final object is to develop a set of practical and commercial localization system for agricultural vehicle.

In future work, the first will be about the landmark model. The proposed landmark color model was effective in our selected environments about the light intensity or in the sun. Because of the changeful natural environment, the landmark should be adapted to adjust the intensity of reflected light to avoid, e.g., a dark background may lead to invisible landmark images and strong sunlight may lead to blurry landmark images. For example, one solution is that the landmark made material adopts transparent plastic or glass and installs a solar cell to keep the landmark brightness balance, which requires some experiments to test its feasibility including effect and cost, etc.

Landmark model standardization should be considered. Its shape and size correlate with the size of landmark in the image and application area size for the system. Landmark setting is a very tedious job. Therefore, landmark model standardization is one of preface for popular practicality. The color threshold for landmark extraction algorithm should be adjusted the value automatically. We should do experiments to find the relation between environmental factors and the color threshold value, then adopt optical sensor to collect environmental data and select the threshold value.

Second, the practical experiment should be progressed. The first step, we will build a standard field installing landmarks with precise accuracy, then integrate all the programs into a set of software and install the omnidirectional vision system on the agricultural vehicle to do the tests in the field by manpower manipulation, which will check the errors and feasibility. We should consider the vibration of vehicle will lead image to be some blurry and consider whether it needs measurements to improve. Now, when we used PC (Intel Core 2, 2.33GHz) to estimate a position via a piece of omnidirectional image resolution 2048×1536, it took about 0.1~0.2 s with our program. We should improve the program faster and develop it

connecting with autonomous vehicle to practice. The next step, we will integrate with the algorithms as a set of software and installed the whole localization including vision sensor, computer and software on the vehicle automated by GPS and other sensors to prove whether the localization system will substitute for GPS for working in practice. The job will be difficult and some specific works to do, such as sensors fusing, mechanical reset and program improvement, etc.

We have done the experiments on the even ground and the system is feasible. We should apply the system working on the slope with considerations such as the landmarks and camera system setting. If the operation environment is very worse, we should consider utilizing angle sensor to adjust the localization result.

Third, it is about the omnidirectional vision camera. The used omnidirectional vision (Vstone, VS-C-300-TK) camera has a wider field of view and high resolution, but which is not a professional camera for our system. There are obvious shortcomings for the navigation, e.g. the adjustment of focal length is not too much and the performance of taking image is erratic, which is very not fit for the real time operation. Via the calibration results, the distortion (Chapter 5.5.3.2) shows that the production of camera is not precise, misalignment between the camera optical axis and the mirror rotational axis or the lens imperfect shape. The hardware of omnidirectional vision selection is one key point to improve the system accuracy.

Forth, it is about the calibration process. Calibration of omnidirectional vision system is a effective work. But the omnidirectional vision system being used is often adjusted the focal length to adapt the environments varying to take images clearly. The calibration costs time and loads down with trivial details for computer. If there are a lot of real-time-calibration processes, it is impossible to adopt the developed calibration program. Self-calibration is necessary, but the author think the calibration will be very difficult to utilize natural features to accomplish and the accuracy dose not promise. Therefore, if we divide the focal length adjustment as three or four grades and apply the developed calibration program to calibrate in the laboratory and obtain the intrinsic and extrinsic parameters to input to program. According with the consideration, the omnidirectional vision system will be reconstructed.

Besides, we will improve our program that can utilize the directional angle of landmarks to improve the accuracy about the field road localization system. For longer distance application, we will study on the prolonging method and landmark installation. We need to improve hardware such as omnidirectional vision sensor and artificial landmark to test in the night to enlarge the application.

Last, about the commercial plan for the system. Besides considering technologies, the economical feasibility, safety and service system should be recognized.

APPENDIX A-POSITION ESTIMATION VIA GEOMETRY

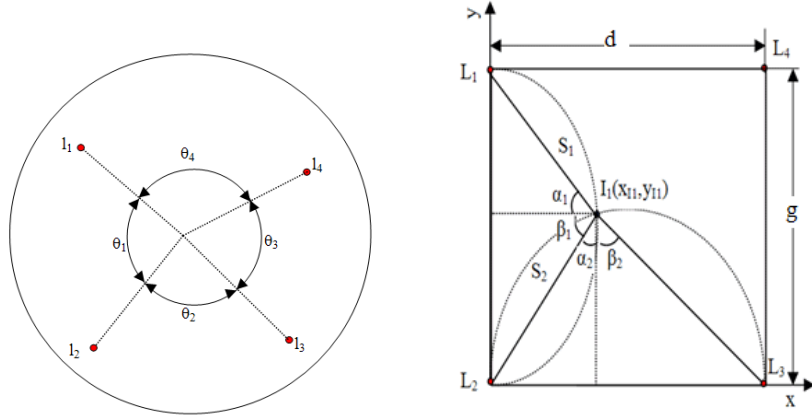


Fig. A-1 Geometrical illustration

From the Fig. A-1, we can obtain:

$$\theta_1 = \alpha_1 + \beta_1 \quad (A1)$$

$$\theta_2 = \alpha_2 + \beta_2 \quad (A2)$$

$$\tan\alpha_1 = \frac{g - y_{11}}{x_{11}} \quad (A3)$$

$$\tan\beta_1 = \frac{y_{11}}{x_{11}} \quad (A4)$$

$$\tan\alpha_2 = \frac{x_{11}}{y_{11}} \quad (A5)$$

$$\tan\beta_2 = \frac{d - x_{11}}{y_{11}} \quad (A6)$$

Then, we deduce that:

$$\tan\theta_1 = \frac{\frac{g}{x_{11}}}{1 - \frac{gy_{11} - y_{11}^2}{x_{11}^2}} = \frac{gx_{11}}{x_{11}^2 + y_{11}^2 - gy_{11}} \quad (A7)$$

$$\tan\theta_2 = \frac{\frac{d}{y_{11}}}{1 - \frac{dx_{11} - y_{11}^2}{y_{11}^2}} = \frac{dy_{11}}{x_{11}^2 + y_{11}^2 - dx_{11}} \quad (\text{A8})$$

Then,

$$\begin{cases} x_{11}^2 + y_{11}^2 - gy_{11} - \frac{gx_{11}}{\tan\theta_1} = 0 \\ x_{11}^2 + y_{11}^2 - dx_{11} - \frac{dy_{11}}{\tan\theta_2} = 0 \end{cases} \quad (\text{A9})$$

We can obtain:

$$\left(\frac{d}{\tan\theta_2} - g \right) y_{11} + \left(d - \frac{g}{\tan\theta_1} \right) x_{11} = 0 \quad (\text{A10})$$

Because in our method, camera position is impossible same to one of landmark positions,

namely, $\frac{d}{\tan\theta_2} - g \neq 0$. We can obtain:

$$y_{11} = \frac{\frac{g}{\tan\theta_1} - d}{\frac{d}{\tan\theta_2} - g} x_{11} \quad (\text{A11})$$

We define:

$$c = \frac{\frac{g}{\tan\theta_1} - d}{\frac{d}{\tan\theta_2} - g} \quad (\text{A12})$$

$$\begin{cases} x_{11} = \frac{g \left(c + \frac{1}{\tan\theta_1} \right)}{1 + c^2} \\ y_{11} = cx_{11} = \frac{gc \left(c + \frac{1}{\tan\theta_1} \right)}{1 + c^2} \end{cases} \quad (\text{A13})$$

APPENDIX B–FOCAL LENGTH CALCULATION VIA GEOMETRY

In Fig. 5-4, let $\theta < 90^\circ$. We have

$$f = |O_c C| = \sqrt{(x - u_0)^2 + (y - v_0)^2} \cot \delta \quad (\text{B1})$$

In $\triangle O_M O_c P_s$, by using the cosine rule, we can obtain:

$$\begin{aligned} |O_c P_s| &= \sqrt{|O_M O_c|^2 + |O_M P_s|^2 - 2 \cos(\pi - \theta) |O_M O_c| |O_M P_s|} \\ &= \sqrt{\xi^2 + 1 + 2 \cos \varphi \xi} \end{aligned} \quad (\text{B2})$$

By applying the sine rule to $\triangle O_M O_c P_s$, the relation:

$$\frac{\sin \delta}{|O_M P_s|} = \frac{\sin(\pi - \varphi)}{|O_c P_s|}$$

Then,

$$\sin \delta = \frac{\sin(\pi - \varphi)}{|O_c P_s|} |O_M P_s| = \sin \varphi \frac{|O_M P_s|}{|O_c P_s|} = \frac{\sin \varphi}{\sqrt{\xi^2 + 1 + 2 \xi \cos \varphi}}$$

We can obtain:

$$\cot \delta = \frac{\cos \delta}{\sin \delta} = \frac{\sqrt{1 - \sin^2 \delta}}{\sin \delta} = \frac{1}{\sqrt{\frac{\xi^2 + 1 + 2 \xi \cos \varphi}{(\xi + \cos \varphi)^2} - 1}} = \frac{1}{\sqrt{\omega - 1}} \quad (\text{B3})$$

Hence, we can obtain:

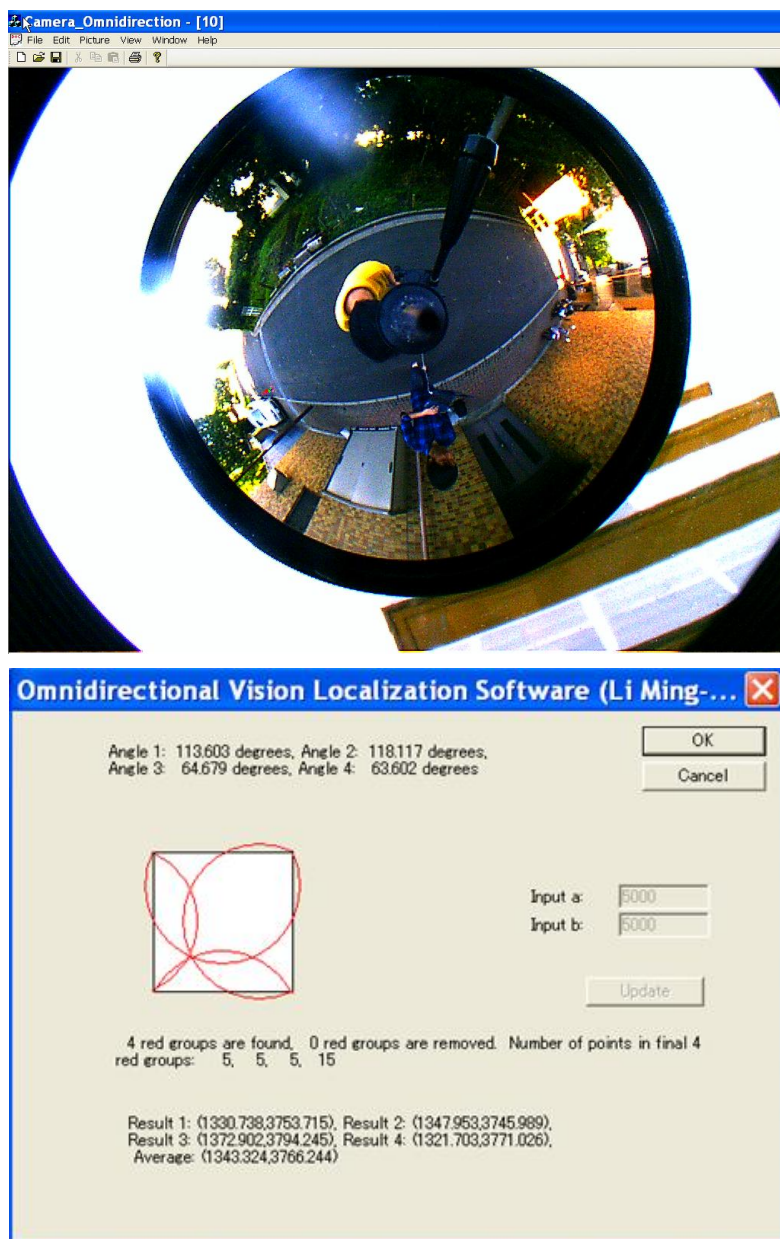
$$\omega = \frac{\xi^2 + 1 + 2 \xi \cos \varphi}{(\xi + \cos \varphi)^2} \quad (\text{B4})$$

Combined B1 with B3, we obtain:

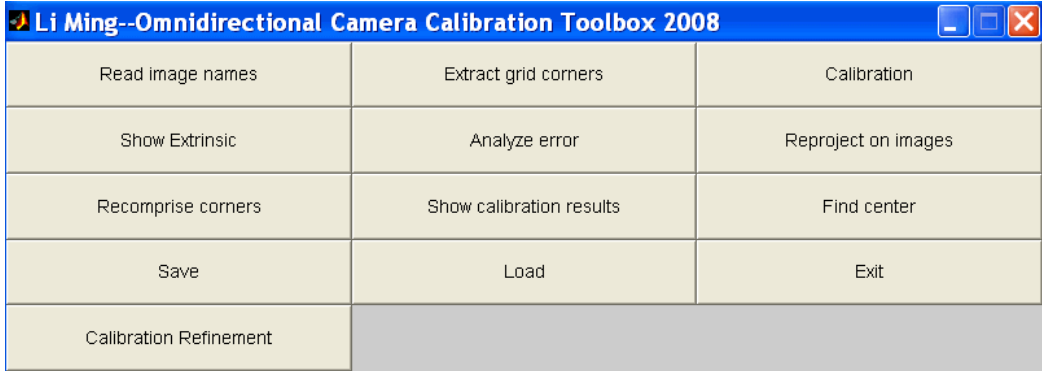
$$f = \sqrt{\frac{(x - u_0)^2 + (y - v_0)^2}{\omega - 1}} \quad (\text{B5})$$

Here, (A4) gives a geometrical explanation for (5-7) and obtain the formula (5-8).

APPENDIX C—SCREENSHOTS OF USER INTERFACES OF PROGRAM



APPENDIX D—SCREENSHOT OF USER INTERFACES OF CALIBRATION PROGRAM



Li Ming--Omnidirectional Camera Calibration Toolbox 2008		
Read image names	Extract grid corners	Calibration
Show Extrinsic	Analyze error	Reproject on images
Recomprise corners	Show calibration results	Find center
Save	Load	Exit
Calibration Refinement		

APPENDIX E–MAIN PROGRAM CODE

```
CCamera_OmnidirectionDoc::CCamera_OmnidirectionDoc()
{
    m_Width = 0;
    m_Height = 0;
    m_bBmpAttach = FALSE;
    m_bPara = FALSE;
    m_pBuf = NULL;
    m_plpoint = NULL;
    m_pJpoint = NULL;
    m_npoint = 0;
    m_plpoint2 = NULL;
    m_pJpoint2 = NULL;
    m_npoint2 = 0;
    m_nmark = 0;
    m_a = 3.5;
    m_b = 5;
    m_c = 6.1;
    m_f = 2.26;
    m_l = 120.0;
    m_w = 90.0;
    m_h = 145.0;
    m_dpi = 7987.4213;
}

CCamera_OmnidirectionDoc::~CCamera_OmnidirectionDoc()
{
    if(m_pBuf!= NULL) delete [] m_pBuf;
    if(m_plpoint!= NULL) delete [] m_plpoint;
    if(m_pJpoint!= NULL) delete [] m_pJpoint;
}

BOOL CCamera_OmnidirectionDoc::OnNewDocument()
{
    if (!CDocument::OnNewDocument())
        return FALSE;
    // (SDI documents will reuse this document)
    return TRUE;
}

CBitmap* CCamera_OmnidirectionDoc::GetBmp()
{
    return &m_pBmp;
}

void CCamera_OmnidirectionDoc::AttachBmp(HBITMAP hBitmap)
{
    m_pBmp.Detach();
    m_pBmp.Attach(hBitmap);
    m_bBmpAttach = TRUE;
}

BOOL CCamera_OmnidirectionDoc::ValidBmpAttach()
{
    return m_bBmpAttach;
}
```

```

}

// CCamera_OmnidirectionDoc serialization

void CCamera_OmnidirectionDoc::Serialize(CArchive& ar)
{
    if (ar.IsStoring())
    {
    }
    else
    {
    }
}

// CCamera_OmnidirectionDoc diagnostics

#ifdef _DEBUG
void CCamera_OmnidirectionDoc::AssertValid() const
{
    CDocument::AssertValid();
}

void CCamera_OmnidirectionDoc::Dump(CDumpContext& dc) const
{
    CDocument::Dump(dc);
}
#endif // _DEBUG

////////////////////////////////////
// CCamera_OmnidirectionDoc commands

void CCamera_OmnidirectionDoc::OnFileOpen()
{
    char szFilter[] = "Bitmap(*.BMP)|*.BMP|";
    CFileDialog dlg(TRUE,NULL,NULL,OFN_HIDEREADONLY,szFilter);
    if(dlg.DoModal() == IDOK)
    {
        CString szPathName = dlg.GetPathName();
        HBITMAP hBitmap =
(HBITMAP)::LoadImage(NULL,szPathName,IMAGE_BITMAP,0,0,LR_LOADFROMFILE);
        if(hBitmap==NULL)
        {
            MessageBox(NULL,"Image format is not correct!","Error",0);
            m_bBmpAttach = FALSE;
            return;
        }

        SetPathName(szPathName);
        AttachBmp(hBitmap);
        BITMAP bm;
        GetBmp()->GetObject(sizeof(BITMAP),&bm);
        m_Width = bm.bmWidth;
        m_Height = bm.bmHeight;
        m_npoint = 0;
        m_npoint2 = 0;
        m_nmark = 0;
        UpdateAllViews(NULL);
        POSITION pos = GetFirstViewPosition();
        CCamera_OmnidirectionView*
pView=(CCamera_OmnidirectionView*)GetNextView(pos);
        pView-> SetScrollSizes(MM_TEXT, GetSize());
    }
}

```

```

    }
}

void CCamera_OmnidirectionDoc::OnPictureCameraPos()
{
// TODO: Add your command handler code here
if(ValidBmpAttach()==FALSE) return;
if(m_bPara==FALSE) OnPictureSetparameter();
// Get Bitmap parameters
CBitmap* pBmp = GetBmp();
BITMAP bm;
pBmp->GetObject(sizeof(BITMAP),&bm);
WORD depth = bm.bmBitsPixel/8;
DWORD dwCount = m_Width*m_Height*depth;
m_pBuf = new BYTE [dwCount];
dwCount = pBmp->GetBitmapBits(dwCount,m_pBuf);
if(dwCount==0) return;
CCameraPos pDiaPos;
// allocate memory
int i,j,ij,ip1_j,im1_j,i_jp1,i_lm1;
int offset = 0;
int x_camera = 534;
int y_camera = 330;
int R,G,B;
int* pRlevel = new int [m_Width*m_Height];
int* pGlevel = new int [m_Width*m_Height];
m_p_lpoint = new int [m_Width*m_Height];
m_p_jpoint = new int [m_Width*m_Height];
m_p_lpoint2 = new int [m_Width*m_Height];
m_p_jpoint2 = new int [m_Width*m_Height];
    int ijcorner_first[10][2];
    int ijcorner_first2[10][2];
double xycorner[10][2],xy[4][2];
double xycorner2[10][2];
double a,aa;
    double b,bb;
    double c,cc, xc, yc, ab_alf1, ab_alf2, eps, xyc[4][2];
double xyca[2];
int ialf0,ialf1,ialf2;

int Rlevel_max = -10000;
int Glevel_max = -10000;
// search four corners
// 1. search all the possible points
m_npoint = 0;
m_npoint2 = 0;
for(i=0;i<m_Width;i++)
{
    for(j=0;j<m_Height-offset;j++)
    {
        ij = j*m_Width+i;
// BGR
        B = m_pBuf[depth*ij];
        G = m_pBuf[depth*ij+1];
        R = m_pBuf[depth*ij+2];
        pRlevel[ij] = R-(B+G)/2-abs(B-G);
        pGlevel[ij] = G-(B+R)/2-abs(B-R);
        if(pRlevel[ij]>Rlevel_max) Rlevel_max = pRlevel[ij];
        if(pGlevel[ij]>Glevel_max) Glevel_max = pGlevel[ij];
    }
}
int dis;

```

```

for(i=1;i<m_Width-1;i++)
{
    for(j=1;j<m_Height-offset-1;j++)
    {
        ij = j*m_Width+i;
        ip1_j = j*m_Width+i+1;
        im1_j = j*m_Width+i-1;
        i_jp1 = (j+1)*m_Width+i;
        i_jm1 = (j-1)*m_Width+i;
        dis = (i-x_camera)*(i-x_camera)
            +(j-y_camera)*(j-y_camera);
        if(pRlevel[ij]>Rlevel_max-20 && dis<m_Height*m_Height*0.4*0.4)
            {
                m_plpoint[m_npoint] = i;
                m_pJpoint[m_npoint] = j;
                m_npoint = m_npoint + 1;
            }
        if(pGlevel[ij]>Glevel_max-30 && dis<m_Height*m_Height*0.4*0.4)
            {
                m_plpoint2[m_npoint2] = i;
                m_pJpoint2[m_npoint2] = j;
                m_npoint2 = m_npoint2 + 1;
            }
    }
}
// 2. divide the possible points into groups
BOOL flag;
int ncorner = 1;
int icorner, ipoint;
ijcorner_first[0][0] = m_plpoint[0];
ijcorner_first[0][1] = m_pJpoint[0];
for(int ipoint=1;ipoint<m_npoint;ipoint++)
{
    flag = TRUE;
    i = m_plpoint[ipoint];
    j = m_pJpoint[ipoint];

    for(icorner=0;icorner<ncorner;icorner++)
    {
        dis = (i-ijcorner_first[icorner][0])*(i-ijcorner_first[icorner][0])
            +(j-ijcorner_first[icorner][1])*(j-ijcorner_first[icorner][1]);
        if(dis < m_Height*m_Height/25)
            {
                flag = FALSE;
                break;
            }
    }
    if(flag==TRUE)
    {
        ijcorner_first[ncorner][0] = i;
        ijcorner_first[ncorner][1] = j;
        ncorner = ncorner+1;
    }
    if(ncorner==10) break;
}
int ncorner2 = 1;
ijcorner_first2[0][0] = m_plpoint2[0];
ijcorner_first2[0][1] = m_pJpoint2[0];
for(int ipoint=1;ipoint<m_npoint2;ipoint++)
{
    flag = TRUE;

```

```

        i = m_plpoint2[ipoint];
        j = m_pJpoint2[ipoint];

for(icorner=0;icorner<ncorner2;icorner++)
{
    dis = (i-ijcorner_first2[icorner][0])*(i-ijcorner_first2[icorner][0])
          +(j-ijcorner_first2[icorner][1])*(j-ijcorner_first2[icorner][1]);
    if(dis < m_Height*m_Height/100)
    {
        flag = FALSE;
        break;
    }
}
if(flag==TRUE)
{
    ijcorner_first2[ncorner2][0] = i;
    ijcorner_first2[ncorner2][1] = j;
    ncorner2 = ncorner2+1;
}
if(ncorner2==10) break;
}
int ngcorner[10];
for(i=0;i<ncorner;i++)
{
    xycorner[i][0]=0;
    xycorner[i][1]=0;
    ngcorner[i]=0;
}
for(ipoint=0;ipoint<m_npoint;ipoint++)
{
    i = m_plpoint[ipoint];
    j = m_pJpoint[ipoint];
    ij = j*m_Width+i;
    for(int icorner=0;icorner<ncorner;icorner++)
    {
        int dis = (i-ijcorner_first[icorner][0])*(i-ijcorner_first[icorner][0])
                  +(j-ijcorner_first[icorner][1])*(j-ijcorner_first[icorner][1]);
        if(dis < m_Height*m_Height/25)
        {
            xycorner[icorner][0] = xycorner[icorner][0]+i;
            xycorner[icorner][1] = xycorner[icorner][1]+j;
            ngcorner[icorner] = ngcorner[icorner]+1;
        }
    }
    int ngcorner2[10];
for(i=0;i<ncorner2;i++)
{
    xycorner2[i][0]=0;
    xycorner2[i][1]=0;
    ngcorner2[i]=0;
}
for(ipoint=0;ipoint<m_npoint2;ipoint++)
{
    i = m_plpoint2[ipoint];
    j = m_pJpoint2[ipoint];
    ij = j*m_Width+i;
    for(int icorner=0;icorner<ncorner2;icorner++)
    {
        int dis = (i-ijcorner_first2[icorner][0])*(i-ijcorner_first2[icorner][0])
                  +(j-ijcorner_first2[icorner][1])*(j-ijcorner_first2[icorner][1]);
        if(dis < m_Height*m_Height/100)
        {

```

```

                xycorner2[icorner][0] = xycorner2[icorner][0]+i;
                xycorner2[icorner][1] = xycorner2[icorner][1]+j;
            ngcorner2[icorner] = ngcorner2[icorner]+1;
        }
    }
}
// Calculate the group center
for(i=0;i<ncorner;i++)
{
    xycorner[i][0]=xycorner[i][0]/ngcorner[i];
    xycorner[i][1]=xycorner[i][1]/ngcorner[i];
}
for(i=0;i<ncorner2;i++)
{
    xycorner2[i][0]=xycorner2[i][0]/ngcorner2[i];
    xycorner2[i][1]=xycorner2[i][1]/ngcorner2[i];
}

m_nmark = 0;
int imark[10],jmark[10];
for(i=0;i<10;i++) imark[i]=1;
int npoint[4];
int ngroup = 0;
for(i=0;i<ncorner;i++)
{
    flag = FALSE;
    for(j=0;j<ncorner2;j++)
    {
        int dis = int((xycorner[i][0]-xycorner2[j][0])*(xycorner[i][0]-xycorner2[j][0])
            +(xycorner[i][1]-xycorner2[j][1])*(xycorner[i][1]-
xycorner2[j][1]));
        if(dis < m_Height*m_Height/100)
        {
            m_nmark = m_nmark+1;
            jmark[m_nmark-1]=j;
            m_xy-mark[m_nmark-1][0]=int(xycorner2[j][0]);
            m_xy-mark[m_nmark-1][1]=int(xycorner2[j][1]);
            flag = TRUE;
            break;
        }
    }
    if(flag==FALSE)imark[i] = 0;
    if(flag==TRUE)
    {
        ngroup = ngroup+1;
        npoint[ngroup-1]=ngcorner[i];
    }
}
UpdateAllViews(0);
    if(m_nmark<2)
    {
        MessageBox(NULL,"Landmarks are not enough","Error",0);
        return;
    }
    if(m_nmark>4)
    {
        MessageBox(NULL,"Landmarks are more than 4","Error",0);
        return;
    }
}
// calculate four angles
for(i=0;i<m_nmark;i++)
{

```

```

xy[i][0] = xycorner2[jmark[i]][0]-x_camera;
xy[i][1] = -xycorner2[jmark[i]][1]+y_camera;
}

for(i=0;i<m_nmark;i++)
{
    if(ngcorner[i]==0)
    {
        MessageBox(NULL,"A Landmark is not found","Error",0);
        return;
    }
}

double r2[4],R2[4],coef1,coef2,side[3];

for(i=0;i<m_nmark;i++)
    m_alf[i] = CalAlf(float(xy[i][0]),float(xy[i][1]));
for(i=0;i<m_nmark;i++)
{
    r2[i] = float(xy[i][0])*float(xy[i][0])+float(xy[i][1])*float(xy[i][1]);
    r2[i] = r2[i]*(2.54/m_dpi)*(2.54/m_dpi);
}

delete [] pRlevel;
delete [] pGlevel;

Prbub(m_alf,r2,m_nmark);
double pi = 3.1415926536;
if(m_nmark==4)
{
    m_alf[0] = m_alf[1]-m_alf[0];
    m_alf[1] = m_alf[2]-m_alf[1];
    m_alf[2] = m_alf[3]-m_alf[2];
    m_alf[3] = 2.e0*pi-m_alf[0]-m_alf[1]-m_alf[2];
}
if(m_nmark==3)
{
    m_alf[0] = m_alf[1]-m_alf[0];
    m_alf[1] = m_alf[2]-m_alf[1];
    m_alf[2] = 2.e0*pi-m_alf[0]-m_alf[1];
}
//
// calculate
for(i=0;i<m_nmark;i++)
{
    coef1 = 4.0*m_b*m_b*m_c*m_c*pow(m_b*m_b-
m_c*m_c,2.0)*m_h*m_h*(m_f*m_f+r2[i]);
    coef2 = (-m_f*(pow(m_b,4.0)-
pow(m_c,4.0))*m_h+pow(coef1,0.5))/(m_f*m_f*pow(m_b*m_b-m_c*m_c,2.0)-
4.0*m_b*m_b*m_c*m_c*r2[i]);
    R2[i]=coef2*coef2*r2[i];
}
}
if(m_nmark==2)
{
    m_alf[0] = m_alf[1]-m_alf[0];
for(i=0;i<m_nmark;i++)
{
    coef1 = 4.0*m_b*m_b*m_c*m_c*pow(m_b*m_b-
m_c*m_c,2.0)*m_h*m_h*(m_f*m_f+r2[i]);

```

```

        coef2 = (-m_f*(pow(m_b,4.0)-
pow(m_c,4.0))*m_h+pow(coef1,0.5))/(m_f*m_f*pow(m_b*m_b-m_c*m_c,2.0)-
4.0*m_b*m_b*m_c*m_c*r2[i]);
        R2[i]=coef2*coef2*r2[i];
    }
}
// calculate position of camera
a = m_l;
b = m_w;
eps = 1.e-10;
// 4 landmarks
if(m_nmark==4)
{
    ab_alf2 = b/tan(m_alf[1])-a;
    if(fabs(ab_alf2)>eps)
    {
        c = (a/tan(m_alf[0])-b)/ab_alf2;
        xc = a*(c+1./tan(m_alf[0]))/(1.+c*c);
        yc = c*xc;
    }
    else
    {
        ab_alf1 = a/tan(m_alf[0])-b;
        if(fabs(ab_alf1)>eps)
        {
            xc = 0.;
            yc = a;
        }
        else
        {
            xc = 0.;
            yc = 0.;
        }
    }
    xyc[0][0] = xc;
    xyc[0][1] = yc;

    ab_alf2 = a/tan(m_alf[2])-b;

    if(fabs(ab_alf2)>eps)
    {
        c = (b/tan(m_alf[1])-a)/ab_alf2;
        xc = b*(c+1./tan(m_alf[1]))/(1.+c*c);
        yc = c*xc;
    }
    else
    {
        ab_alf1 = b/tan(m_alf[1])-a;
        if(fabs(ab_alf1)>eps)
        {
            xc = 0.;
            yc = b;
        }
        else
        {
            xc = 0.;
            yc = 0.;
        }
    }
    xyc[1][0] = b - yc;
    xyc[1][1] = a - xc;

    ab_alf2 = b/tan(m_alf[3])-a;

```

```

    if(fabs(ab_alf2)>eps)
    {
        c = (a/tan(m_alf[2])-b)/ab_alf2;
        xc = a*(c+1./tan(m_alf[2]))/(1.+c*c);
        yc = c*xc;
    }
    else
    {
        ab_alf1 = a/tan(m_alf[2])-b;
        if(fabs(ab_alf1)>eps)
        {
            xc = 0.;
            yc = a;
        }
        else
        {
            xc = 0.;
            yc = 0.;
        }
    }
    xyc[2][0] = b - xc;
    xyc[2][1] = yc;

ab_alf2 = a/tan(m_alf[0])-b;

    if(fabs(ab_alf2)>eps)
    {
        c = (b/tan(m_alf[3])-a)/ab_alf2;
        xc = b*(c+1./tan(m_alf[3]))/(1.+c*c);
        yc = c*xc;
    }
    else
    {
        ab_alf1 = b/tan(m_alf[3])-a;
        if(fabs(ab_alf1)>eps)
        {
            xc = 0.;
            yc = b;
        }
        else
        {
            xc = 0.;
            yc = 0.;
        }
    }
    xyc[3][0] = yc;
    xyc[3][1] = xc;

    xyca[0] = 0.25*(xyc[0][0]+xyc[1][0]+xyc[2][0]+xyc[3][0]);
    xyca[1] = 0.25*(xyc[0][1]+xyc[1][1]+xyc[2][1]+xyc[3][1]);
}

// 3 landmarks
if(m_nmark==3)
{
// calculate the length of 3 sides
for(i=0;i<m_nmark;i++)
{
    double bb = pow(R2[i],0.5);
    double cc = pow(R2[(i+1)%m_nmark],0.5);
    side[i]= pow(bb*bb+cc*cc-2.0*bb*cc*cos(m_alf[i]),0.5);
}
}

```

```

// judge the longest side
double sidem;
sidem = side[0];
int imax;
imax = 0;
for(i=1;i<m_nmark;i++)
{
    if(side[i]>sidem)
    {
        sidem=side[i];
        imax = i;
    }
}

double sidem2;
sidem2 = -10000.;
int imax2;
imax2 =0;
for(i=0;i<m_nmark;i++)
{
    if(i!=imax&&side[i]>sidem2)
    {
        sidem2=side[i];
        imax2 = i;
    }
}

// the vertex
ialf0 = imax2;
ialf1 = 3-imax2-imax;
ialf2 = imax;

    ab_alf2 = b/tan(m_alf[ialf1])-a;
    if(fabs(ab_alf2)>eps)
    {
        c = (a/tan(m_alf[ialf0])-b)/ab_alf2;
        xc = b*(1.+c/tan(m_alf[ialf1]))/(1.+c*c);
        yc = c*xc;
    }
    else
    {
        ab_alf1 = a/tan(m_alf[ialf0])-b;
        if(fabs(ab_alf1)>eps)
        {
            xc = 0.;
            yc = a;
        }
        else
        {
            xc = b;
            yc = a;
        }
    }
xyc[0][0] = xc;
xyc[0][1] = yc;

ab_alf2 = a*(1./tan(m_alf[ialf0])+1./tan(m_alf[ialf2]))-b;

    if(fabs(ab_alf2)>eps)
    {
        c = (b/tan(m_alf[ialf2]))/ab_alf2;
        yc = a*c*(c-1.0/tan(m_alf[ialf0]))/(1.+c*c);
    }

```

```

        xc = c*(a-yc);
    }
    else
    {
        yc = a;
        yc = a/tan(m_alf[ialf0]);
    }
    xyc[1][0] = xc;
    xyc[1][1] = yc;

ab_alf2 = b*(1./tan(m_alf[ialf1])+1./tan(m_alf[ialf2]))-a;

    if(fabs(ab_alf2)>eps)
    {
        c = (a/tan(m_alf[ialf2]))/ab_alf2;
        xc = b*c*(c-1.0/tan(m_alf[ialf1]))/(1.+c*c);
        yc = c*(b-xc);
    }
    else
    {
        xc = b;
        yc = b/tan(m_alf[ialf1]);
    }
    xyc[2][0] = xc;
    xyc[2][1] = yc;

    xyca[0] = (xyc[0][0]+xyc[1][0]+xyc[2][0])/3.0;
    xyca[1] = (xyc[0][1]+xyc[1][1]+xyc[2][1])/3.0;
}

if(m_nmark==2)
{
// calculate the length of side
    bb = pow(R2[0],0.5);
    cc = pow(R2[1],0.5);
if (m_alf[0]>pi)
{
    m_alf[0]=2*pi-m_alf[0];
}

    aa = pow(bb*bb+cc*cc-2.0*bb*cc*cos(m_alf[0]),0.5);
    double cosa,sina;
    cosa = (aa*aa+bb*bb-cc*cc)/(2.*aa*bb);
    sina = sqrt(1.-cosa*cosa);
    xyca[0] = bb*sina/aa;
    xyca[1] = bb*cosa/aa;
}
// display the results
    CString sBuf;

    if(m_nmark==4)
    {
        sBuf.Format("Angle 1: %8.3f degrees, Angle 2: %8.3f degrees,\nAngle 3: %8.3f degrees,
Angle 4: %8.3f degrees",
        m_alf[0]*180./pi,m_alf[1]*180./pi,m_alf[2]*180./pi,m_alf[3]*180./pi);
        pDiaPos.m_info = sBuf;

        sBuf.Format("Result 1: (%8.3f,%8.3f), Result 2: (%8.3f,%8.3f), \nResult 3: (%8.3f,%8.3f), Result 4:
(%8.3f,%8.3f),\n Average: (%8.3f,%8.3f)",
        xyc[0][0],xyc[0][1],xyc[1][0],xyc[1][1],xyc[2][0],xyc[2][1],xyc[3][0],xyc[3][1],xyca[0],xyca[1]);
        pDiaPos.m_results = sBuf;
    }
}

```

```

for(i=0;i<4;i++) pDiaPos.m_alf[i] = m_alf[i];
    for(i=0;i<4;i++)
        for(j=0;j<2;j++)
            pDiaPos.m_xyc[i][j] = xyc[i][j];
sBuf.Format("%3d red groups are found, %3d red groups are removed. Number of points in final 4
red groups: %5d,%5d,%5d,%5d",
    ncorner,ncorner-4,npoint[0],npoint[1],npoint[2],npoint[3]);
pDiaPos.m_points = sBuf;
}
if(m_nmark==3)
{
    sBuf.Format("Angle 1: %8.3f degrees, Angle 2: %8.3f degrees,\nAngle 3: %8.3f degrees",
        m_alf[jalf0]*180./pi,m_alf[jalf1]*180./pi,m_alf[jalf2]*180./pi);
pDiaPos.m_info = sBuf;

    sBuf.Format("Result 1: (%8.3f,%8.3f), Result 2: (%8.3f,%8.3f), \nResult 3: (%8.3f,%8.3f), \n Average:
(%8.3f,%8.3f)",
        xyc[0][0],xyc[0][1],xyc[1][0],xyc[1][1],xyc[2][0],xyc[2][1],xyca[0],xyca[1]);
pDiaPos.m_results = sBuf;
pDiaPos.m_alf[0] = m_alf[jalf0];
pDiaPos.m_alf[1] = m_alf[jalf1];
pDiaPos.m_alf[2] = m_alf[jalf2];
    for(i=0;i<m_nmark;i++)
        for(j=0;j<2;j++)
            pDiaPos.m_xyc[i][j] = xyc[i][j];
sBuf.Format("%3d red groups are found, %3d red groups are removed. Number of points in final 3
red groups: %5d,%5d,%5d",
    ncorner,ncorner-3,npoint[0],npoint[1],npoint[2]);
pDiaPos.m_points = sBuf;
}
if(m_nmark==2)
{
    sBuf.Format("Angle 1: %8.3f degrees",
        m_alf[0]*180./pi);
pDiaPos.m_info = sBuf;

sBuf.Format("Result (relative value): (%8.3f,%8.3f)",
    xyca[0],xyca[1]);
pDiaPos.m_results = sBuf;

pDiaPos.m_alf[0] = m_alf[0];

pDiaPos.m_r1 = bb/aa;
pDiaPos.m_r2 = cc/aa;
pDiaPos.m_xyc[0][0] = xyca[0];
pDiaPos.m_xyc[0][1] = xyca[1];

sBuf.Format("%3d red groups are found, %3d red groups are removed. Number of points in final 2
red groups: %5d,%5d",
    ncorner,ncorner-2,npoint[0],npoint[1]);
pDiaPos.m_points = sBuf;
}

pDiaPos.m_a=m_l;
pDiaPos.m_b=m_w;
pDiaPos.m_nmark=m_nmark;

pDiaPos.DoModal();

```

```

        if(m_pBuf!= NULL)
    {
        delete [] m_pBuf;
        m_pBuf = NULL;
    }
}

double CCamera_OmnidirectionDoc::CalAlf(float x, float y)
{
    double theta=atan2(y,x);
    return theta;
}

void CCamera_OmnidirectionDoc::Prbub(double* p,double* q,int n)
{
    int m,k,j,i;
    double d;
    k=0; m=n-1;
    while (k<m)
    {
        j=m-1; m=0;
        for (i=k; i<=j; i++)
            if (p[i]>p[i+1])
            {
                d=p[i]; p[i]=p[i+1]; p[i+1]=d; m=i;
                d=q[i]; q[i]=q[i+1]; q[i+1]=d;
            }
        j=k+1; k=0;
        for (i=m; i>=j; i--)
            if (p[i-1]>p[i])
            {
                d=p[i]; p[i]=p[i-1]; p[i-1]=d; k=i;
                d=q[i]; q[i]=q[i-1]; q[i-1]=d;
            }
    }
    return;
}

void CCamera_OmnidirectionDoc::OnPictureSetparameter()
{
    CParaDlg paradlg;
    paradlg.m_a = m_a;
    paradlg.m_b = m_b;
    paradlg.m_c = m_c;
    paradlg.m_f = m_f;
    paradlg.m_l = m_l;
    paradlg.m_w = m_w;
    paradlg.m_h = m_h;
    paradlg.m_dpi = m_dpi;

    if(paradlg.DoModal() == IDOK)
    {
        m_a= paradlg.m_a;
        m_b= paradlg.m_b;
        m_c= paradlg.m_c;
        m_f= paradlg.m_f;
        m_l= paradlg.m_l;
        m_w= paradlg.m_w;
        m_h= paradlg.m_h;
        m_dpi= paradlg.m_dpi;
        m_bPara=TRUE;
    }
}

```

LIST OF PUBLICATIONS

JOURNAL PAPERS

1. Ming Li, Kenji Imou, Katsuhiko Wakabayashi, Shinya Yokoyama. Review of research on agricultural vehicle autonomous guidance. *International Journal of Agricultural and Biological Engineering*, 2009, 2(3):1-17.
2. Ming Li, Kenji Imou, Katsuhiko Wakabayashi, Shirou Tani, Shinya Yokoyama. Position estimation method using artificial landmarks and omnidirectional Vision, *Transactions of the ASABE* (accepted), February, 2010.
3. Ming Li, Kenji Imou, Katsuhiko Wakabayashi, Shinya Yokoyama. Artificial landmark self-localization for agricultural vehicle field road navigation using omnidirectional vision. *International Journal of Control, Automation, and Systems* (in press).

CONFERENCE PAPERS

1. Ming Li, Kenji Imou, Shirou Tani, Shinya Yokoyama. Localization of agricultural vehicle using landmark based on omni-directional vision. Proceedings of 2009 International Conference on Computer Engineering and Applications. Manila, Philippine, June, 2009, pp. 140-144.
2. Ming Li, Kenji Imou, Shinya Yokoyama. Artificial landmark localization system for agricultural vehicle using omnidirectional vision. Joint Conference on Environmental Engineering in Agriculture 2009 (CD). Tokyo, Japan, September, 2009.
3. Ming Li, Kenji Imou, Katsuhiko Wakabayashi, Shinya Yokoyama. A new agricultural vehicle localization system. IEEE proceedings of the 2009 International Conference on Computer and Computing Technology Applications in Agriculture. Beijing, China, October, 2009 (in press).
4. Ming Li, Kenji Imou, Katsuhiko Wakabayashi, Shinya Yokoyama. Localization system based on artificial landmark and omnidirectional vision. IEEE International Conference on Information Engineering and Computer Science, Wuhan, China, December, 2009.

REFERENCES

- Abdul B, Robert S. Landmark Based Global Self-localization of Mobile Soccer Robots. P.J. Narayanan et al. (Eds.): ACCV2006, pp.842–851. 2006.
- Abidine A Z, Heidman B C, Upadhyaya S K Hills D J. Application of RTK GPS based auto-guidance system in agricultural production. ASAE Paper No. O21152. ASAE, St. Joseph, MI. 2002.
- Ahamed T, Takigawa T, Koike M, Honma T, Yoda A, Hasegawa H, Junyusen P, Zhang Q. Characterization of laser range finder for in-field navigation of autonomous tractor. In: Proceedings of the Automation Technology for Off-road Equipment, Kyoto, Japan. 2004.
- Aihara N, Iwasa H, Yokoya N, Takemura H. Memory based Self-localization Using Omnidirectional Images. In: ICPR'98, 1799–1803. 1998.
- Aliaga D G. Accurate catadioptric calibration for real-time pose estimation in room-size environments. In: Proceedings of the 8th International Conference on Computer Vision. IEEE, pp.127–134, 2001.
- Andreasson H, Treptow A, Duckett, T. Self-localization in non-stationary environment using omni-directional vision. *Robotics and Autonomous System*, 2007; 55: 541–551.
- Åstrand B, Baerveldt A J. A vision based row-following system for agricultural machinery. *Mechatronics*. 2005; 15(2): 251–269.
- Åstrand B. Vision based perception or mechatronic weed control. Doctor of Philosophy Thesis, Chalmers and Halmstad Universities, Sweden. 2005.
- Bais A, Sablating R. Landmark Based Global Self-localization of Mobile Soccer Robots. P.J. Narayanan et al. (Eds.) ACCV2006. LNCS, vol. 3852, pp. 842-851. Springer Heidelberg, 2006.
- Baker S, Nayar S. A theory of single-viewpoint catadioptric image formation. *International Journal of Computer Vision*, 35(2), November 1999, pp. 175–196.

- Barawid J O C, Mizushima A, Ishii K, Noguchi N. Development of an autonomous navigation system using a two-dimensional laser scanner in an orchard application. *Biosystems Engineering*. 2007; 96(2):139–149.
- Barreto J P, Araujo H. Geometry properties of central catadioptric line images and application in calibration. *IEEE Transactions on Pattern Analysis and Machine Intelligence*. 2005; 27(8): 1327–1333.
- Barreto J P, Araujo H. Issues on the geometry of central catadioptric image formation. In *CVPR*, 2001.
- Barshan B, Durrant-Whyte H F. Inertial Navigation Systems for Mobile Robots. *Transactions on Robotics and Automation*, 1995; 1(3): 328–342.
- Bell T. Automatic tractor guidance using carrier-phase differential GPS. *Comput. Electron. Agric.* 2000; 25 (1-2), 53–66.
- Benson E, Reid J F, Zhang Q. Machine vision-based guidance system for agricultural grain harvesters using cut-edge detection. *Biosystems Engineering*. 2003; 86(4):389–398.
- Benson E, Stombaugh T, Noguchi N, Will J, Reid J F. An evaluation of a geomagnetic direction sensor for vehicle guidance in precision agriculture applications. *ASAE Paper 983203*. ASAE. St. Joseph, MI. 1998.
- Bergeijk J V, Goense D, Keesman K J, Speelman L. Digital filters to integrate global positioning system and dead reckoning. *J. Agric. Eng. Res.* 1998; 70(2): 135–143.
- Bevly D M, Gerdes J C, Parkinson B W. A new yaw dynamic model for improved high speed control of a farm tractor. *Journal of Dynamic System, Measurement, and Control*. 2002; 124(4): 659–667.
- Billingsley J, Schoenfisch M. The successful development of a vision guidance system for agriculture *Comput. Electron. Agric.* 1997; 16(2):147–163.
- Borenstein J, Everett H R, Feng L. *Navigating Mobile Robots: Systems and Techniques*. A. K. Peters, Ltd. 1996.
- Bouton N, Lenain R, Thuilot B, Martinet P. Backstepping observer dedicated to tire cornering stiffness estimation application to an all terrain vehicle and a farm tractor. *Proceedings of*

- the 2007 IEEE/RSJ International Conference on Intelligent Robots and Systems San Diego, CA, USA, Oct 29 - Nov 2, 1763–1768. 2007.
- Briechele K. and U. D. Hanebeck 2004. Localization of a Mobile Robot Using Relative Bearing Measurements. In: IEEE Trans. On Robotics and Automat.20(1):36–44.
- Briggs A J, Scharstein D, Braziunas D, Dima C, Wall P. Mobile Robot Navigation Using Self-Similar Landmark. In Proc. of IEEE International Conference on Robotics and Automation, 2000; 1428-1434. San Francisco, CA, USA.
- Cam View2.5 Information, <http://www.ff-net.ne.jp/ffhome/camview.html>.
- Cassandra A, Kaelbling L P, Kurien J. Acting under uncertainty: Discrete Bayesian models for mobile-robot navigation. In: Proceedings of the International Conference on Intelligent Robots and Systems, IROS, IEEE/RSJ, pp. 963–972 ,1996.
- Chenavier F, Crowley J. Position Estimation for a Mobile Robot Using Vision and Odometry. Proceedings of IEEE International Conference on Robotics and Automation, Nice, France, May 12-14, pp. 2588–2593. 1992.
- Cho S I, Lee J H. Autonomous speed sprayer using differential global positioning system, genetic algorithm and fuzzy control. Journal of Agriculture Engineering and Research. 2000; 76: 111–119.
- Deng X M, Wu F C, Wu Y H. An Easy Calibration Method for Central Catadioptric Cameras. Acta Automatica Sinica. 2007; 33(8):801–808.
- Duckett T, Nehmzow U. Mobile robot self-localization and measurement of performance in middle scale environments, Robotics and Autonomous Systems .1998; 24 (1–2): 57–69.
- Ehsani M R, Sullivan M D, Zimmerman T L, Stombaugh T. Evaluating the dynamic accuracy of low-cost GPS receivers. In: Proceedings of the ASAE Annual International Meeting, Nevada, USA. 2003.
- Fang H, Ruixia F, Thuilot B, Martine P. Trajectory tracking control of farm vehicles in presence of sliding. Robotics and Autonomous Systems. 2006; 54(10):828–839.
- Feng L, He Y, Bao Y, Fang H. Development of trajectory model for a tractor-implement system for automated navigation applications. IMTC 2005 – Instrumentation and Measurement Technology Conference Ottawa, Canada, 17-19 May, 1330–1334. 2005.

- Freeland S R, Wilkerson B J, Hart E W. Instrumentation for measurement of tractor yaw. ASAE Paper No. 92-3552. ASAE, St. Joseph, MI. 1992.
- Gander W, Golub G H, Strebel R. Least-squares fitting of circles and ellipses. BIT Numerical Mathematics. 1994; 34(4): 558–578.
- Gan-Mor S, Ronen B, Josef S, Bilanki Y. Guidance of autonomous vehicle for greenhouse transportation, Acta Hortic. 1997; 443: 99–104.
- Gan-Mor S, Upchurch B L, Clark R L, Hardage D. Implement guidance error as affected by field conditions using automatic DGPS tractor guidance. ASAE Paper No. 021153. ASAE, St. Joseph, MI. 2002.
- Garacía-Pérez L, Garacía-Alegre M C, Ribeiro A, Guinea D. An agent of behavior architecture for unmanned control of a farming vehicle. Comput. Electron. Agric. 2008; 60(1): 39–48.
- Geyer C, Daniilidis K. A unifying theory for central panoramic systems and practical implications. In ECCV, pages 445–461, 2000.
- Geyer C, Daniilidis K. Paracatadioptric camera calibration. IEEE Transactions on Pattern Analysis and Machine Intelligence. 2002; 24(5): 687–695.
- Gezici S, Tian Z, Biannakis G B, Kobayashi H, Molisch A F, Poor H V, Sahinoglu Z. Localization via ultra-wideband radios. IEEE Signal Processing Magazine. 2005; 22 (4):70–84.
- Hague T, Marchant J A, Tillett N D. Ground Based Sensing Systems for Autonomous Agricultural Vehicles. Comput. Electron. Agric. 2000; 25(1):11–28.
- Hague T, Tillett N D. A bandpass filter-based approach to crop row location and tracking. Mechatronics. 2001; 11(1):1–12.
- Han S, Zhang Q, Ni B, Reid J F. A guidance directrix approach to vision-based vehicle guidance systems. Comput. Electron. Agric. 2004; 3(43):179–197.
- Harper N L, McKerrow P J. Recognition of plants with CTFM ultrasonic range data using a neural network, In Proc. IEEE International Conference on Robotics and Automation, Albuquerque, NM, 3244–3249,1997.
- Harper N, McKerrow P. Recognising plants with ultrasonic sensing for mobile robot navigation. Robotics and Autonomous Systems 34:71–82. 2001.

- Harrell R C, Adsit P D, Pool T A, Hoffman R. The Florida robotic grove lab. Transactions of the ASAE. 1990; 33: 391–399.
- Heikillä J, Silv'en O. A four-step camera calibration procedure with implicit image correction. In Computer Vision and Pattern Recognition, 1997.
- Holmqvist R. A laser–optic navigation system for driverless vehicle, Arnex Navigation AB, R. Holmqvist, ARNBL 344:15. 1993.
- Imou K, Ishida M, Okado A, Takenaga H, Shibuya Y, Honda Y, Itokawa W. Yaw Angle Measurement on an Autonomous Tractor --- Influence of Tilt of a Tractor on Yaw Angle Measurement with a 1-axis Gyroscope. Journal of the Japanese Society of Agricultural Machinery. 1997; 59(4), 79-86. (in Japanese)
- Imou K, Okamoto T, Kaizu Y, Ishida M, Sawamura A, Sumida Y. Ultrasonic Doppler sensor for measuring vehicle speed in forward and reverse motions including low speed motions. Agricultural Engineering International: the CIGR Journal of Scientific Research and Development, Vol. III. 2001.
- Imou K, Okamoto T, Kaizu Y, Yoshii H. Ultrasonic Doppler Speed Sensor for Autonomous Vehicles. Journal of the Japanese Society of Agricultural Machinery. 2001; 63(2): 39–46.
- Imou K, Okamoto T, Torii T, Ishida M, Takanaga H, Okado A, Itokawa N. Autonomous Tractor for Forage Production, In Pro. 13th International Congress on Agricultural Engineering. 1998; 3:361–368.
- Imou K, Tani S, Yokoyama S. Position detection of vehicle using an omni–directional camera. In Proc. ISMAB, Taiwan. 2008.
- Inoue K, Otuka K, Sugimoto M, Murakami N. Estimation of place of tractor and adaptive control method of autonomous tractor using INS and GPS, Preprints of the International Workshop on Robotics and Automated Machinery for Bio–Productions, EurAgEng, Gandia, 27–736. 1997.
- Ishida M, Imou K, Okado A, Takenaga H, Honda Y, Itokawa N, Shibuya Y. Autonomous tractor for forage production. Journal of the Japanese Society of Agricultural Machinery. 1998; 60(2): 59–66 (in Japanese).

- Iwasa H, Aihara N, Yokoya N, Takemura H. Memory-based self-localization using omnidirectional images. *Systems and Computers in Japan*. 2003; 34(5):56–68.
- Jang G, Kim S, Lee W, Kweon I. Color Landmark Based Self-Localization for Indoor Mobile Robots. In *Proc. IEEE International Conference on Robotics and Automation*, 1037– 1042. Washington D.C., USA. 2002.
- Junior V G, Junior J O. Development of an Omnidirectional Vision System. *J. of the Braz. Soc. of Mech. Sci. & Eng.* 2006; (XXVIII) 1:58–68.
- Kaizu Y, Imou K. A dual-spectral camera system for paddy rice seedling row detection. *Comput. Electron. Agric.* 2008; 63(1):49–56.
- Kalman R E. A new approach to linear filtering and prediction problem. *Trans. ASME: J. Basic Eng.* 1960; 82(3): 35–40.
- Kang S B. Catadioptric self-calibration. In: *Proceedings of IEEE Conference on Computer Vision and Pattern Recognition*. IEEE, 201–207, 2000.
- Kise M, Noguchi N, Ishii K, Terao H. Development of agricultural autonomous tractor with an RTK-GPS and a FOG. *Proceedings of the Fourth IFAC Symposium on Intelligent Autonomous Vehicles*, Sapporo, Japan, 99–104. 2001.
- Kise M, Noguchi N, Ishii K, Terao H. The development of the autonomous tractor with steering controller applied by optimal control. *Proceedings of Automation Technology for Off-Road Equipment*, Chicago, USA, 367–373. 2002.
- Kise M, Zhang Q, Rovira M F. A stereovision-based crop row detection method for tractor-automated guidance. *Biosystems Engineering*. 2005; 90(4):357–367.
- Kodagoda K R S, Wijesoma W S, Teoh E K. Fuzzy speed and steering control of an AGV. *IEEE Trans. Control Syst. Technol.* 2002; 10 (1):112–120.
- Kubo Y, Kindo T, Ito A, Sugimoto S. DGPS/INS/wheel sensor integration for high-accuracy land-vehicle positioning. In *Proc. 12th International Technical Meeting of the Satellite Division of the Institute of Navigation*, 555–564. ION GPS-99. Fairfax, Va.: The Institute of Navigation. 1999.

- Ladd A M, Bekris K E , Rudys A P , Wallach D S, Kavraki L E. On the Feasibility of Using Wireless Ethernet for Indoor Localization. *IEEE Transactions on Robotics and Automation*. 2004; (20)3:555–559.
- Larsen W E, Nielsen G A, Tyler D A. Precision navigation with GPS. *Comput. Electron. Agric.* 1994; 11(1): 85–95.
- Lawitzky G, Feiten W, MÖller M. Sonar sensing for low-cost indoor mobility. *Robotics and Autonomous Systems*. 1995; 14(2-3):149–157.
- Lee J W, Choi S U, Lee Y J, Lee K S. A study on recognition of lane and movement of vehicles for port AGV vision system. In: *Proceedings of the 40th SICE Annual Conference. International Session Papers, 25–27 July*, pp. 38–41. 2001.
- Leemans V, Destain M F. Line cluster detection using a variant of the Hough Transform for culture row localization. *Image and Vision Computing*. 2006; 24(5): 541–550.
- Lenain R, Thuilot B, Cariou C, Martinet P. High accuracy path tracking for vehicles in presence of sliding: application to farm vehicle automatic guidance for agricultural task. *Auton Robot*. 2006; 21: 79–97.
- Lenain R, Thuilot B, Cariou C, Martinet P. Model predictive control for vehicle guidance in presence of sliding: application to farm vehicles path tracking. *International Conference on Robotics and Automation, Barcelona, Spain*, 897–902. 2005.
- Madhukar B R, Nayak R A, Ray J K, Shenoy M R. GPS/DR integration using low-cost sensors. In *Proc. 12th International Technical Meeting of the Satellite Division of the Institute of Navigation*, 537–544. ION GPS–99. Fairfax, Va.: The Institute of Navigation. 1999.
- Makadia A, Daniilidis K. Direct 3D-rotation estimation from spherical images via a generalized shift theorem. In *Proc. CVPR 2*:217–224. 2003.
- Marchant J A, Brivot R. Real-time tracking of plant rows using a hough transform. *Real-Time Imag*. 1995 ; (1): 363–371.
- Marchant J A. Tracking of row structure in three crops using image analysis. *Comput Electron Agric*. 1997; 15(2):161–179.

- Marques, C.F. and P.U. Lima. 2001. A Localization Method for a Soccer Robot Using a Vision based Omni-directional Sensor, Robot Cup 2000: Robot Soccer World Cup IV, 96–107. LNCS.
- Matsuo Y, Yukumoto O, Aburata K, Noguchi N. Research on tilling robot (part 4)-unmanned operation with the total station of automatic tracking type. Japanese Society of Agriculture Machinery 56th Annual Meeting, 57–58, 1997.
- Mehta S S, Bruks T F, Dixo W E. Vision-based localization of a wheeled mobile robot for greenhouse applications: A daisy-chaining approach. *Comput. Electron. Agric.* 2008; 63(1): 28–37.
- Mei C, Rives P. Single view point omnidirectional camera calibration from planar grids. In: Proc. 2007 IEEE International Conference on Robotics and Automation, Rome, Italy, pp. 3945–3950. IEEE Computer Society Press, Los Alamitos (2007)
- Micusik B, Pajdla T. Autocalibration & 3D Reconstruction with Non-central Catadioptric Cameras. Proc. of IEEE Conference on Computer Vision and Pattern Recognition, pp. 58–65, 2004.
- Morgan K E. A step towards an automatic tractor. *Farm mech.* 1958; 10 (13): 440–441.
- Morimoto E, Suguri M, Umeda M. Vision-based navigation system for autonomous transportation vehicle. *Precision Agriculture.* 2005; 6:239–254.
- Motomura A, Matsuoka T, Hasegawa T. Self-localization method using two landmarks and dead reckoning for autonomous mobile soccer robots. In: RoboCup 2003: Robot Soccer World Cup VII, 526–533. LNCS. 2003.
- Murakami N, Ito A, Will J D, Inoue K, Kita K, Miyarua S. Environment identification technique using hyper Omni-vision and image map, In: Proc. 3rd IFAC Int. Workshop Bio-Robotics, Sapporo, Japan, 2006; 317–320.
- Nagasaka Y, Umeda N, Kanetai Y, Taniwaki K Sasaki Y. Automated rice transplanter using global positioning and gyroscopes. *Comput. Electron. Agric.* 2004; 43 (3): 223–234.
- Nagasaka, Y, Saito H, Kitagawa H, Kobayashi K, Seki M, Tamaki K, Taniwaki K, Miyazaki M, Tateishi K. Development of Autonomous Rice Transplanter (Part 2) (in Japanese), *Journal of JSAM.* 2008; (71)1:79–84.

- Nayar S K. Catadioptric omnidirectional camera. Proc. of IEEE Computer Vision and Pattern Recognition. 1997; pp. 482– 488.
- Nishimura S, Honda Y, Imou K, Takenage H, Itokawa N. Automatic tractor steering system for forage harvesting. Journal of JSAM (in Japanese with English abstract). 1996; 58(2): 31–38.
- Noguchi N, Kise M, Ishii K, Terao H. Field automation using robot tractor. In: Proceedings of the Automation Technology for Off-road Equipment, ASAE, Chicago, IL, 239–245. 2002.
- Noguchi N, Terao H. Path planning of an agricultural mobile robot by neural network and genetic algorithm. Comput. Electron. Agric. 1997; 18(2-3): 187–204.
- Noguchil N, Ishii K, Terao H. Development of an agricultural mobile robot using a geomagnetic direction sensor and image sensors. Journal of Agricultural Engineering Research. 1997; 67:1–15.
- Nørremark M, Griepentrog H W, Nielsen J, Søggaard H T. The development and assessment of the accuracy of an autonomous GPS-based system for intra-row mechanical weed control in row crops. Biosystems Engineering. 2008; 101(4): 396–410.
- O'Connor M, Bell T, Elkaim G, Parkinson B. Automatic Steering of Farm Vehicles Using GPS. Paper presented at 3rd International Conference on Precision Agriculture, ASA, CSSA, and SSSA, Madison, WI. 1996.
- Okamoto H, Hamada K, Kataoka T, Terawaki M, Hata S. Automatic guidance system with crop row sensor. Automation Technology for Off-Road Equipment Proceedings, Conference (Chicago, Illinois, USA) 701P0502, 307–316. 2002
- Otsason V, Varshavsky A, Lamarca A, Lara E. Accurate GSM Indoor Localization. UbiComp 2005, LNCS 3660, 141–158.
- Pinto F A C, Reid J F, Zhang Q, Noguchi N. Vehicle guidance parameter determination from crop row images using principal component analysis. Journal of Agricultural Engineering Research. 2000; 75(3), 257–264.
- Qiu H, Zhang Q, Reid J F, Wu D. Nonlinear feedforward-plus-PID control for electrohydraulic steering systems. In Fluid Power Systems and Technology 6: 89–94. New York, N.Y.: ASME. 1999.

- Reid J F, Zhang Q, Noguchi N, Dickson M. Agricultural automatic guidance research in North America. *Comput. Electron. Agric.* 2000; 25: 155–167.
- Rudolph v d M, Eric A W. Sigma-Point Kalman Filters for Integrated Navigation. In Proceedings of the 60th Annual Meeting of the Institute of Navigation (ION), Dayton, OH, Jun. 2004.
- Ryerson A E F, Zhang Q. Vehicle path planning for complete field overage using genetic algorithms. *Agricultural Engineering International: the CIGR Ejournal*. Manuscript ATOE 07014. Vol. IX. July. 2007.
- Scaramuzza A, Martinelli D, Siegwart R. A toolbox for easy calibrating omnidirectional cameras. In IROS, 2006.
- Schönberg T, Ojala M, Suomela J, Torpo A, Halme A. Positioning an autonomous off-road vehicle by using fused DGPS and inertial navigation. *International Journal of Systems Science*. 1996; 27(8):745–752.
- Shimshoni I. On Mobile Robot Localization from Landmark Bearings. In: *IEEE Transactions on Robotics and Automation*. 2002; 18(6).
- Sissons R. Plowing in circles saves time. *The Prairie Farmer*. 1939; 111 (20): 7.
- Slaughter D C, Giles D K, Downery D. Autonomous robotic weed control systems: A review. *Comput. Electron. Agric.* 2008; 61(1): 63–78.
- Søgaard H T, Olsen H J. Determination of crop rows by image analysis without segmentation. *Comput. Electron. Agric.* 2003; 2(38):141–158.
- Spacek, L. and C. Burbridge. 2007. Instantaneous robot self-localization and motion estimation with omnidirectional vision. *Robotics and Autonomous Systems* 55:667–674.
- Stoll A, Kutzbach H D. Guidance of a Forage Harvester with GPS. *Precision Agriculture*. 2000; 2: 281–291.
- Subramanian V, Burks T F, Arroyo A A. Development of machine vision and laser radar based autonomous vehicle guidance systems for citrus grove navigation. *Comput. Electron. Agric.* 2006; 53(2):130–143.
- Sutherland, K. T. and W. B. T. Hompson. 1993. Inexact navigation. In: *IEEE International Conference on Robotics and Automation (ICRA' 93)*. PP. 1–7.

- Tamaki K. Agriculture and robot. Tokyo Univ. of Agric., 2006; 50(4): 83–94. (in Japanese)
- Tamimi H, Andreasson H, Treptow A, Duckett T, Zell A. Localization of mobile robots with omnidirectional vision using Particle Filter and iterative SIFT. *Robotics and Autonomous Systems*. 2006; 54:758–765.
- Tatsuno J, Tajima K, Terada Y, Ishii T, Kato M, Tamaki K. 2-D localization of autonomous farm vehicle using laser distance sensor. *Journal of the Japanese Society of Agricultural Machinery*. 2005; 67(5): 45–53.
- Terada A, Ando Y, Mizukawa M. Autonomous agricultural robot with a seeding function-self localization using Omni-directional vision. *Nippon Kikai Gakkai Robotikusu, Mekatoronikusu Koenkai Koen Ronbunshu (CD-ROM), 2A1-B13*. 2006. (in Japanese).
- Tillett N D, Hugue T. Computer-Vision-based Hoe Guidance for Cereals- an Initial Trial. *Journal of Agricultural Engineering Research*. 1999; 74(3): 225–236.
- Tillett N D. Automatic guidance sensors for agricultural field machines: a review. *Journal of Agricultural Engineering Research*. 1991; 50(33): 167–187.
- Tofael A, Tomohiro T, Masayuki K, Tsuyoshi H, Hideo H, Zhang Q. Navigation Using a Laser Range Finder for Autonomous Tractor (Part 1)-Positioning of Implement. *Journal of the Japanese Society of Agricultural Machinery*. 2006; 68 (1): 68–77.
- Tsubota, R, Noguchi N, Mizushima A. Automatic guidance with a laser scanner for a robot tractor in an orchard. In: *Proceedings of the Automation Technology for Off-road Equipment, Kyoto, Japan*. 2004.
- Vasseur P, Mouaddib E M. Central catadioptric line detection. In: *Proceedings of the British Machine Vision Conference*. London, U K: BMVA Press, 2004
- Weng J, Cohen P, Herniou M. Camera calibration with distortion models and accuracy evaluation. *PAMI*. 1992; 14(10):965–980.
- Willrodt F L. Steering attachment for tractors. 1924, U.S. Patent No. 1506706.
- Winters N, Santos-Victor J. Omni-directional Visual Navigation. In: *Proc. of the 7th Int. Symp. On Intelligent Robotic Systems (SIRS'99), Coimbra, Portugal* 9:109–118, 1999.
- Wu D, Zhang Q, Reid J F. Adaptive steering controller using a Kalman estimator for wheel-type agricultural tractor. *Robotica*. 2001; 19:527–533.

- Yekutieli O, Pegna F G. Automatic guidance of a tractor in a vineyard. In: Proceedings of the Automation Technology for Off-road Equipment, Illinois, USA. 2002.
- Ying X, Hu Z. Catadioptric camera calibration using geometric invariants. IEEE Transactions on Pattern Analysis and Machine Intelligence. 2004; 26(10): 1260–1271.
- Yu B, Jain A K. Lane boundary detection using a multiresolution hough transform. Proceedings. International Conference on Image Processing, 1997; 2: 748–51.
- Yukumoto O, Matsuo Y, Noguchi N. Navigation technology for tilling robots. Robotisation of agricultural vehicles and the outline of navigation system for tilling robot. Proc. International Symposium on Mobile Agricultural Bus-System Lab and PA for the Large Scale Farm Mechanization, Sapporo, Japanese Society of Agricultural Machinery, 1997; pp.59–78.
- Yukumoto O, Matsuo Y, Noguchi N. Robotization of agricultural vehicles—description of the tilling robot. Journal of Agricultural Engineering Research. 2000; 34: 107–114.
- Zhang Q, Reid J F, Noguchi N. Agricultural vehicle navigation using multiple guidance sensors, In: Proceedings of International Conference on Field and Service Robotics. Pittsburgh, PA, USA, 1999; 293–298.
- Zhang Q, Wu D, Reid J F, Benson E R. Model recognition and validation for an off-road vehicle electrohydraulic steering controller. Mechatronics. 2002; 12(6): 845–858.
- Zhang Y, Gao L, Tian L. INS/GPS integrated navigation for wheeled agricultural robot based on sigma-point Kalman Filter. Asia Simulation Conference — 7th Intl. Conf. on Sys. Simulation and Scientific Computing. pp.1425-1431. 2008.
- Zhu Z X, Torisu R, Takeda J I, Mao E R, Zhang Q. Neural network for estimating vehicle behavior on sloping terrain. Biosystems Engineering. 2005; 91(4): 403–411.

ACKNOWLEDGEMENTS

First, I would like to express my profound gratitude and sincere appreciation to my academic advisor, Associate Professor Dr. Kenji Imou, for his availability, expertise and advice, motivation, and encouragement to move forward. It is my great pleasure to express indebtedness, deepest sense of gratitude, sincere appreciation to Professor Shinya Yokoyama for his kind advice, scholastic guidance and encouragement guided me to walk on this research avenue and complete my study. Great sincere thanks for Professor Hideo Sakai, Professor Kenji Omasa and Professor Seiichi Oshita. They spent some time and painstaking effort on reviewing my thesis and gave me a lot of good advices and comment for improvement my thesis.

I acknowledge my gratitude to the Embassy of Japan and the Ministry of Education of China for selecting me as a candidate for Monbukagakusho scholarship. Also thanks goes to the Ministry of Education, Culture, and Science of Japan for granting the scholarship that covered my study and stay in Japan.

Special gratitude is expressed to my seniors and juniors for their kind assistance and suggestions in both academic concern and daily life during the three years. Especially, special thanks should be expressed to Mr. Katsuhiko Wakabayashi and Mr. Shiro Ito, Mr. Hideo Sekino, Ms. Keiko Kita, Mr. Fumio Hasagawa, Mr. Yongwei Xiong and other friends in my laboratory for their memorable help.

In addition, sincere special thanks are for my friends in Japan Dr. Feiyong Chen, Dr. Yang Guo, Dr. Jinying Qiu and Mr. Shinya Kanai. Thanks for their moral support, study help and economical assistance when I was in the wrong box in Japan.

I should thank my organization the Hunan Agricultural University in China in which I have worked for 7years and is paying my salaries until now.

At last, sincere expressions of gratitude are for my family including my kindly parents, my loving wife and my cute baby. I remember their moral support, unflinching patience and encouragement while I stay in Japan alone. I am thankful to my sister for her support and help.

I will memory all the love and I must work harder in future.